SOLUTION AND SOLID STATE NMR STUDIES OF FLUORINE TAGGING REAGENTS

by

Michael Phillip Spratt

Dissertation submitted to the Graduate Faculty of the
Virginia Polytechnic Institute and State University
in partial fulfillment of the requirements for the degree of

DOCTOR OF PHILOSOPHY

in

Chemistry

APPROVED:

Harry C. Dorn, Chairman

Larry T. Taylor

John G. Dillard

John C. Schug

Harold M. Bell

June, 1985

Blacksburg, Virginia

To

Acknowledgements

In completing this tome I stand humbled and grateful for the support rendered from many sources. Dr. Harry Dorn's technical advice, friendship, and moral support was consistent throughout my graduate career. Thanks to and for many useful discussions and advice. Also, I would like to thank the members of my committee for reading, correcting, and the useful suggestions given toward the objective of making this dissertation a more useful piece of scientific literature. Also, to , who has patiently typed and retyped this work, my deepest gratitude. Finally, to my loving wife and my babies, they have shown me the things that are most important and dearest in this life. Beside them all else pales in importance.

TABLE OF CONTENTS

LIST OF FIGURES

Figure

Figure

Figure

Figure

LIST OF TABLES

Table

Introduction

This dissertation concerns applications of the fluorine tagging reagent, p-fluorobenzoyl chloride. The base-catalyzed reactions of p-fluorobenzoyl chloride provide a convenient method for ^{19}F NMR analysis of alcohols, phenols, carboxylic acids, amines, and thiols in simple model systems. The ^{19}F chemical shifts indicate a wide shift range (~10 ppm) for a large number of compounds with well resolved chemical shift regions for most functional groups. On the basis of this study, p-fluorobenzoyl chloride was an attractive analytical reagent for characterization of active hydrogen functional groups in complex mixtures.

This dissertation is in chapter form; Chapters I and III have appeared as publications in Analytical Chemistry (1,2). Chapter I describes the characterization of sterols and amino acid model compounds by derivatization with p-fluorobenzoyl chloride. This study showed the reagent to be useful in analyzing compounds of biological interest. Chapter II describes the applicabiliy of the reagent for analysis of more complex mixtures (e.g., characterizing various coal-related materials such as extraction products). Chapters III and IV describe the extension of p-fluorobenzoyl chloride into roles as a dual tagging reagent and as a prederivatizing reagent for LC-^{19}F NMR.

Chapter V leaves the theme of using fluorine tagging reagents as an analytical reagent in solution state ^{19}F NMR and focuses on the benefits of utilizing fluorine tagging reagents in solid state NMR

studies. The purpose of this work is to tag active sites on solids with a fluorine tagging reagent; then use ^{13}C -^{19}F dipole coupling interactions to assign chemical shift domains in solid state NMR spectra. Solid state ^{13}C NMR data is presented for a number of derivatized 1-adamantyl and sterol fluorobenzoate samples. Silica gel surfaces derivatized with fluorine tagging reagents were studied by solid state ^{29}Si NMR. The solid state NMR work was, in part, motivated by results obtained by Lin and Ward (3) and Pfeffer, et al. (4). It is highly recommended that these papers be reviewed before reading Chapter V.

CHAPTER I

CHARACTERIZATION OF AMINO ACIDS AND STEROIDS BY FLUORINE-19 NUCLEAR MAGNETIC RESONANCE SPECTROMETRY OF p-FLUOROBENZOYL DERIVATIVES

Introduction

For several years, fluorinated derivatives have been used by a number of groups to analyze biological compounds. Cairns and co-workers (5) quantitatively characterized trifluoroacetate derivatives of hydroxyestrogens in complex mixtures derived from pregnant mare's urine by using gas chromatography/chemical ionization mass spectrometry (GC-MS). H. Ehrsson et al. (6-9) have used fluorinated derivatives to quantitatively analyze pharmaceuticals by gas chromatography (GC) and mass spectrometry (MS). However, spectroscopic examination of complex biological mixtures by nuclear magnetic resonance (NMR) seldom permits speciation, due to excessive spectral overlap of closely related compounds. This is particularly true in ^{1}H NMR analysis where extremely complex spectra are observed for most macromolecules.

An alternate approach that easily complements ^{1}H and/or ^{13}C NMR data for complex biological systems is ^{19}F NMR. One advantage of ^{19}F NMR is that few biological systems of interest contain fluorine, thus, reducing a potentially significant background problem. Also, the ^{19}F nucleus is much more sensitive to subtle changes in chemical structure relative to the ^{1}H nucleus. This is indicated by the large ^{19}F NMR

chemical shift range (~375 ppm) for a large number of compounds.

A number of papers have appeared in the literature concerning the use of ^{19}F NMR and fluorine derivatizing reagents for analyzing amino acids in proteins and peptides. An effective sulfhydryl specific fluorinating reagent for proteins and peptides is 3-bromo-1,1,1-trifluoropropanone (BrTFA). Brown and Seamon (10) have demonstrated that BrTFA is a simple and quantitative method for characterizing cysteine residues present in these systems. The general reaction is:

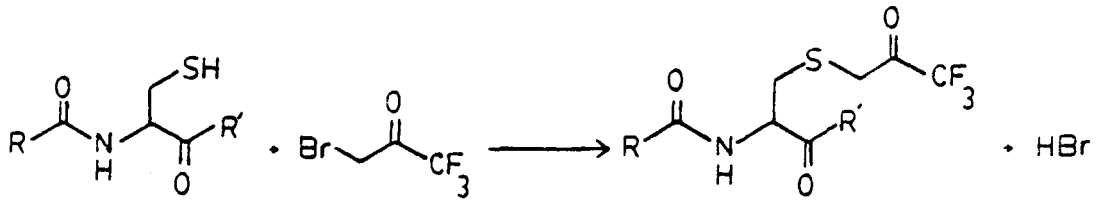

Other groups have used the BrTFA reagent to tag active site cysteines of glyceraldehyde-3-phosphate dehydrogenase (11, 12) which is a key enzyme in the glycolytic cycle. In addition, the cooperative interactions in hemoglobin (13) were studied by tagging the cysteine-93 residue with BrTFA. The ^{19}F chemical shifts of the TFA group have also been shown to be dependent on the conformation of surrounding amino acids in the protein complex (14) and the pH of the aqueous media containing the protein or enzyme (15).

M. R. Bendall and G. Lowe (16, 17) have studied active sites of papain by preparing derivatives of these enzymes utilizing SS-(2,2,2-trifluoro -1,1-dideuteroethyl)-O-methyldithioperoxycarbonate

and trifluoromethyl mercuric bromide as illustrated below:

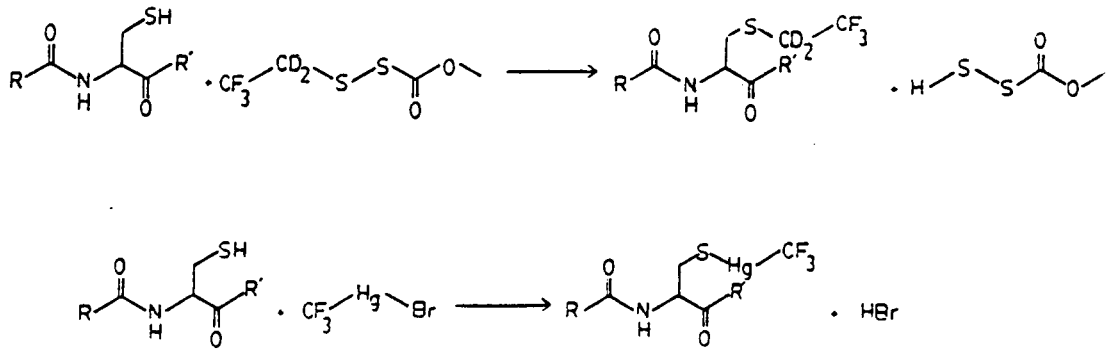

Huestis and co-workers (18) used ethyl thiotrifluoroacetate to specifically derivatize lysine residues 1 and 7 on ribonuclease S. In a similar study, Paselk and Levy (19) also used ethyl thiotrifluoroacetate to study glycine, phenylalanine and the ε-amino group of lysine in insulin.

Gaffield and Lundin (20) have used hexafluoroacetone derivatives and ^{19}F NMR, as a means of determining nitrosoaminoalcohols and amines in foods. Zuber and co-workers (21) have also used pentafluoropropionic anhydride to analyze pharmaceuticals by ^{19}F NMR. However, only a paucity of published reports are in the literature regarding the use of fluorinated derivatives to characterize steroids by ^{19}F NMR. One example, is the study by Bayer and coworkers (22) where the trifluoroacetate derivatives of hydroxypregnanes were characterized by ^{19}F NMR. They found a ^{19}F chemical shift range of approximately 0.9 ppm.

Experimental Section

Apparatus

JEOL PS-100 and JEOL FX-200 nuclear magnetic resonance spectrometers were used to obtain ^{19}F nuclear magnetic resonance (NMR) spectra at 94.08 and 187.7 MHz, respectively, for the model compounds. Both spectrometers operate in the Fourier Transform (FT) mode. The NMR spectrometers were used with internal deuterium lock systems operating at 15.14 and 30.3 MHz, respectively. 1,2-Difluorotetrachloroethane (Peninsular Chem Research) was used as the ^{19}F chemical shift reference with chloroform-d as solvent. Chemical shifts (δ ^{19}F) were measured in parts per million (ppm) with a negative value indicating shielding relative to the reference.

Procedures

Preparation of steroid p-fluorobenzoates

In a flask 0.1 millimole of the steroid was added to 10 mL of anhydrous pyridine (distilled and stored over KOH pellets). A 10% molar excess of the equivalent amount of p-fluorobenzoyl chloride was slowly added. The reaction mixture was then stirred for 24 hours at room temperature under nitrogen.

After 24 hours the pyridine was removed by vacuum distillation. The remaining residue was redissolved in 25 mL ethyl acetate and washed twice with 20 mL of 5% $NaHCO_3$ and once with 20 mL distilled H_2O. The ethyl acetate was dried over $MgSO_4$ and removed *in vacuo*.

An optional technique used to isolate the product (23), employed

dilution of the reaction mixture with 20 mL of a 50/50 benzene/ethyl acetate solution. This was washed twice with 20 mL of 5% $NaHCO_3$ and three times with 1M $CuSO_4$ which complexes with the pyridine and forms a dark blue precipitate. The remaining solvent was washed once with distilled water, dried over $MgSO_4$ and removed in vacuo. The resulting material in most cases was a crude solid which was purified by recrystallization from ethyl acetate. Yields were highly dependent on whether the hydroxyl group of the steroid was primary, secondary or tertiary (24).

Preparation of N-p-fluorobenzoyl amino acid derivatives

The method used to derivatize amino acids with p-fluorobenzoyl chloride was similar to the derivatization technique developed by Kingston and LeFevre (25). The general procedure is as follows: The amino acid model (1 millimole) was added to 10 mL of 1 N NaOH and stirred using a magnetic stirrer until dissolved. To this solution 10 mL of ethyl ether was added followed by slow addition of 5 mL of ethyl ether containing 1.1 millimole (or a 10 percent excess of the equivalent amount in cases of more than one functional group) of p-fluorobenzoyl chloride. The aqueous and ethyl ether solutions were mixed and the pH of the reaction mixture was occasionally checked to assure that the pH was always greater than 10. If the pH was less than 10, 1N NaOH was added in dropwise fashion to obtain a pH $>$ 10. After the p-fluorobenzoyl chloride was added, the heterogeneous solution was vigorously stirred at room temperature for a 24 hour period. After 24 hours the solution was placed in a separatory funnel and acidified with 6N HCl to

a pH of 1. The solution was extracted three times with 20 mL portions of ethyl acetate. The organic portions were combined, dried over $MgSO_4$, and the ethyl acetate removed in vacuo. The resulting residue in most cases was a crystalline solid. Upon recrystallization, (ethyl acetate/hexane) all samples yielded white crystalline product.

Results and Discussion

The general reaction for the preparation of the p-fluorobenzoate derivatives is illustrated below:

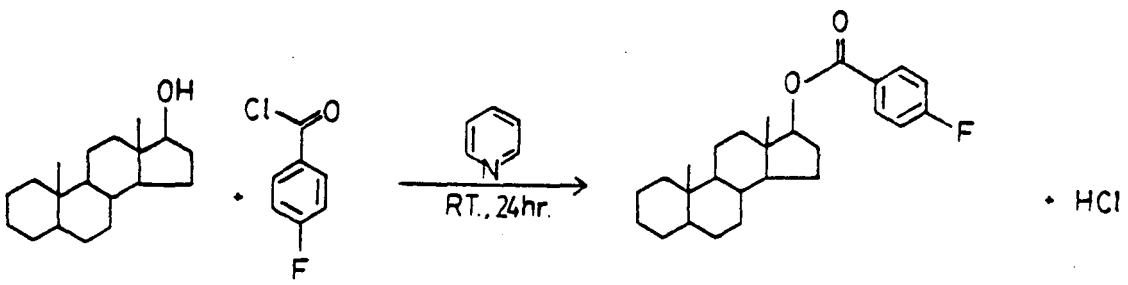

The ^{19}F chemical shifts for a number of p-fluorobenzoates of sterols are presented in Tables 1.1 to 1.5. The ^{19}F spectral assignments for some of the di-and tri-p-fluorobenzoate sterol derivatives in Tables 1.1 to 1.5 are tentative (e.g., cholestane-3β, 5α, 6β-triol). However, in some cases ^{19}F spectral assignments were based on the relative intensities of the ^{19}F signals obtained when a limiting amount of the p-fluorobenzoyl chloride was used in the derivative preparation. As an example, one would expect (and observes) a more rapid reaction at the C21 position (primary alcohol) as opposed to the α-C17 position (tertiary alcohol) in Δ^4-pregnen-17α,21-diol-3,20-dione (Table 1.3). Where appropriate, the ^{19}F spectral assignments are

Table 1

^{19}F NMR CHEMICAL SHIFTS FOR p-FLUOROBENZOATE DERIVATIVES OF 5α - STEROIDS

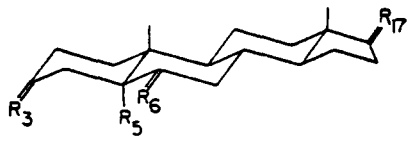

STEROID		δ_F, PPM R_3	R_5	R_6	R_{17}	R_{20}
5α-androstan-3β-ol-17-one	R_3: 3β-OH ; R_5: —H ; R_6: 6β-H ; R_{17}: =O	-38.90(n)				
5α-androstan-3α-ol-17-one	R_3: 3α-OH ; R_5: —H ; R_6: 6β-H ; R_{17}: =O	-38.73(d)				
5α-androstan-17β-ol-3-one	R_3: =O ; R_5: —H ; R_6: 6β-H ; R_{17}: 17β-OH				-38.66(n)	
5α-pregnan-3β,20β-diol	R_3: 3β-OH ; R_5: —H ; R_6: 6β-H ; R_{17}: 17β-H, 20β-OH	-38.86(n)[1]				-38.83(n)[1]
cholestane-3β,5α,6β-triol	R_3: 3β-OH ; R_5: —OH ; R_6: 6β-OH ; R_{17}: 17β-H, 20-isooctyl	-38.55(n)[1]	-38.69(a)[1]	-38.10(n)[1]		

1) ^{19}F Chemical Shifts have been tentatively assigned.

Table II

^{19}F NMR CHEMICAL SHIFTS FOR p-FLUOROBENZOATE DERIVATIVES OF 5α - STEROIDS

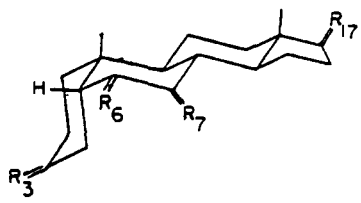

STEROID	δ_F, PPM R_3	R_6	R_7	R_{20}
5α-androstan-3β-ol-17-one	-38.89(1)			
5α-androstan-3α-ol-17-one	-38.78(α)			
5α-pregnan-3α,6α-diol-20-one	-38.41(α)[1]	-38.51(α)[1]		
5α-pregnan-3α,20α-diol	-38.77(α)[1]			-38.82(α)[1]
5α-cholanic acid-3α,7α-diol	-38.78(α)[1]		-37.58(α)[1]	

1) ^{19}F Chemical Shifts have been tentatively assigned.

indicated as they appear in Tables 1.1 to 1.5. The range of ^{19}F chemical shifts for the p-fluorobenzoates of the sterols (Figure 1.1) are approximately twice the range found for the trifluoroacetates for nearly the same sterol model set (22).

In Tables 1.1 and 1.2 are summarized the ^{19}F chemical shifts for a number of C3 substituted steroids with the A/B ring system having cis and trans geometries at the C5 ring junctions. The ^{19}F chemical shifts are nearly insensitive to the cis and trans geometries at the C5 ring junction (e.g., 5β-androstan-3β-ol-17-one vs. 5α-androstan-3β-ol-17-one) Tables 1.2 and 1.1, respectively. However, examination of the four isomers of androstan-3-ol-17-one reveals that the ^{19}F chemical shifts for these p-fluorobenzoates allow spectral identification of the α or β isomer at the C3 carbon. For example, the ^{19}F chemical shift for 5β-androstan-3β-ol-17-one is -38.89 ppm while for 5β-androstan-3α-ol-17-one the ^{19}F resonance is -38.78 ppm. One observes the same ^{19}F chemical shift trend for the 5α-androstane isomers, (e.g., 5α-androstan-3β-ol-17-one, -38.90 ppm and 5α-androstan-3α-ol-17-one, -38.75 ppm).

The introduction of a second p-fluorobenzoyl group at the C6 position typically has a deshielding influence on the C3 p-fluorobenzoate ^{19}F chemical shift (e.g., 5β-pregnan-3α, 6α-diol-20-one). The observation of a deshielding effect by introduction of a second aromatic ring is similar to data obtained in simple model systems (24). The influence is apparently not observed when the second p-fluorobenzoyl group is introduced at the C7 and/or a position further removed from C3.

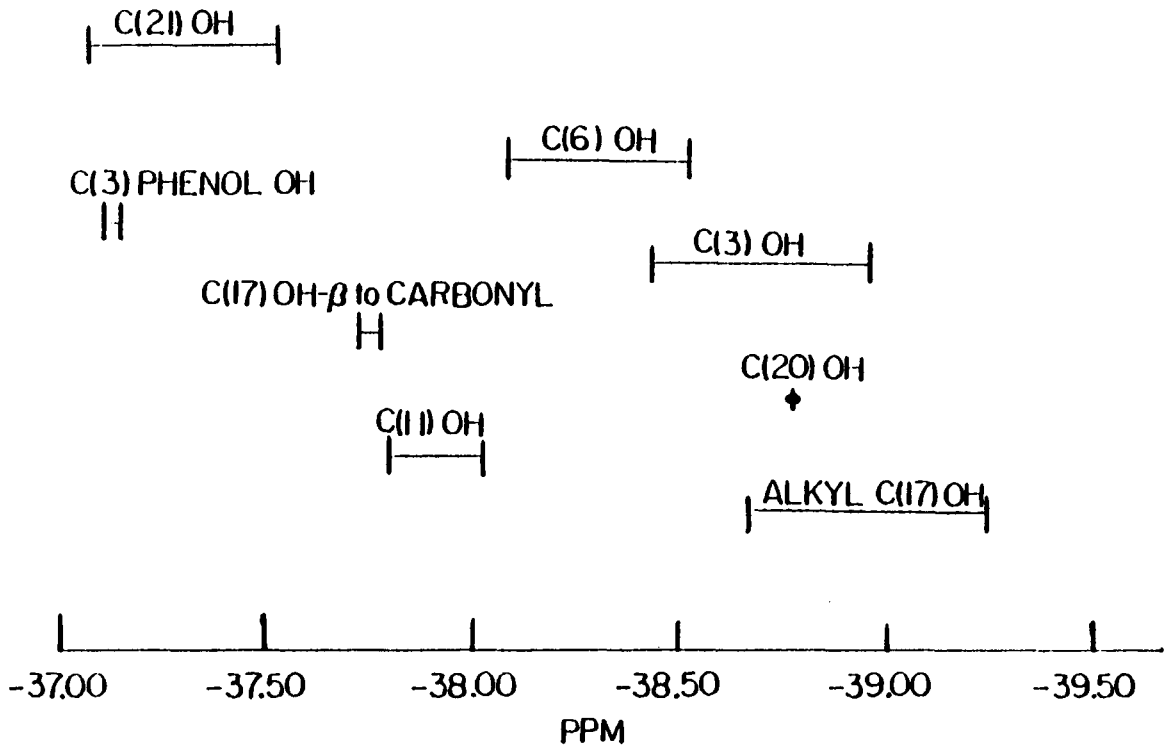

FIGURE 1.1 ^{19}F chemical shift range for p-fluorobenzoyl derivatives of sterols.

The ^{19}F chemical shifts for a number of Δ^4-steroids are presented in Table 1.3. One major feature of the data in Table 1.3 is the influence of a β-carbonyl group on the ^{19}F chemical shift of the p-fluorobenzoate group which causes a deshielding of the ^{19}F nucleus. For example, comparing the ^{19}F chemical shift of the C21 p-fluorobenzoate ester of ^{4}-pregnen-21-ol-3,20-dione (-37.54 ppm) to the n-butyl p-fluorobenzoate ester (-38.86 ppm) (24), one observes a deshielding of the ^{19}F nucleus by 1.32 ppm. The deshielding of the ^{19}F nucleus by the β-carbonyl functional group was expected in light of our previous study (24). In this study it was found that p-fluorobenzoyl anhydride derivatives of carboxylic acids had ^{19}F chemical shifts significantly more deshielded than other alcohol derivative (~3.5 ppm). This effect was also observed for trifluoroacetates of C21 sterols containing a β-carbonyl group (22).

For the sterols with a tertiary alcohol group at C17 (e.g., Δ^4-pregnen-17α-21-diol-3,20-dione), the ^{19}F chemical shifts for these C17 p-fluorobenzoate groups are much lower (more deshielded) than normally encountered for tertiary alcohol derivatives. For example, the ^{19}F chemical shift for the p-fluorobenzoate of t-butanol is -39.69 ppm (24). However, the presence of the β-carbonyl group and the second p-fluorobenzoate ring in reasonably close proximity substantially deshield the p-fluorobenzoate group at C17. Thus, the relatively constant ^{19}F shifts of approximately -37.7 ppm at C17 are understandable in terms of these factors. It is also interesting to note that the ^{19}F chemical shift for the Δ^4-androstan-17β-ol-3-one p-fluorobenzoate

Table IV

^{19}F NMR CHEMICAL SHIFTS FOR p-FLUOROBENZOATE DERIVATIVES OF Δ^4 - STEROIDS

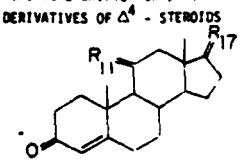

STEROID	R_{11}	δ_F, PPM R_{17}	R_{21}
Δ^4-pregnen-21-ol-3,20-dione	R_{11} = ; R_{17} = 		-37.54
Δ^4-pregnen-21-ol-3,11,20-trione	R_{11} = =O ; R_{17} =		-37.49
Δ^4-pregnen-11β,21-diol-3,20-dione	R_{11} = ; R_{17} =	-38.02(n)	-37.37
Δ^4-pregnen-17α,21-diol-3,20-dione	R_{11} = ; R_{17} = 	-37.73(a)[1]	-37.34[1]
Δ^4-pregnen-17α,21-diol-3,11,20-trione	R_{11} = =O ; R_{17} =	-37.77(a)[1]	-37.15[1]
Δ^4-pregnen-11β,17α,21-triol-3,20-dione	R_{11} = ; R_{17} =	-37.81(n)	-37.74(a)[1] -37.10[1]
Δ^4-androsten-17β-ol-3-one	R_{11} = ; R_{17} =	-38.63(n)	

1) ^{19}F Chemical Shifts have been tentatively assigned.

derivative is in fair agreement with the value obtained for the simple model cyclohexanol (-38.88 ppm) (24). The p-fluorobenzoate derivatives at the secondary C11 position are substantially deshielded for Δ^4-pregnen-11β-21-diol-3,20-dione and Δ^4-pregnen-11β,17α,21-triol-3,20-dione with ^{19}F chemical shifts of -38.02 and -37.81 ppm, respectively. This could be due in part to the aromatic ring interactions of the second and third aromatic systems with the p-fluorobenzoate ring at the C11 position.

In Table 1.4 several Δ^5-steroid p-fluorobenzoate derivatives are reported. Once again, the narrow range (-39.90 to -39.71 ppm) of ^{19}F chemical shifts for the C3 p-fluorobenzoate group is very similar to the simple cyclohexanol derivative (-38.88 ppm) (24). In addition, the C17 ^{19}F chemical shift for the 17α-methyl-5-androstan-3β,17β-diol derivative is close to the expected value for tertiary alcohol derivatives.

The sterols in Table 1.5 are easily characterized by the phenolic C3 p-fluorobenzoate ^{19}F resonance at approximately -37.19 ppm for estrone, β-estradiol, and estriol. As Figure 1.2 clearly shows, the two ^{19}F resonances for the phenol (-37.19 ppm) and the C17 secondary alcohol (-38.67 ppm) groups on β-estradiol are well resolved in the ^1H decoupled ^{19}F spectrum and can be assigned easily. The estriol is easily characterized by the C16 and C17 secondary p-fluorobenzoate ^{19}F resonances at -37.98 and -38.08 ppm. In similar manner to other systems discussed (vide supra), vicinal p-fluorobenzoate ring interactions at C16 and C17 deshield the ^{19}F nucleus.

A limited number of amino acids were also characterized using

Table VI

^{19}F NMR CHMICAL SHIFTS FOR p-FLUOROBENZOATE DERIVATIVES OF Δ^5 - STEROIDS

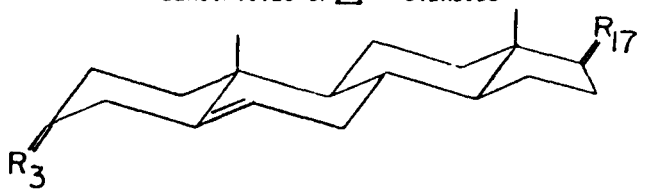

STEROID	δ_F, PPM R_3	R_{17}
Δ^5-cholesten-3ß-ol cholesterol	-38.90(ß)	
Δ^5-androsten-3ß-ol-17-one	-38.86(ß)	
Δ^5-pregnen-3ß-ol-20-one pregnenolone	-38.71(ß)	
17α-methyl-5-androsten-3ß,17ß-diol methylandrostenediol	-38.74(ß)	-39.24(ß)

Table V

^{19}F NMR CHEMICAL SHIFTS FOR p-FLUOROBENZOATE DERIVATIVES OF $\Delta^{1,3,5}$ – ESTRATRIENE STEROIDS

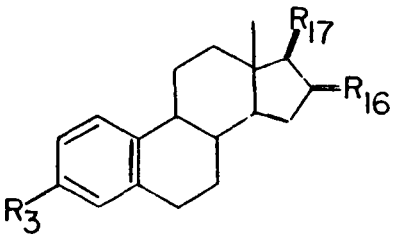

STEROID		δ_F, PPM R_3	R_{16}	R_{17}
$\Delta^{1,3,5}$-estratrien-3-ol-17-one Estrone	R_3 = OH ; R_{16} =  ; R_{17} = =O	-37.19		
$\Delta^{1,3,5}$-estratrien-3,17β-diol β-Estradiol	R_3 = OH ; R_{16} =  ; R_{17} = 	-37.19		-38.67(β)
$\Delta^{1,3,5}$-estratrien-3,16α,17β-triol Estriol	R_3 = OH ; R_{16} =  ; R_{17} = 	-37.14	-37.94(α)[1]	-38.08(β)[1]

1) ^{19}F Chemical Shifts have been tentatively assigned.

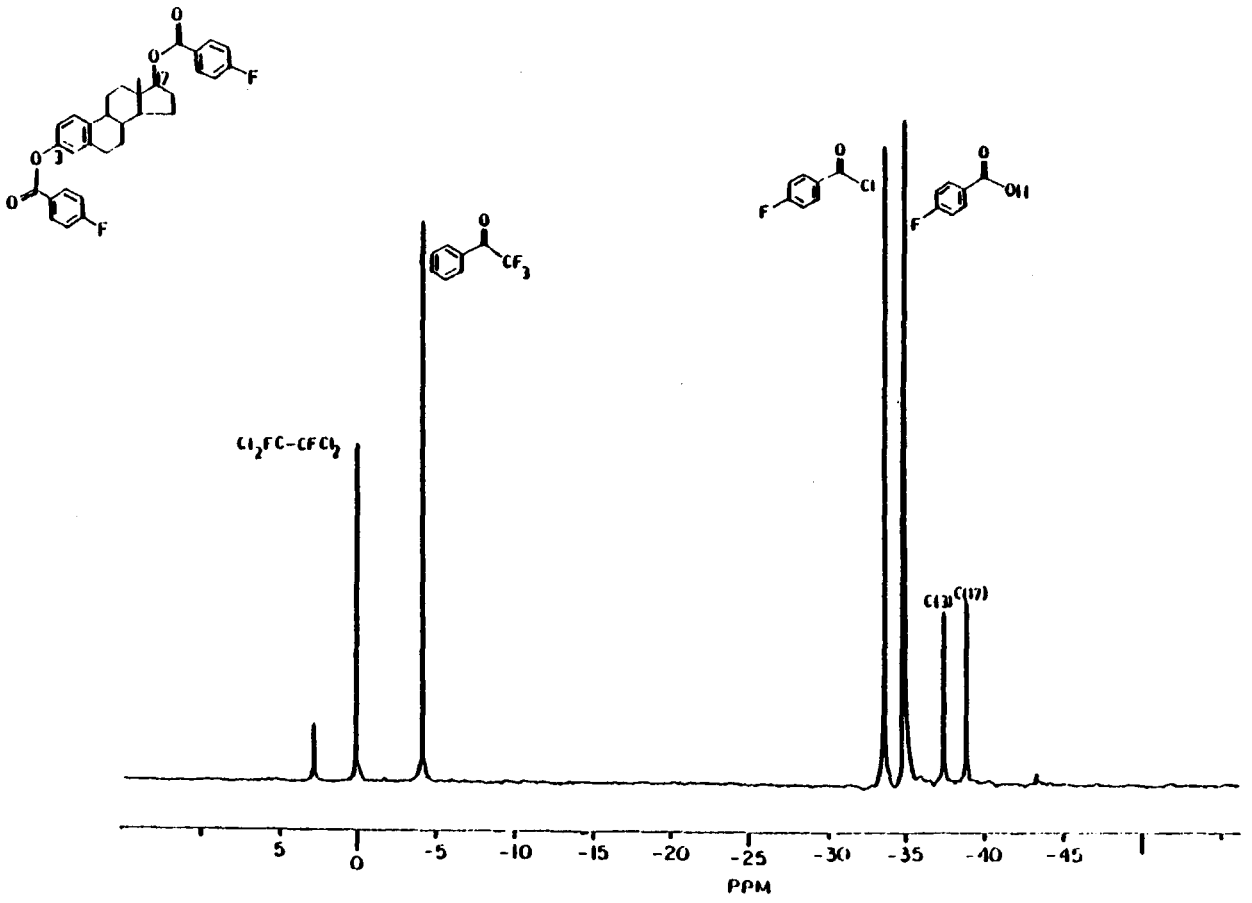

FIGURE 1.2 ^{1}H decoupled ^{19}F spectrum for p-fluorobenzoate derivative of $\Delta^{1,3,5}$-Estratrien-3,17$_{\beta}$ diol (β-Estradoil)

p-fluorobenzoyl chloride. The ^{19}F chemical shift data for the p-fluorobenzamides of the amino acids are listed in Table 1.6. The ^{19}F chemical shifts observed are characteristic for primary amine derivatives (24). The overall ^{19}F chemical shift range for the p-fluorobenzamides is only ~0.36 ppm for the limited number of amino acids examined. These results reflect the fact that the ^{19}F test nucleus is eight and/or nine bonds removed from the reaction site.

In spite of the large interatomic distances between the fluorine test nucleus and the structural changes of the amino acid, it is still possible to observe the effect of alkyl and/or phenyl substitution on alanine. These effects although greatly attenuated are similar to the results previously obtained for alcohol derivatives (24). The ^{19}F chemical shift data can also be used to characterize amino acids containing other functional group such as threonine where the hydroxyl functional group is also derivatized; the ^{19}F chemical shifts for these are indicated in Table 1.6.

Conclusion

The results of the present study demonstrate the potential utility of ^{19}F NMR for characterizing sterols and amino acids . That is, the ^{19}F chemical shift parameter for p-fluorobenzoyl derivatives is sufficiently sensitive to allow spectral identification of several types of sterols and even differences in structure at the β-position of amino acids. The ^{19}F chemical shifts are influenced by: 1) the position of p-fluorobenzoate on the steroid ring system, 2) the type of hydroxyl

Table VI

^{19}F NMR Chemical Shifts for
N-p-fluorobenzoate Derivatives of
Amino and Nucleic Acids

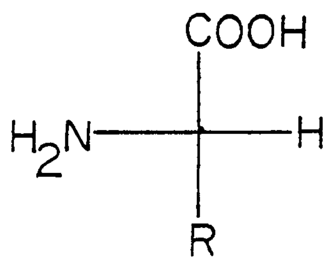

STRUCTURE OF R	AMINO ACID	δ_F, PPM
$-CH_3$	(D,L)-ALANINE	-41.05
$-CH(CH_3)_2$	(D,L)-VALINE	-41.14
$-CH_2CH(CH_3)_2$	(D,L)-LEUCINE	-41.07
$-CH(CH_3)CH_2CH_3$	(D,L)-ISOLEUCINE	-41.10
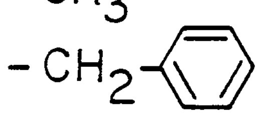	(D,L)-PHENYLALANINE	-40.91
$-CH_2CH_2SCH_3$	(D,L)-METHIONINE	-40.85
$-CH(OH)CH_3$	THREONINE	-40.78 -37.15 2° (OH)

group (e.g. 1°, 2° or 3° alcohols), 3) ring interactions between mono, di-and tri-p-fluorobenzoate groups and 4) substituent effects for groups in close proximity to the p-fluorobenzoate group (e.g., β-carbonyl). Although ^{19}F spectral overlap of a few steroid derivatives is observed, nevertheless, unique ^{19}F shifts are obtained for most of the sterols. Thus, the modest range of ^{19}F chemical shifts (~ 2 ppm for all hydroxyl groups) and ease of derivative preparation suggests an important role for p-fluorobenzoyl chloride in characterizing sterols.

CHAPTER II

DERIVATIZATION OF COAL WITH FLUORINE TAGGING REAGENTS: CHARACTERIZATION OF ACTIVE HYDROGEN FUNCTIONAL GROUPS BY NMR TECHNIQUES

Introduction

It is generally acknowledged that heteroatom compound formation and/or dissolution during coal liquefaction is of paramount importance in terms of coal conversion. From the physical dissolution viewpoint, heteroatom compounds (e.g. phenols, amines, carboxylic acids, etc.) form strong hydrogen bond complexes which can hinder dissolution or thermal solvolysis. Sternberg for many years has called attention to the identification of scissle bonds in coal and their corresponding role in coal conversion (26).

Neavel (27) has pointed out the need to classify various fundamental properties for the vitrinite in coals. Neavel suggests that four structural properties of major importance to classification are the following: a) the nature of cyclic structures (e.g. ring condensation index, aromaticity, heteroatoms), b) scissle bridging structures (e.g. ethers, sulfides, polymethylenes), c) functional group characteristics (especially oxygen-and sulfur-containing), and d) the nature of the hydrogen bonding and physical entanglement that cohere molecular moieties. One technique by which many of these properties are studied is by analysis of extractable products.

During the last few years several groups have studied the alkylation and/or acylation of coal using various reagents and conditions. In the case of alkylation, Sternberg's reductive alkylation procedure, using alkali metals and electron transfer reagents, has received considerable attention (28, 29). Studies have shown (30) reductive alkylation of solid fuels yield a soluble product representing about 80% of the original coal material. Alemany, et. al. (31), by reductively butylating coal, showed that electron transfer, proton abstraction, ether cleavage, and elimination reactions were all possible reactions that different coal moieties may undergo. In a more recent study, Alemany et. al. (32), analyzed methylated and butylated coals by solid state ^{13}C CP/MAS NMR and determined the degree of alkyl substitution in the coal products. They also determined the oxygen/carbon alkylation ratios for the methylation and butylation reactions.

The work of Hodek (33) and Larsen (34) have shown that bituminous coal can be readily acylated using Friedel-Craft conditions (i.e. $AlCl_3$). Hodek reported that the pyridine solubility of the acylated coal was dependent on the alkyl chain length of the acid chloride employed. Hodek reported weight-average molecular weights in the range of 2 -3 x 10^3 daltons. Other work by Hombach (35) suggested much higher values ~10^5. Larsen has interpreted these results in terms of acylation at the surface of the coal particles. He states that increasing the alkyl chain length of the acyl groups promotes favorable solvent interactions (alkyl chains-solvents) analogous to "reversed micelle" formation (34). Larsen (34, 36) also reported ^1H and ^{13}C NMR

spectra which indicated the presence of the acyl chains, but few resonances were observed for the carbon and hydrogen of the actual coal. This is consistent with the hypothesis that the alkyl chains would exhibit more motion (e.g. rotational motion of the methylene groups) on the surface of the coal particles and thereby be NMR observable. In contrast, the hydrogen and carbon in the coal would have relatively little motion (solid-like) and not be observable using solution NMR techniques.

Franz and Skiens (37) have reported that numerous naphthol derivatives may be formed as by-products when coal is reductively alkylated. Sharma and co-workers (38) have cited that the harsh reaction conditions used to alkylate coal usually disrupt the original structure of coal and severely changes the original carbon framework. Therefore, they have reported milder acylation techniques where the acylating reagents were carboxylic acids, acid anhydrides, and N-hydroxy methyl amides. In a similar manner, Ouchi and Makabe (39, 40) developed a technique to reduce coal in hexamethylphosphoramide with NaOH and t-butyl alcohol. From analysis of the pyridine soluble products they determined molecular weight distributions and the average size of the aromatic rings. Conversely, oxidation of coal by hydrogen peroxide (H_2O_2) and trifluoroacetic acid (TFA) completely degrades the aromatic ring structure of coals while leaving the aliphatic structure relatively intact (41). Verheyen and Johns (42) have used ^1H NMR techniques to quantitatively determine the aliphatic structure of these aromatic oxidative degradation products. In addition, silylation of the chemical

functionalities using ^{1}H and/or ^{29}Si NMR spectroscopy is a well characterized method for studying active hydrogen functional sites on coal (43-47).

Although GC-MS fluorine derivatization techniques have been used to characterize coal liquids (48-51), few reports have been written concerning the use of ^{19}F NMR tagging reagents (52). Dorn, et. al. have recently reported the use of p-fluorobenzoyl chloride as a fluorine tagging reagent and have used it successfully to characterize a number of biological model systems (1, 24, 53). A large ^{19}F chemical shift range for the p-fluorobenzoyl derivatives, (e.g., ~10 ppm) allows relatively easy characterization of hydroxyl, amine, and thiol functionalities. In this chapter we wish to illustrate how whole coal samples can be extracted using quinoline and p-fluorobenzoyl chloride. A number of ^{1}H, ^{13}C, and ^{19}F NMR techniques have been used to analyze the resulting liquid products. However, the ^{19}F NMR spectra yield specific data regarding the hydroxyl and amine content of these samples.

Experimental

Two different coals have been derivatized using p-fluorobenzoyl chloride as the tagging reagent. The coals studied were a Virginia bituminous coal obtained from United Coal Co. Western and an Illinois #6 bituminous coal obtained from the Monterey mine. Specifically, 5 g of coal and 5 g of p-fluorobenzoyl chloride (Aldrich Chem. Co.) were mixed with quinoline (10 mL) which served as the solvent and basic catalyst. The mixture was stirred at a temperature of 200°C for 20 hours under an inert nitrogen atmosphere. In addition, a control reaction of quinoline

and p-fluorobenzoyl chloride (no coal present) was also conducted using same reaction conditions and work-up procedure.

The work-up procedure consists of cooling the reaction flask to room temperature and exhaustively extracting the coal residue into chloroform with a Soxhlet extractor. The chloroform extract is then washed 3-4 times with cold 2N hydrochloric acid (to remove the quinoline), 5% aqueous $NaHCO_3$, and distilled water. After drying the extract over anhydrous magnesium sulfate, the chloroform is removed in vaccuo. Several preliminary observations should be noted.

There was only a small amount of intractable solid material remaining in the Soxhlet extraction thimble after extraction with chloroform. This would suggest that most of the coal was "soluble" in chloroform after derivatization. Seyferth, et. al. (43) have shown that silylation can be used to solubilize solvent refined coals (SRC) and pyridine extracts of a high volatile bituminous coal in benzene. This is presumably due to the removal of most hydrogen-bonding interactions. Although some of the "soluble" derivatized product was undoubtably "reversed micelle" material, analogous to the material described by Larsen (34, 36), a significant portion of the derivatized coal is clearly soluble material as indicated by the ^{1}H, ^{13}C, and ^{19}F NMR results discussed below.

Instrumentation

A JEOL FX-200 nuclear magnetic resonance (NMR) spectrometer

equipped with an Oxford 4.7 T superconducting solenoid magnet (52/mm bore) was used to obtain high resolution ^{19}F, ^{13}C, and ^{1}H NMR spectra at 187.70 MHz, 50.10 MHz, and 199.50 MHz frequencies,respectively. A floppy disk system was used for data storage and each spectrum contained 8096 data points. The NMR spectrometer was used with an internal deuterium lock system operating at 30.28 MHz.

For all the ^{19}F NMR spectra, 1,2-difluorotetrachloroethane (Penninsular Chemical Research) was used as the ^{19}F chemical shift reference with chloroform-d as the solvent. Chemical shifts (δ ^{19}F) were measured in parts per million (ppm) with a negative value indicating shielding relative to the reference.

Hexamethyldisiloxane (Aldrich Chemical Co.) was used as the ^{1}H (0.07 ppm relative to TMS) and ^{13}C (1.98 ppm relative to TMS) chemical shift reference with chloroform-d as the solvent. In all ^{13}C experiments the complete ^{1}H decoupling mode was used. Details for the ^{13}C INEPT (insensitive nucleus enhancement by polarization transfer) pulse sequence have been previously described (54).

Results and Discussion

Figure 2.1a is the ^{19}F NMR spectrum for the derivatized Illinois No. 6 coal products. The chemical shift reference, 1,2-difluorotetrachloroethane, is indicated, as well as a strong signal due to p-fluorobenzoic acid, one of the major by-products of the reaction. However, the ^{19}F signal characterizing the acid, 34.84 ppm, is well

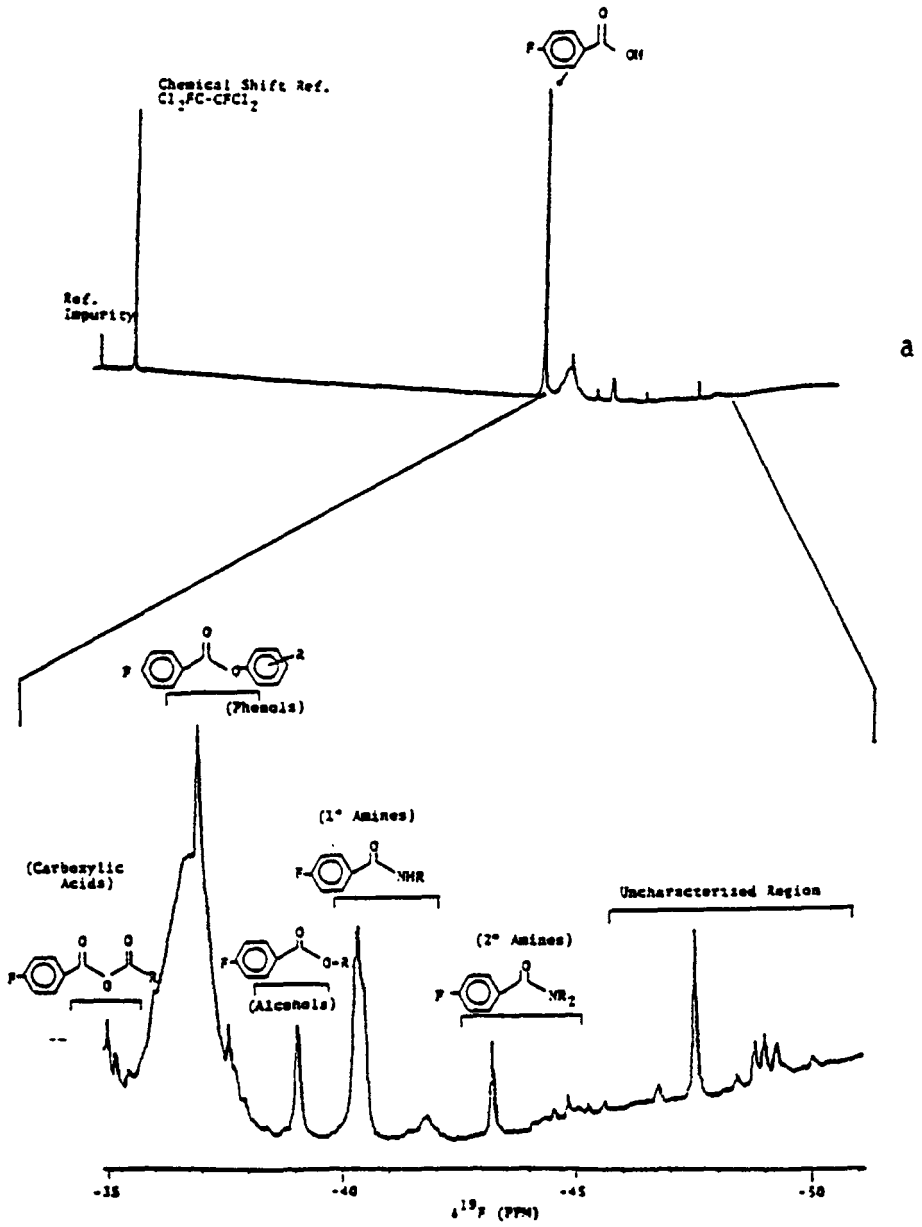

FIGURE 2.1 The 187.7 MHz ^{19}F NMR spectrum for p-fluorobenzoyl derivatives of Illinois #6 extraction material (a) and the expanded ^{19}F NMR spectral region (-35 to -50 ppm) for derivatized Illinois #6 coal (b).

removed from the chemical shift region of the p-fluorobenzoyl derivatives. Figures 2.1b and 2.2 are the expanded ^{19}F NMR spectral regions (-35.0 to -50.0 ppm) for the chloroform soluble derivatized Illinois No. 6 and Western Virginia coals, respectively. As indicated in these spectra a preponderance of phenols is clearly derivatized. Moreover, a number of derivatized amines, alcohols, and carboxylic acids are also present in both coal samples. Previous work (53) with derivatized SRC (SESC) coal samples did not indicate levels as high for any of these particular heteroatom compounds (SESC is an acronym for sequential Elution by Selective Solvent Chromatography, a chromatographic technique developed at Mobil Oil which divides liquid coal products into classes containing various functional groups (55). To illustrate this point Figure 2.3 is the ^{19}F NMR spectra for the SRC SESC fraction #5 obtained from the Illinois No. 6 coal (53). The preponderance of phenol derivatives is clearly indicated with only very small amounts of amines or carboxylic acids. This was generally true for the other SESC fractions and for the total SRC sample (53). This may indicate that the more severe SRC reaction conditions (e.g. 400-450°C) may lead to extensive losses for certain heteroatom functionalities (e.g. carboxylic acid). This could mask the actual functional groups involved in the initial phases of liquefaction.

Comparing Figures 2.1b and 2.2, there are subtle differences in the functionality content of these two coals. In Figure 2.1b the phenol region of the Illinois No. 6 coal is divided into two distinct regions, one sharp peak centered at -36.99 ppm and a broad shoulder at -36.63

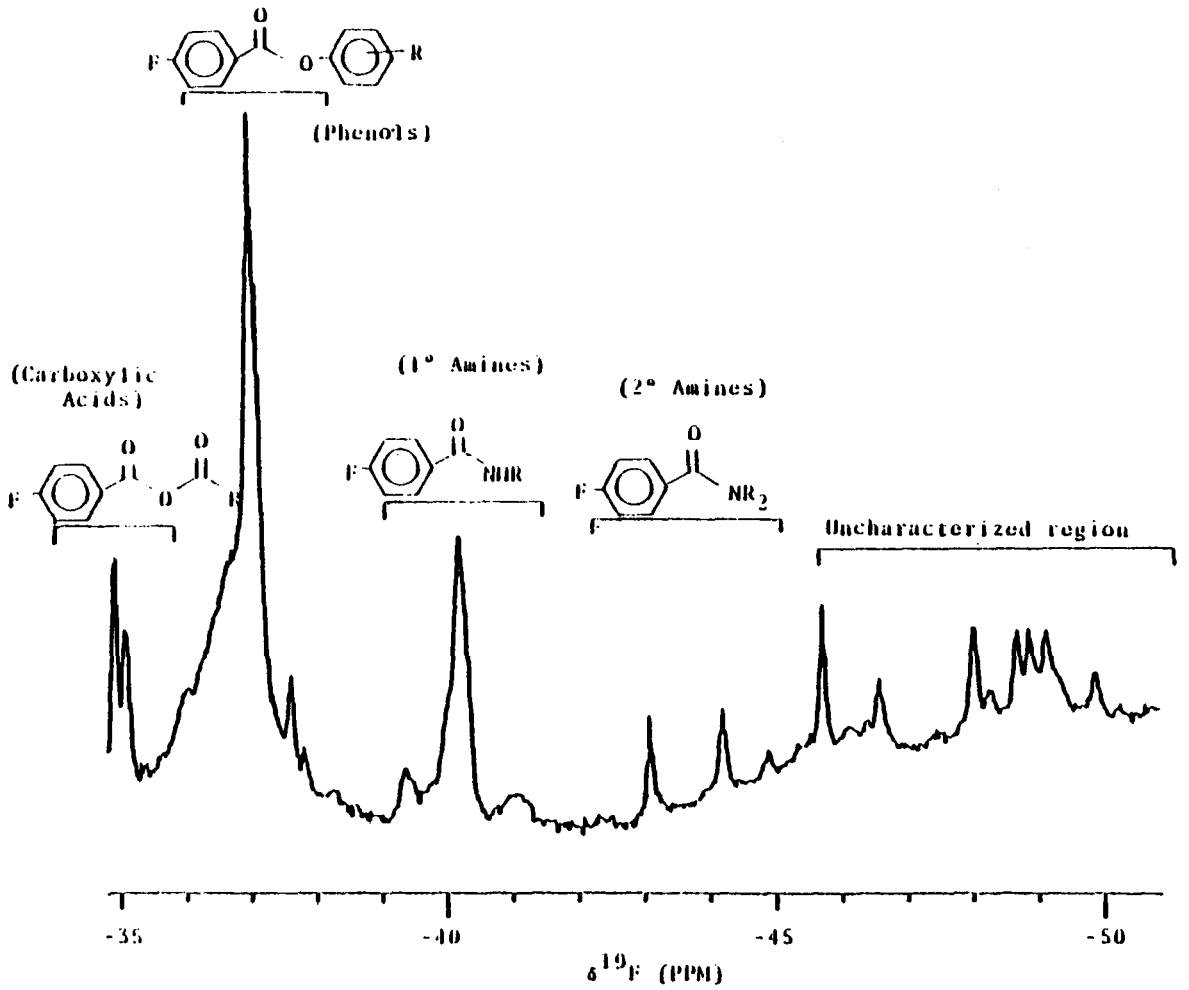

FIGURE 2.2 The expanded ^{19}F NMR spectral region (-35 to -50 ppm) for derivatized Western Virginia Coal.

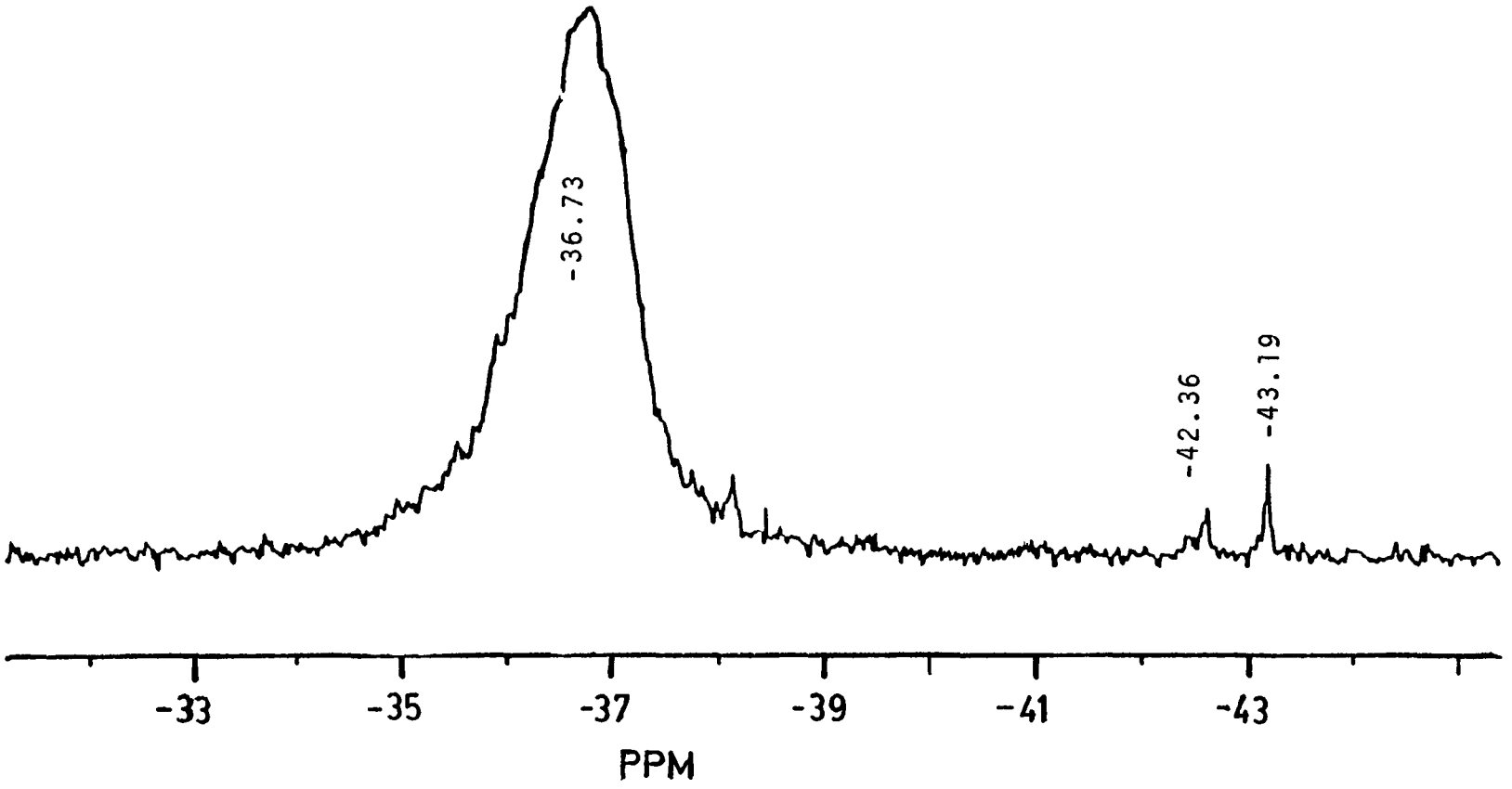

FIGURE 2.3 Expanded 56.13 MHz ^{19}F NMR spectral region (-33 to -45 ppm) for an Illinois #6 Solvent Refined Coal SESC fraction #5 (52).

ppm. It is interesting to note that the ^{19}F chemical shifts for these two regions are in fair agreement with the values obtained for simple models. The region centered at -36.99 ppm corresponds to simple phenols (e.g. β-naphthol, -37.06 ppm or phenylphenols, -36.99 ppm) (24) and the region centered at -36.63 ppm is indicative of a larger fused ring and/or polyfunctional phenols (e.g. phenanthrols, -36.84 ppm; catechol -36.62 ppm; or resorcinol, -36.78 ppm) (24). While many of the same signals are also present in the ^{19}F spectrum for the Western Virginia coal (Figure 2.2), the polyfunctional phenol region is not as well defined or as intense as found in the ^{19}F spectrum for the Illinois coal.

Each ^{19}F spectrum for the two coals indicates that a few carboxylic acids groups have been derivatized. From previous studies (24) these ^{19}F resonances are characteristic of fused ring carboxylic acids or carboxylic acids with phenyl substituents (e.g. 1-naphthoic acid, -35.18 ppm or diphenylacetic acid, -35.02 ppm). A second ^{19}F chemical shift region common to both coals is a broad resonance centered at -40.36 ppm. It should be noted that primary aromatic p-fluorobenzamide derivatives have ^{19}F chemical shifts characteristic of this region (anilines, naphthal amines, pyrene amines, etc). One ^{19}F chemical shift region that is significantly more prominent in the Illinois coal spectrum versus the Virigina coal spectrum is a broad ^{19}F envelope centered at -39.05 ppm. Secondary amines contained within a heterocyclic ring exhibit ^{19}F chemical shifts in this region. The ^{19}F spectra for both coals also exhibit a variety of secondary alkyl amine derivatives (-42.00 to -45.00 ppm). One region (45.50-50 ppm) of these ^{19}F NMR

spectra contained ^{19}F resonances that were not characterized in previous model studies (1, 24).

It is also interesting to note that some soluble coal and/or coal derivatives were obtained using this procedure. Support for this may be illustrated in the ^{1}H and ^{13}C NMR spectra for the derivatized Virginia and Illinois No. 6 coals (Figures 2.4 and 2.5). Specifically, the aliphatic ^{1}H NMR spectral region (~1-3.5 ppm) for both derivatized coals, Figure 2.4a and 2.4b, clearly indicate various strong signals. Since neither p-fluorobenzoyl chloride or quinoline contain aliphatic hydrogen, these signals are clearly the result of soluble and/or derivatized coal products. In addition, chloroform was the only organic solvent used in the work-up procedure. Thus, these signals could not have originated from the work-up procedure. The signals at ~ 1-1.5 ppm (Figures 2.4a and 2.4b) are clearly indicative of long chain alkyl carbons. Other prominent signals between 2-3 ppm are characteristic of methyl groups attached to aromatic rings. The aromatic region (~ 6.7-9 ppm) clearly contains signals due to soluble coal fragments as well as the aromatic hydrogen of the p-fluorobenzoyl derivatives. However, as indicated in a recent report by Hellgeth and Taylor (56), the solubility of several components in coal residuum may be enhanced by nitrogen adduction. Because quinoline was the principle solvent used in the coal extraction/ derivatization work, this may also be a possible explanation for the solubility of several components in the mixture.

The ^{13}C spectra for these two coals (Figure 2.5a and 2.5b) also clearly indicate the presence of aromatic and aliphatic carbons. The

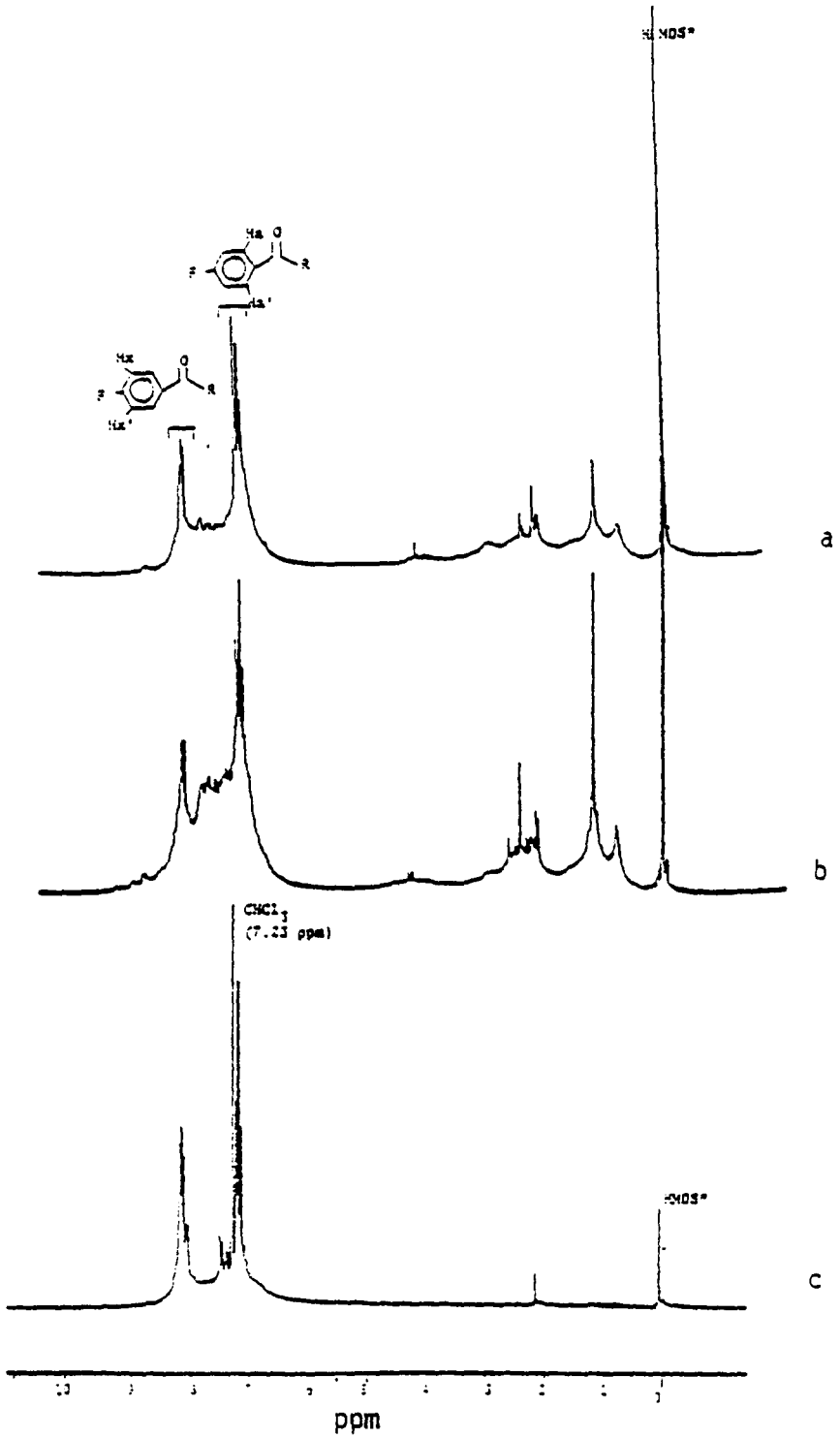

FIGURE 2.4 The 200 MHz ^{1}H NMR spectra for p-fluorobenzoyl derivatives of Illinois #6 coal (a), Western Virginia coal (b), and the control reaction mixture (c).

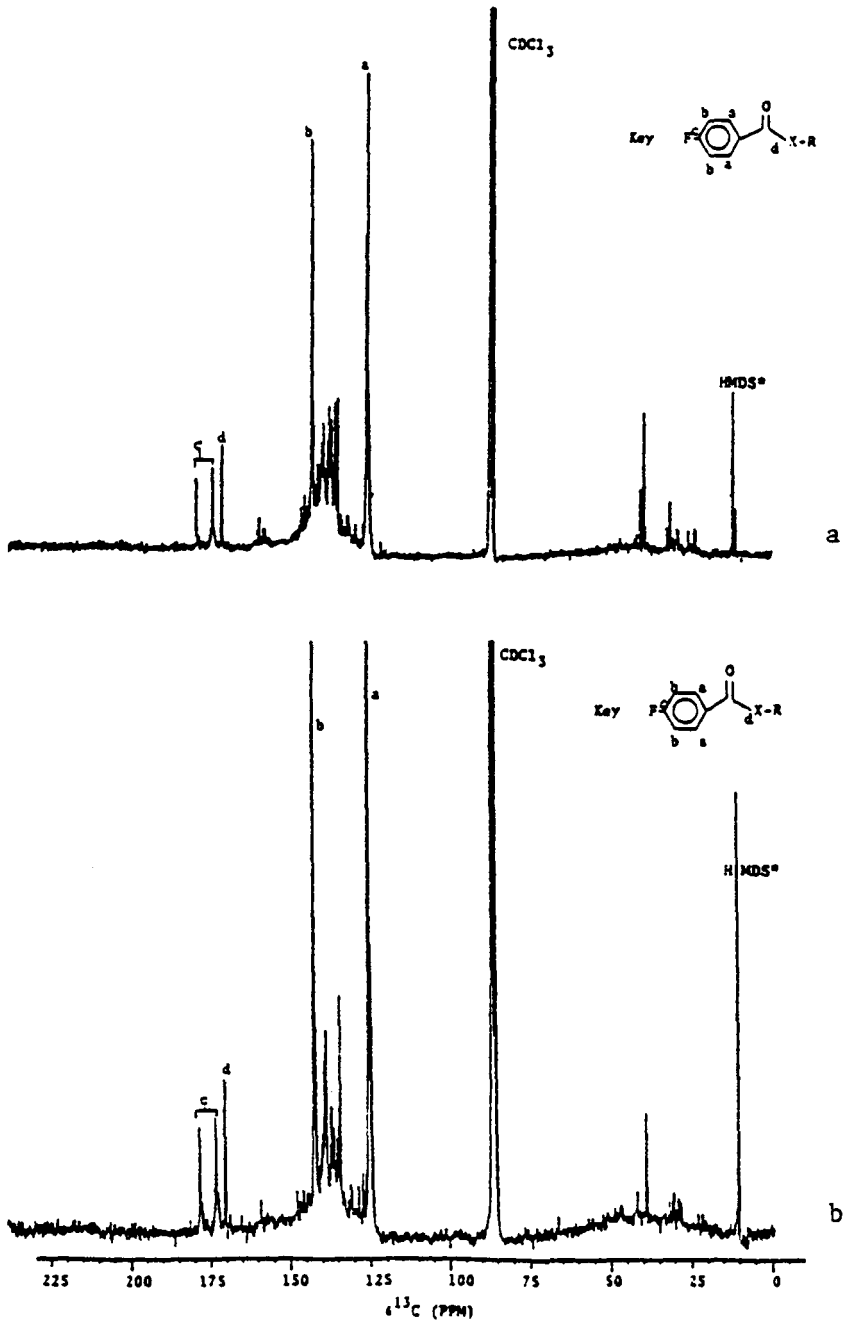

FIGURE 2.5 The 50.1 MHz ^{1}H decoupled ^{13}C NMR spectra for p-fluorobenzoyl derivatives of Illinois #6 coal (a) and Western Virginia coal (b).

^{13}C resonances for the p-fluorobenzoyl derivatives are easily assigned, as indicated. Because a large chemical shift range exists for ^{13}C NMR, there is adequate resolution among many of the ^{13}C aromatic resonances of the coal samples. These ^{13}C chemical shifts closely match those for model compounds (e.g. pyrene, naphthalene, phenanthrene, biphenyl, acenaphthalene, and fluorene).

In Figures 2.6 and 2.7 are shown the expansions of the alkyl regions from the ^{13}C INEPT spectra of the derivatized Illinois and Western Virginia coals. The spectra suggest that compounds similar to acenaphthalene and fluorene are present in these complex mixtures, as noted by the two methylene resonance peaks at 36.7 and 30.2 ppm (Figures 2.6C and 2.7C). A number of methyl ^{13}C resonances are also present in Figure 2.6 and 2.7, which are typical of methyl carbons attached to aromatic systems.

It should also be mentioned that the ^{1}H and ^{13}C spectra for the control reaction are also generally devoid of signals for the spectral regions discussed above. For example, Figure 2.4c is the ^{1}H NMR spectrum for the control reaction mixture. This spectrum clearly shows the lack of signals in the aliphatic region (~ 1-3.5 ppm) and reduced aromatic signals when compared with Figure 2.4 and 2.6. Similar results were also obtained for the ^{19}F spectrum of the control reaction mixture.

Conclusion

The results obtained in this study indicate that whole coals can

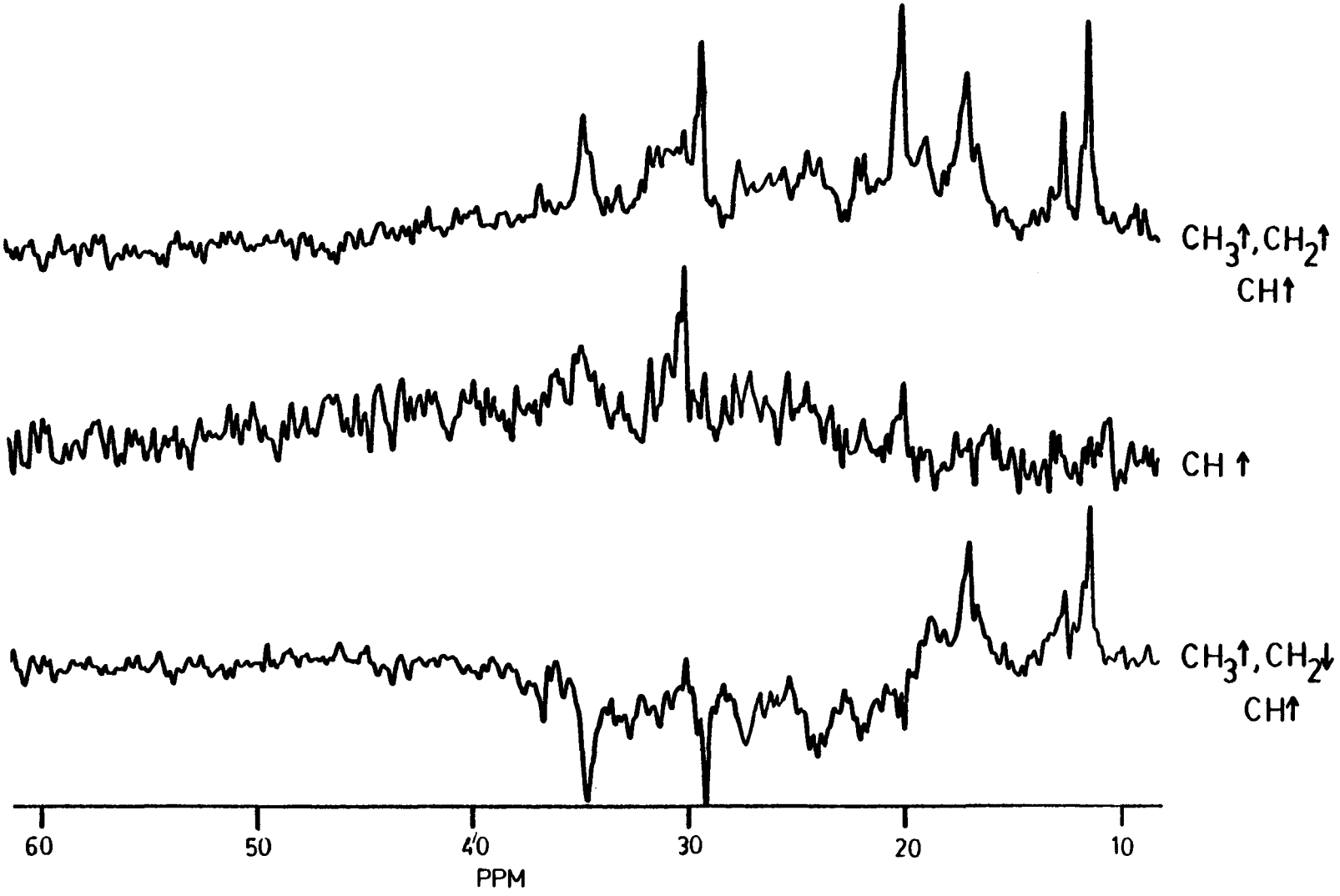

FIGURE 2.6 Expansion of the alkyl region for the 50.1 MHz ^{13}C INEPT spectrum for derivatized Illinois #6 coal.

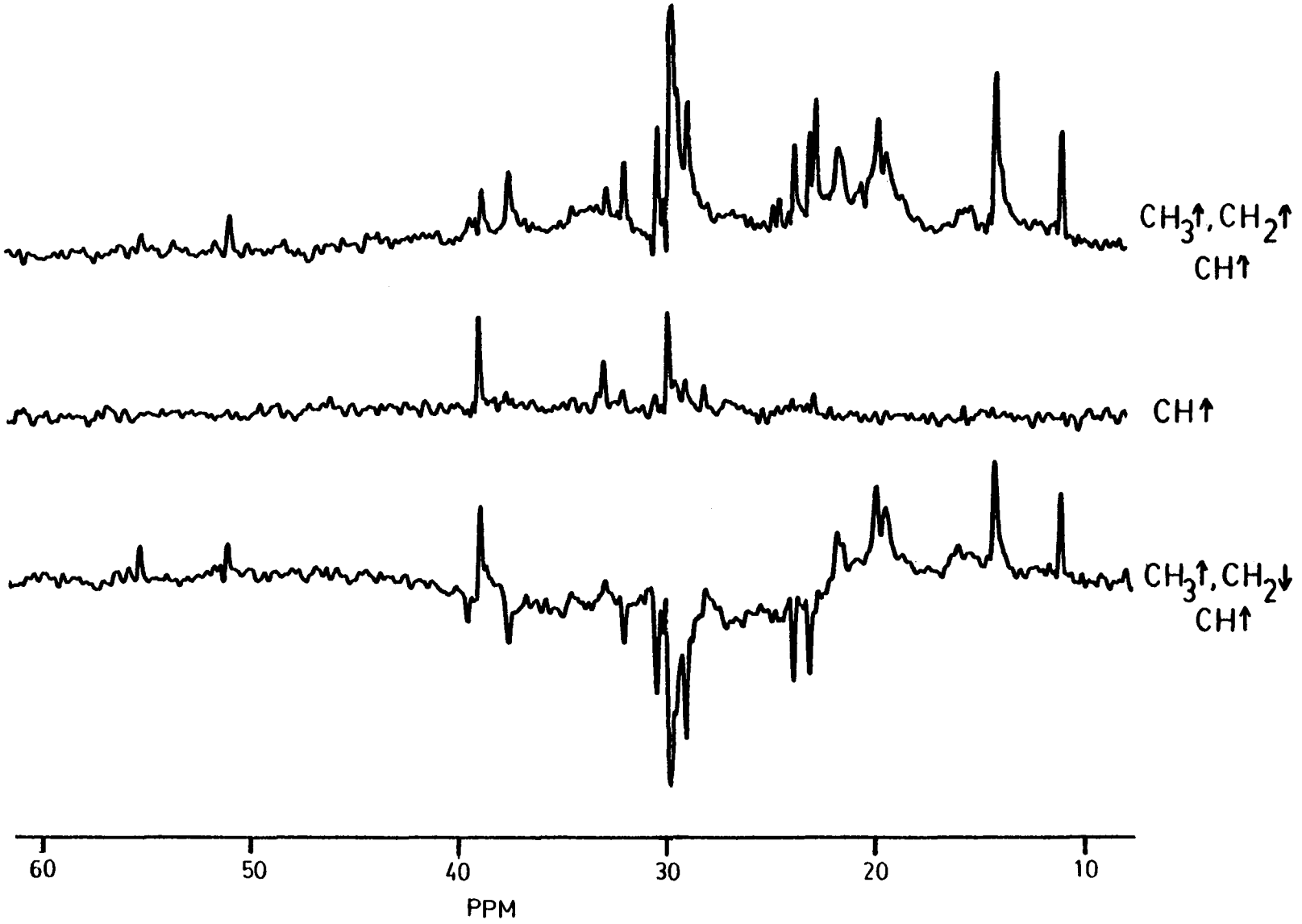

FIGURE 2.7 Expansion of the alkyl region for the 50.1 MHz ^{13}C INEPT spectrum for derivatized Western Virginia coal.

be readily characterized by treatment with a fluorine tagging reagent and subsequently analyzed by ^{19}F NMR. The large ^{19}F chemical shift range for p-fluorobenzoyl derivatives allows easy characterization of a number of phenol, amine, and carboxylic acid groups. The reaction appears to increase the solubility of the coal products. Two mechanisms that may be responsible for the increase in the solubility is: derivatized active hydrogen functional sites (i.e., phenols, carboxylic acids, and amines, etc.) which may alleviate strong hydrogen bonding interactions making the coal products more soluble. Also, adduction of active sites to the nitrogen base may increase solubility. Both mechanisms are consistent with previously reported data (36, 56).

CHAPTER III

CARBON-13 AND FLUORINE-19 NUCLEAR MAGNETIC RESONANCE CHEMICAL SHIFT STUDIES OF CARBON-13 ENRICHED p-FLUOROBENZOYL DERIVATIVES

Dorn and coworkers (24) have reported the use of p-fluorobenzoyl chloride as a ^{19}F NMR tagging reagent for characterizing molecules with active hydrogen functional groups. The base catalyzed reaction of p-fluorobenzoyl chloride has provided a convenient method for ^{19}F NMR analysis of alcohols, phenols, carboxylic acids, amines, and thiols. More recently, the p-fluorobenzoyl chloride reagent has been used to characterize biological systems such as steroids and amino acids (1). In most cases, the p-fluorobenzoyl derivatives provide a simple and usually quantitative method for introducing a fluorine tagging group. An attractive feature of this fluorinating reagent is the large ^{19}F chemical shift range (~10 ppm) for a large number of p-fluorobenzoate derivatives (24) . Furthermore, derivatives for chemical classes (e.g., phenols, alcohols, amines, etc.) have fairly well resolved chemical shift regions. Nevertheless, in more complex mixtures and larger substrates, spectral overlap in the ^{19}F spectrum can still be a problem.

In this chapter another spectral dimension of the p-fluorobenzoyl chloride tagging reagent is discussed. That is, its potential use as a dual tag (e.g., ^{19}F and ^{13}C nuclei). This is accomplished by enriching

the carbonyl carbon to a level of 90% with the ^{13}C isotope. The ^{13}C enriched p-fluorobenzoyl chloride can be synthesized as outlined below:

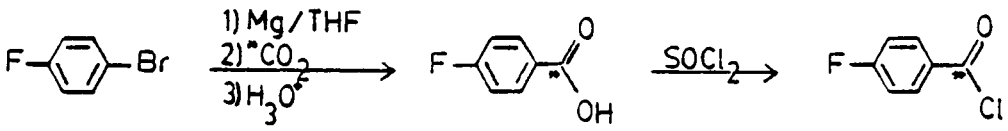

There have been a number of fluorine-19 NMR tagging reagents reported in the literature during the last several years (21, 57-61). However, the ^{13}C-enriched p-fluorobenzoyl chloride reagent is one of the first examples for analysis of molecules containing active hydrogen functional groups. The general reaction is:

In this chapter, we report the ^{13}C and ^{19}F chemical shifts for a limited model study of alcohols, phenols, and amine derivatives.

Experimental

Instrumentation

The ^{13}C and ^{19}F nuclear magnetic resonance (NMR) spectra were obtained utilizing a JEOL FX-200 NMR spectrometer operating at 50.10 and

56.20 MHz, respectively. Experimental details have been discussed in the previous two chapters.

Preparation of ^{13}C-enriched p-fluorobenzoyl chloride

The p-fluorophenyl magnesium bromide was prepared by adding 0.12 mole (2.90 g) of magnesium turnings to a 250 mL flame dried flask surmounted with a condenser, under nitrogen. To this was added 25 mL of anhydrous tetrahydrofuran (THF) (distilled from lithium aluminium hydride) and two to three crystals of I_2. A solution of 50mL of THF and 0.12 mole (21.0g) p-fluorobromobenzene (Aldrich Chem.) was added dropwise to the magnesium turnings via an addition funnel. The Grignard reaction was started with 3-5 mL of the halide solution. After the reaction was initiated, the remaining p-fluorobromobenzene solution was added over a 30 minute period of time with gentle heating . After addition of the halide, the mixture was stirred for 1 hour under nitrogen.

Utilizing a vacuum line apparatus, 90% ^{13}C enriched $^{13}CO_2$ was generated from 0.12 mole (23.68 g) $Ba^{13}CO_3$ by slowly adding 2.4 moles (126 mL) of concentrated H_2SO_4. The liberated $^{13}CO_2$ was condensed immediately into the flask containing the p-fluorophenyl magnesium bromide, which was cooled to -196°C via a liquid nitrogen bath. The flask was then slowly warmed to -60°C via a xylene/liquid nitrogen slurry. The $^{13}CO_2$ was rapidly absorbed by the solution at this temperature. This mixture was stirred at -60°C for 1.5 hours and

slowly warmed to room temperature. The mixture was stirred for an additional three hours.

After stirring, 100 mL of 3N HCL and ice was added to the reaction mixture which immediately formed separated aqueous-oil layers. The oil was extracted from the aqueous layer with three, 200 mL portions of ethyl ether. The solvent was concentrated in vacuo to yield a white solid. This solid was redissolved in ethyl ether and extracted with 200 mL of 1.5N NaOH. The aqueous layer was acidified again with 3N HCL to a pH of 1. A white solid precipitated during the addition of the aqueous HCl. The solid was extracted with three, 100 ml portions of ethyl ether. The solvent was dried over anhydrous $MgSO_4$ and removed in vacuo to yield 14.09 g (83.9% yield) of ^{13}C labelled p-fluorobenzoic acid. The product was used without further purification.

To 100 mL of tetrahydrofuran was added 0.07 mole (10g) of ^{13}C-enriched p-fluorobenzoic acid and 0.091 moles (0.23g) of I_2. To this solution 0.28 moles (21 ml) of thionyl chloride was slowly added under nitrogen. The mixture was stirred under reflux for 15 hours. The product was purified by vacuum distillation (b.p. 88-90° C at 20 mmHg). A yield of 10.2g (90%) of ^{13}C-enriched p-fluorobenzoyl chloride was obtained.

Derivatives of ^{13}C-enriched p-fluorobenzoyl chloride were prepared according to previously described procedures (24).

Results and Discussion

The ^{13}C and ^{19}F chemical shifts for a number of ^{13}C-enriched

derivatives of alcohols, phenols, amines, and carboxylic acids are reported in Table 3.1. The range of ^{13}C chemical shifts for the carbonyl group of the ester, amide, and anhydride derivatives is ~9ppm. Characteristic ^{13}C chemical shift regions were observed for ester, amides, and anhydride derivatives, as illustrated in Figure 3.1. Figure 3.2. illustrates the ^{19}F and ^{13}C spectra for the p-fluorobenzoate derivative of benzyl alcohol. In each case, the ^{19}F and ^{13}C spectra were obtained using twenty accumulations. This Figure illustrates the separate spectral domains (i.e., ^{19}F and ^{13}C spectra) obtainable by this approach.

A crucial problem in complex mixture analysis is chemical shift overlap in both chemical shift domains. Table 3.2 compares the ^{19}F and ^{13}C (carbonyl) chemical shifts for several model systems obtained from Table 3.1. As indicated, the two discrete compounds present in a complex mixture may have approximately the same ^{19}F chemical shifts (n-butylamine, -41.50 ppm and sec-butylamine -41.59 ppm), but in this case they have significantly different ^{13}C (carbonyl) chemical shifts (166.37 and 166.85 ppm, respectively). The converse case is also illustrated, for example, p-methoxy benzyl alcohol and phenethyl alcohol have approximately the same ^{13}C (carbonyl) chemical shifts, but are distinguished by separate ^{19}F chemical shifts.

In summary, from this limited model study, a chemical shift range of ~9 ppm is observed for both ^{19}F and ^{13}C derivatives. The remarkable feature of this data is the fact that ^{19}F chemical shifts are not attenuated relative to the ^{13}C chemical shifts even though the ^{19}F

Table 3.1

^{13}C and ^{19}F Chemical Shift Data for p-Fluorobenzoate Derivatives[24]

Sample	δC^1	δF^2
1-butanol	165.59	-38.86
2-butanol	165.49	-38.65
2-methyl-2-propanol	164.37	-39.69
1-propanol	165.59	-38.81
phenethyl alcohol	165.43	-38.54
benzhydrol	164.44	-37.98
benzyl alcohol	165.35	-38.29
p-methoxybenzyl alcohol	165.44	-38.39
1-octanol	165.15	-39.11
choesterol	164.44	-38.90
n-butylamine	166.37	-41.50
sec-butylamine	166.85	-41.59
diethylamine	170.21	-44.11
n-ethyl-n-butylamine	170.40	-44.16
carbazole	166.85	-40.38
phenol	169.19	-37.23
m-phenylphenol	169.48	-36.90
benzoic acid	161.26	-35.05

1. The ^{13}C chemical shift were internally referenced to the middle peak of chloroform-d and referred in the table to tetramethylsilane by the following relationship, $\delta C = 77.0 + \delta C$ observed.
2. The ^{19}F chemical shift were referenced to 1,2-difluorotetachloroethane
3. Increasing positive δC and δF values denote a decrease in shielding.

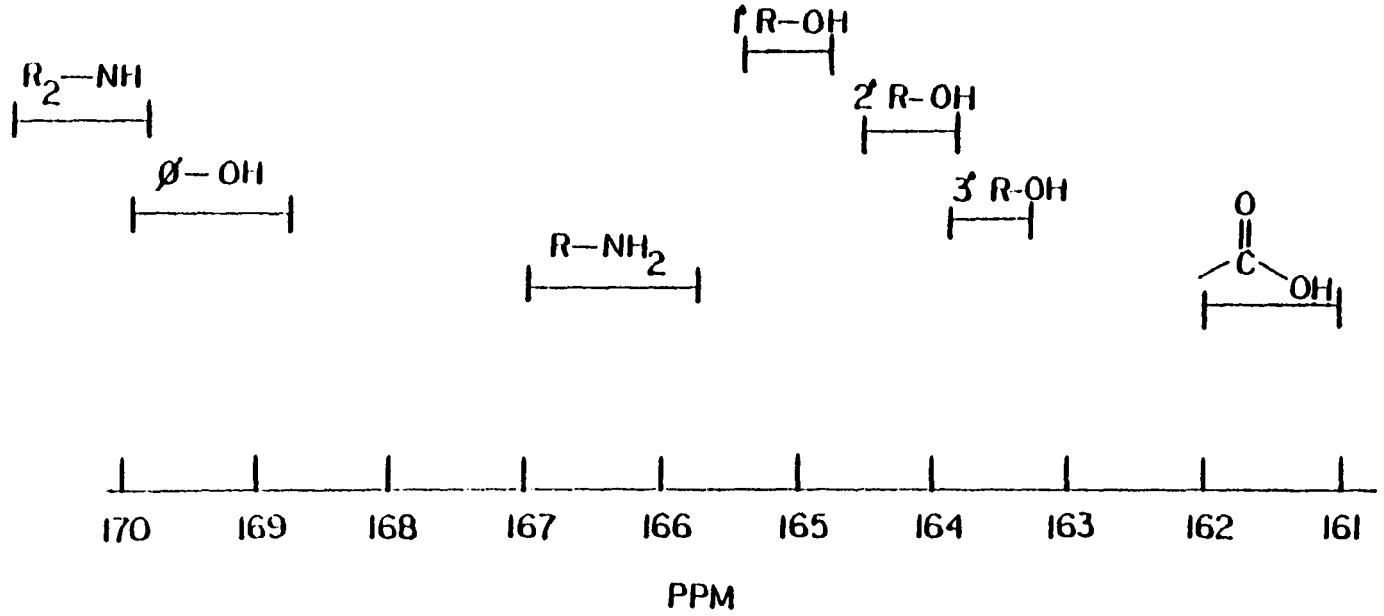

FIGURE 3.1 The range of carbonyl ^{13}C chemical shifts for p-fluorobenzoyl derivatives.

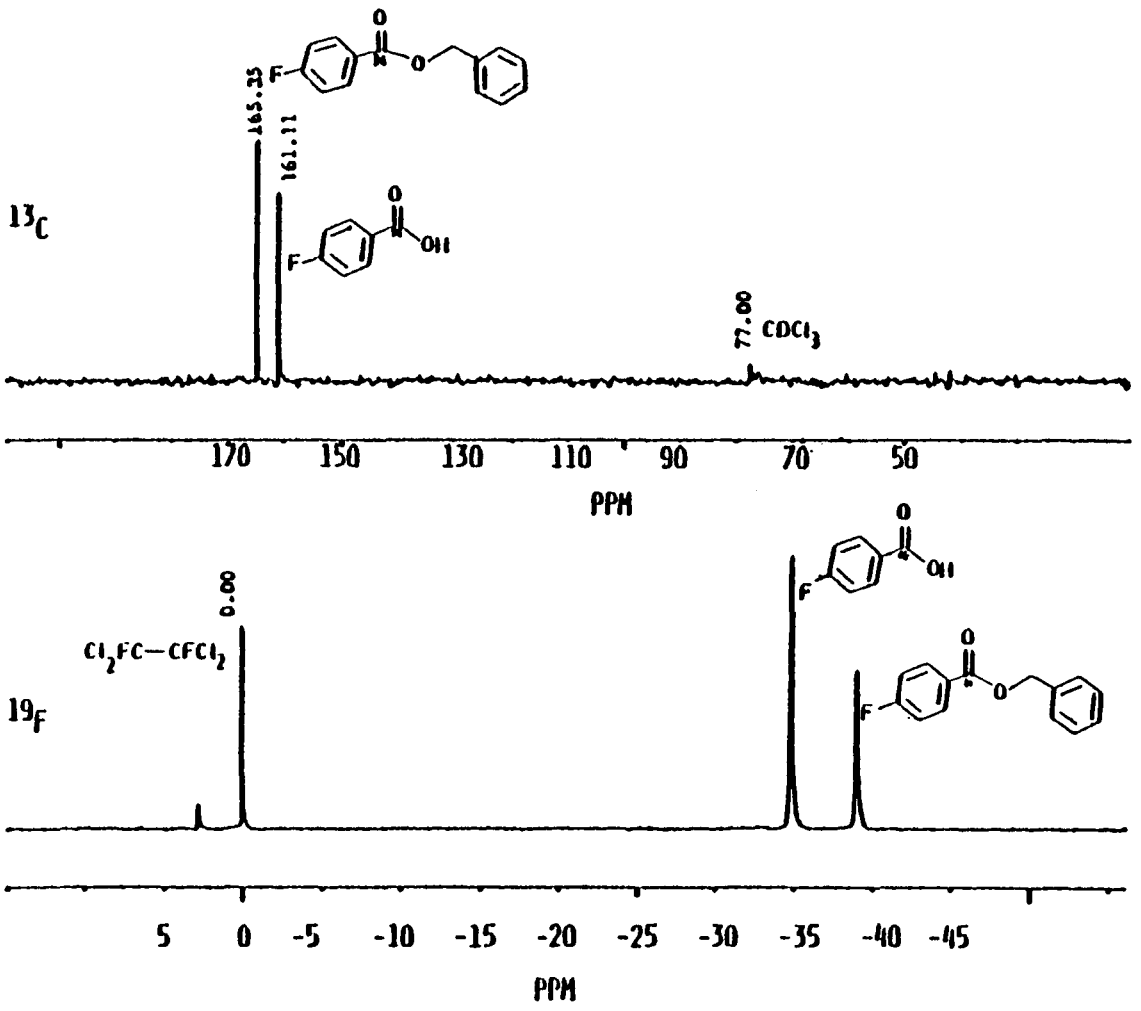

FIGURE 3.2 The decoupled ^{19}F and ^{13}C spectra for the p-fluorobenzoate derivative of benzyl alcohol.

nuclide is 5 more bonds removed from these structural changes. These data reflect the known facile ability for transmission of substituent effects to the para postion (62) in substituted aromatic systems.

Table 3.2

^{13}C and ^{19}F Chemical Shift Comparison Data
for Various p-Fluorobenzoyl Derivatives

Sample	δC^1	diff. (ppm)	δF^1	diff. (ppm)	
n-butanol	165.59		-38.86		^{13}C Chemical Shifts overlap, but ^{19}F Chemical Shifts are different
		0.1		0.21	
iso-butanol	165.49		-38.65		
p-methoxybenzyl alcohol	165.44		-39.39		
		0.01		0.15	
phenethyl alcohol	165.43		-38.54		
n-butylamine	166.37		-41.50		^{19}F Chemical Shifts overlap, but ^{13}C Chemical Shifts are different
		0.48		0.09	
sec-butylamine	166.85		-41.59		
diethylamine	170.21		-44.11		
		0.19		0.05	
n-ethyl-n-butylamine	170.40		-44.16		

1. (See Table 3.1).

CHAPTER IV

ANALYSIS OF ACTIVE HYDROGEN FUNCTIONAL GROUPS IN COMPLEX MIXTURES BY FLOW LIQUID CHROMATOGRAPHY DIRECTLY COUPLED TO FLUORINE-19 NUCLEAR MAGNETIC RESONANCE SPECTROMETRY (LC- ^{19}F NMR)

Introduction

The feasibility of directly coupling a liquid chromatography (LC) system to a proton nuclear magnetic resonance spectrometer (^{1}H NMR) was first demonstrated by Watanabe (63) in 1978. This initial report used a stop-flow system yielding static ^{1}H NMR examination of chromatographic fractions. The first continuous-flow LC-^{1}H NMR experiments were reported by Bayer and co-workers (64) in 1979. These and other preliminary LC-^{1}H NMR studies (63-68) used electromagnetic based spectrometers with detection limits which were on the order of 0.1-1 mg, using 30-s observation times.

Obviously, sensitivity was one of the major disadvantages encountered in using this information rich chromatographic detector. As reported (69-72), detection limits for a 200 MHz superconducting system were approximately 10-20 μg for compounds in the 100-300 dalton range with continuous-flow LC-^{1}H NMR (~30-s observation time). A disadvantage in using the stop-flow technique was the longer experimental time. Methods to improve S/N in LC-NMR are currently being studied by Dorn and co-workers (73, 74) (i.e., improving the receiver coil and sample cell designs). Many of these techniques, and others, have been

discussed in greater detail in a recent review (75).

To date, LC-^{1}H NMR has been used to characterize a variety of complex mixtures such as fuels (68, 70-72), samples of biological interest (69, 76, 77), and analysis of organic reaction mixtures (78). Haw, et. al. (79) demonstrated that quantitative data could easily be obtained from the LC-^{1}H NMR method. LC-^{1}H NMR has also been used as a detector for all the common liquid chromatographic separation modes including size exclusion (71) and reversed-phase (69) systems.

Besides the limited sensitivity of the ^{1}H NMR detector, another potential problem concerns the narrow ^{1}H chemical shift range, approximately 10 ppm. This becomes more important for samples with a wide range of ^{1}H chemical shifts (i.e., typically large molecular systems and/or very complex mixtures). As an example, Haw and coworkers (72) found that normal-phase chromatography of coal conversion recycle solvents allows relatively easy separation and characterization of chemical classes (e.g., monocyclic aromatics and aliphatics). However, identification of each compound in these chemical classes is still sometimes difficult because of overlap in the ^{1}H NMR spectral domain.

For samples that can be easily derivatized with fluorine tagging reagents, monitoring the ^{19}F NMR nuclide has certain advantages. The ^{19}F nucleus is an excellent candidate based on sensitivity considerations and its NMR sensitivity is comparable to the ^{1}H nucleus. In addition, the ^{19}F nucleus is very sensitive to subtle changes in chemical structure as indicated by the large chemical shift range for ^{19}F NMR (400 ppm for a number of compounds). Another important

consideration is that few complex mixtures of interest contain fluorine. This avoids a significant ^{19}F NMR spectral background problem. Also, a wider range of chromatographic and/or NMR-acceptable solvent systems are also possible. For example, reversed-phase LC-^{19}F NMR may be feasible because of the lack of background signals in the ^{19}F NMR spectrum for most reversed phase solvent systems (e.g., water/acetonitrile mixtures). Whereas, commonly used reverse phase solvent systems still have significant ^{1}H NMR signals, even when deuterated solvents are employed (e.g., D_2O-D_3CCN). Even if a fluorinated solvent is used, the ^{19}F background signals due to solvent may be well removed from the chemical shift region of interest.

Prederivatization techniques using ^{19}F tagging reagents have been used successfully in several gas chromatographic studies. Prederivatization of amines by trifluoroacetic anhydride (48) and pentafluoropropionic anhydride (49) have proven useful in identifing amine compounds by gas chromatography/mass spectroscopy (GC-MS). This is necessary because many of the underivatized nitrogen compounds are not resolved by GC due to very similar physical and chemical properties. The derivatized compounds are also more volatile and are therefore more easily studied by GC-MS. In a similar fashion, Cairn et. al (5) quantitatively characterized trifluoroacetate derivatives of hydroxyestrogens in complex mixtures obtained from pregnant mare's urine using GC/MS.

The fluorine tagging reagent used in the present study is p-fluorobenzoyl chloride. Previous studies (1, 24) on simple models,

such as phenols, alcohols, amines, carboxylic acids, and more complex biological compounds have shown that the ^{19}F nucleus for this tagging reagent is sensitive to subtle chemical structural changes among these substrates, as reflected by a 12 ppm chemical shift range. Also, p-fluorobenzoyl derivatives are resistant to hydrolysis and can be separated by normal phase chromatographic modes. One disadvantage of the p-fluorobenzoyl derivatives is the long-range J_{HF} coupling between the fluorine and ring protons which broadens the ^{19}F spectral lines. This problem could be avoided by ^{1}H decoupling and/or deuterium labelling.

Experimental

Two different series of p-fluorobenzoyl derivatized model systems are discussed, p-fluorobenzoates of estrogen sterols and phenols. The preparation of these derivatives, including ^{19}F chemical shift data, have been reported (1, 24).

A Whatman Magnum-9 silica gel-PAC column (250 x 9 mm i.d.) was used for normal phase separations. The PAC column was activated with chloroform-d_1 (99.8% D, Aldrich) and then equilibrated with the appropriate solvent system, this depended upon the model system studied and whether LC-^{1}H NMR or LC-^{19}F NMR results were desired.

The solvent system used to obtain the LC-^{1}H NMR of the derivatized phenol and sterol mixtures was a 50:50 mixture of d-chloroform and Freon-113. A flow rate of 1 mL/min was used for each experiment. The LC-^{19}F NMR profiles were collected using an 80:20 mixture of pentane and chloroform. The two solvent systems have very similar polarity (P^1)

values (80), the polarity of the 50:50 d-chlorofrom/Freon-113 mixture was ~1.00 the polarity of the 80:20 pentane/chloroform mixture was ~0.95. Flow rates of 0.1 mL/min and 0.5 mL/min were used in the LC-^{19}F NMR to separate the derivatized sterol and phenol mixtures, respectively.

Hexamethyldisiloxane (HMDS) was added to the solvent as the chemical shift reference for the LC-^{1}H NMR to make a concentration of 0.01% by volume. Fluorobenzene was used as the ^{19}F NMR chemical shift reference, once again in a concentration of 0.01% by volume. All solvents were degassed before use.

The pump was a Waters M-45 solvent delivery system. A Valco injection valve with a 100 µl sample loop was used throughout. All samples were diluted in the appropriate solvent system to yield 1M solutions. A Laboratory Data Control Model 1107 refractive index (RI) detector was used to obtain initial chromatograms. The NMR flow cell was connected directly to the outlet of the RI detector via a length of a Telfon tubing (i.d. ~1mm), 1.5 meters in length. Effluent was removed from the NMR flow cell through a Telfon tube and into a waste container.

A JEOL FX-200 nuclear magnetic resonance spectrometer equipped with an Oxford 4.7-T superconducting solenoid magnet (54 mm bore) was used to obtain ^{1}H spectra at 199.50 MHz and ^{19}F spectra at 187.7 MHz. A floppy disk system was used for data storage and each diskette had sufficient data storage for 58 (1024 points) LC-NMR files. Acquisition of additional files could be accomplished by exchanging diskettes without interrupting data collection. A transfer time of approximately 3-s

created a short dead time between each file.

Results and Discussion

The two model systems discussed in this chapter were chosen to illustrate how LC-^{19}F NMR can complement the LC-^{1}H NMR approach. In these two circumstances analysis of the mixtures by LC-^{1}H NMR was hindered by ^{1}H NMR spectral and/or chromatographic overlap. The first model set to be discussed is a mixture of three derivatized steroids. The static 200 MHz ^{1}H NMR spectra and structures for these derivatized steroids are presented in Figure 4.1. It is worth noting the complexity of each high resolution ^{1}H spectrum (each spectrum was taken under high resolution conditions with 0.2 Hz spectral resolution), in the alkyl (~0.9-0.30 ppm) and aromatic (~6.9-8.5 ppm) chemical shift region. A notable exception are the ^{1}H signals at approximately 5 ppm, which are characteristic of methine hydrogen atoms attached to carbons bearing the steroid-ester linkage. For the p-fluorobenzoate of estrone this ^{1}H resonance is absent because the derivative is located at the phenolic C-3 site of the steroid. However, for the β-estradiol the methine proton appears as a characteristic triplet at 5.01 ppm. For estriol the two methine resonances representing C-16 and C-17 are deshielded to 5.6 ppm (multiplet) and 5.3 ppm (doublet), respectively.

The flow LC-^{1}H NMR profiles for these derivatives are presented in Figure 4.2. Each proton spectrum is the result of 224 accumulations with an acquisition time of 0.512 sec. It is apparent in this profile that chromatographic separation is not good. The normal refractive

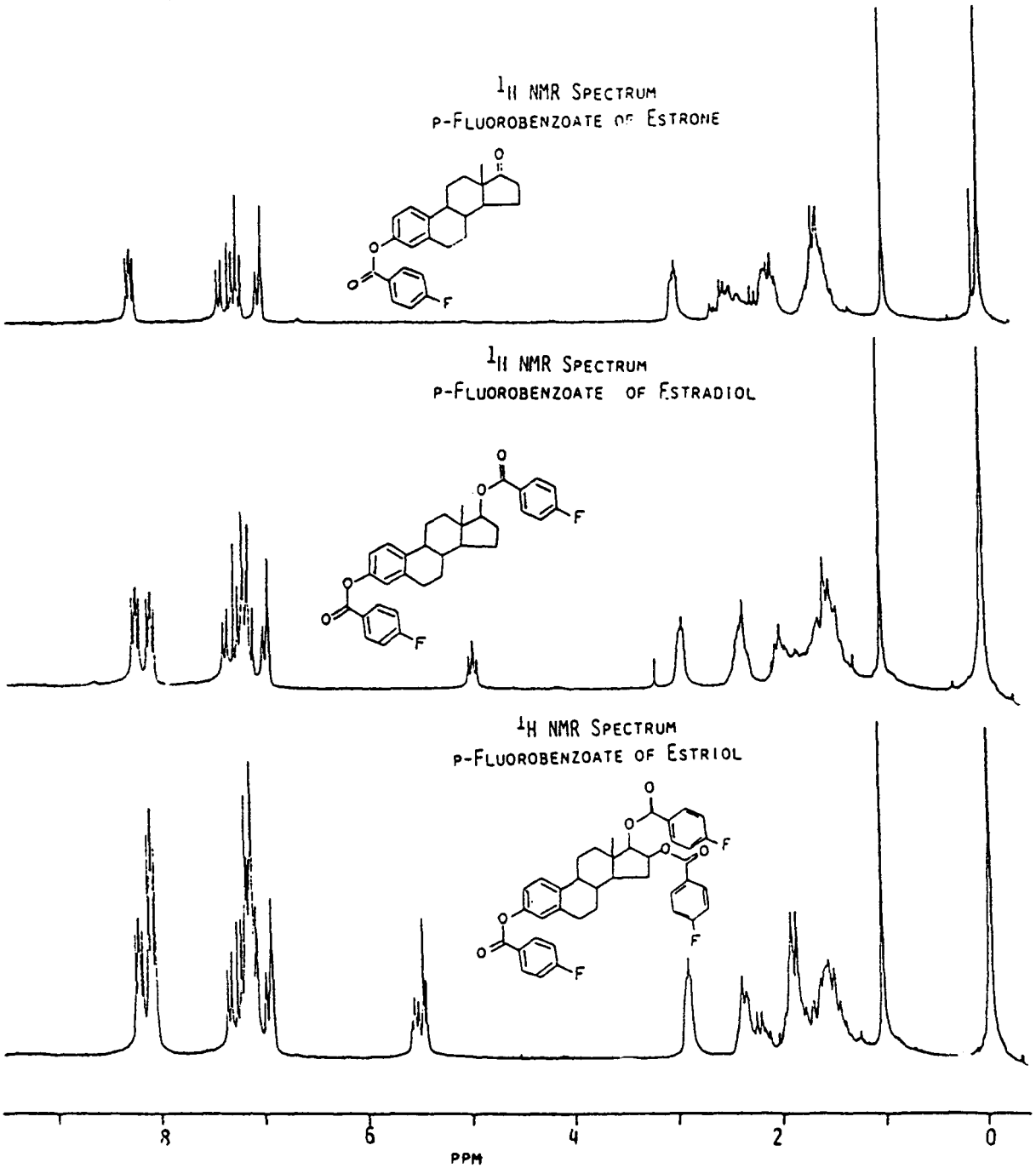

FIGURE 4.1 Static 200-MHz ^{1}H-NMR spectra for the p-fluorobenzoate derivatives of estrone (E_1), estradiol (E_2), and estriol (E_3).

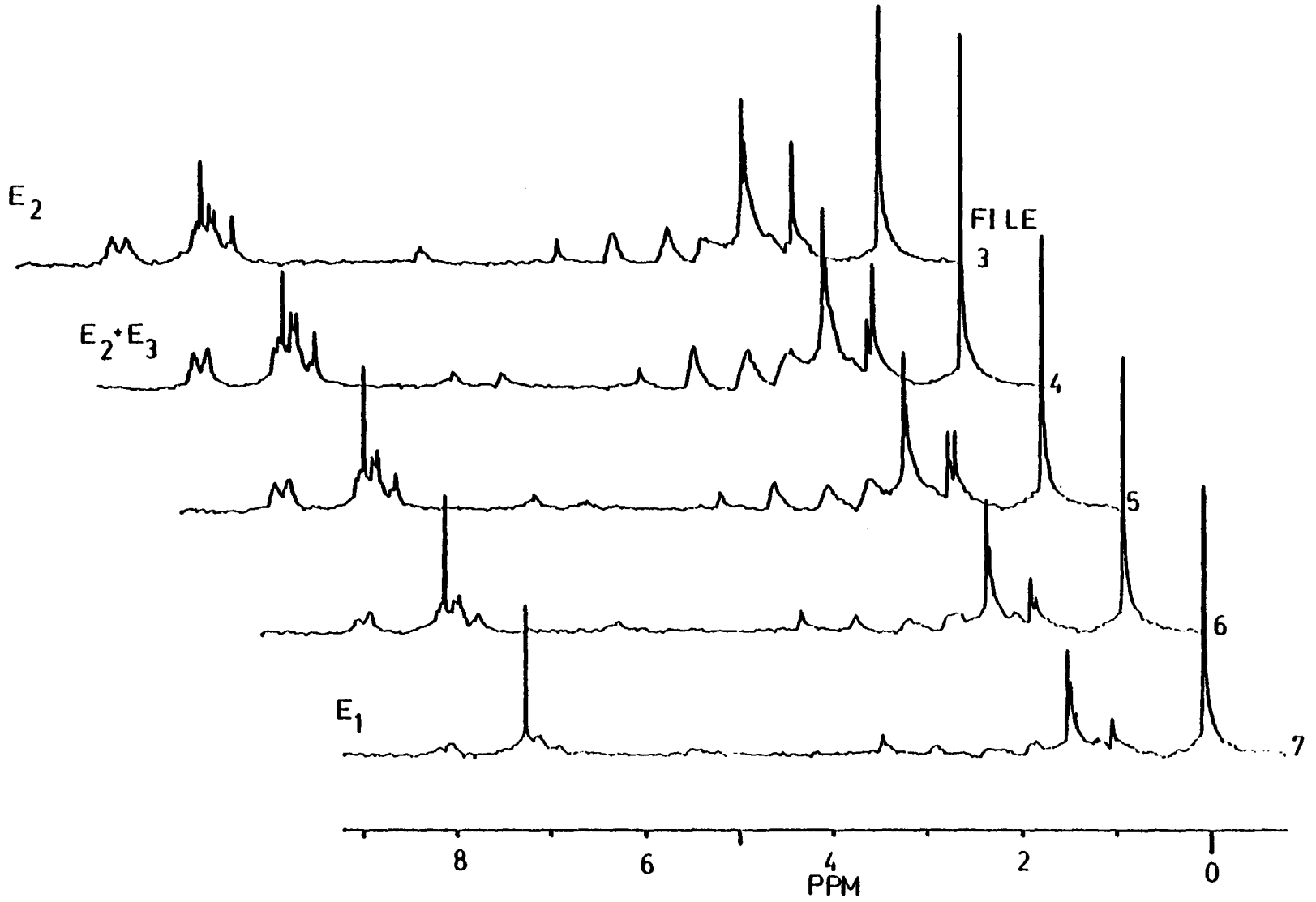

FIGURE 4.2 LC-^{1}H-NMR profiles of steroid derivatives (E_1, E_2, and E_3). Files are 120 s wide. The solvent is a 50:50 mixture of d-chloroform and Freon-113. The chromatographic column is a Whatman Magnum - 9 PAC column with a flow rate of 1 ml/min.

index (RI) trace obtained for this mixture indicates no significant chromatographic separation of the three compounds and appears as one broad envelope with a retention time of several minutes. Yet it is interesting to note that, at least, some separation is detected in the LC-^{1}H NMR profile. Clearly the β-estradiol p-fluorobenzoate derivative (E_2) is the first component to elute in file 3. This is indicated by the broad resonance centered at ~5.01 ppm characteristic of the C-17 methine proton, vida supra. Estriol (E_3) begins to coelute with β-estradiol in file 4 and continues to elute over files 5 and 6, as indicated by the ^{1}H resonance at ~5.3 ppm. Estrone (E_1) may begin to elute as early as file 6, but clearly is eluting in file 7.

For this model system, the chromatographic separation is very poor and considerable ^{1}H chemical shift overlap occurs in the LC-^{1}H NMR profiles. One method attempted to improve chromatographic resolution was to change solvent systems. By changing the solvent system from 50:50 d-chloroform/freon 113 to 80:20 pentane/chloroform we hoped to retain solvent systems of comparable polarity, but which would have different separation selectives for the components in the model mixture. Little improvement in chromatographic resolution was observed due to changing solvents. However, from Table 4.1 notice that these same steroid p-fluorobenzoates can be easily characterized on the basis of one, two, or three ^{19}F resonances in the ^{19}F NMR chemical shift domain. Hence, in sharp contrast to the LC-^{1}H NMR profile, the LC-^{19}F NMR profile (Figure 4.3) of these derivatized steriods indicates that the ^{19}F chemical shifts are clearly separated. Each ^{19}F spectrum is the

Table 4.1

^{19}F NMR Chemcial Shifts For p-Fluorobenzoate Derivatives Relative to Fluorobenzene

p-Fluorobenzoate Derivative	δF Relative to Fluorobenzene
phenol	8.12
o-tertbutylphenol	8.24
9-phenanthrol	8.84
β-naphthol	8.29
Estrone	8.16
β-Estradiol	C(3) 8.16
	C(17) 8.68
Estriol	C(3) 8.21
	C(16) 7.41
	C(17) 7.25

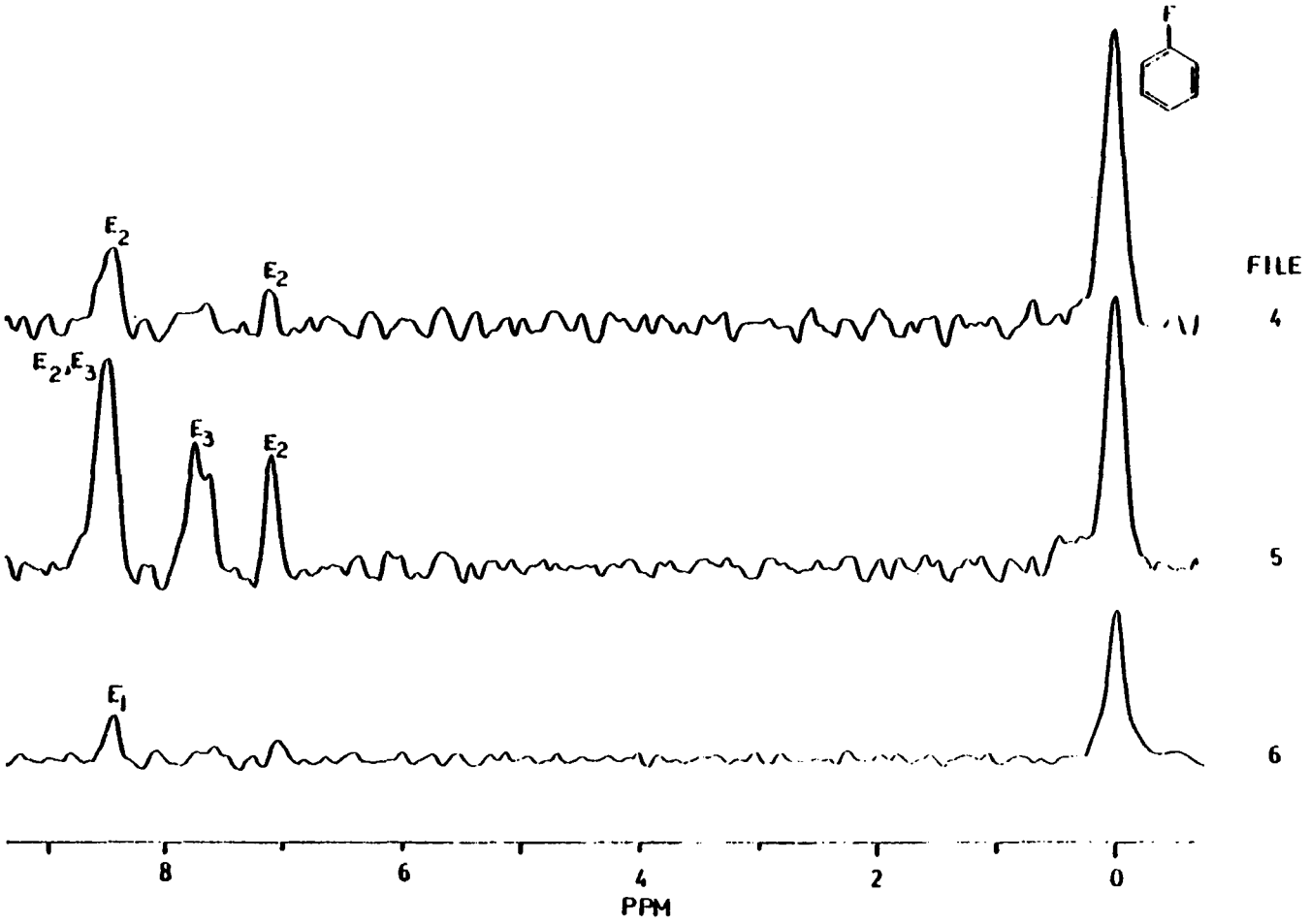

FIGURE 4.3 LC-^{19}F-NMR profile of steroid derivatives (E_1, E_2, and E_3). Files are 120 s wide. The internal reference is fluorobenzene. The solvent is an 80:20 mixture of pentane:chloroform. The chromatographic column is a Whatman Magnum-9 PAC column with a flow rate of 0.1 ml/min. Resolution (~30 Hz) is degraded because of J_{HF} coupling and excessive exponential apodization of the free induction decay.

result of 169 accumulations with 0.6820 s acquisition time.

A second series of models, p-fluorobenzoate phenol derivatives, illustrate again how LC-^{19}F NMR may be used to complement LC-^{1}H NMR. In this case the chromatographic separation between the four components of the model mixture (composed of phenol, β-naphthol, 9-phenanthrol, and ortho-tertbutyl phenol) is somewhat better. However, the LC-^{1}H NMR profile, (Figure 4.4) is difficult to interpret due to the complex aromatic chemical shift region. The only phenol that is positively identified is o-tertbutylphenol, with a characteristic signal for the methyl resonance at 1.2 ppm. As indicated in Table 4.1, the phenols are characterized by their respective ^{19}F resonances. Using LC-^{19}F NMR the compounds are easily identified as they elute from the column by a single ^{19}F resonance (Figure 4.5).

There is one problem, however, in using p-fluorobenzoyl chloride as the fluorine derivatizing reagent for LC-^{19}F NMR; that is, the protons on the aromatic ring, ortho and meta to the fluorine test nuclide reduce its intensity by extensive J_{HF} spin coupling. The ^{19}F coupled spectrum (Figure 4.6) for a single nuclide shows a nine line multiplet over 30 Hz wide. The results presented in each LC-^{19}F NMR profile are the results of extensive exponential apodization of the corresponding free induction decay (FID) and line widths at half height are approximately 30 Hz. The addition of a ^{1}H decoupling channel should make the LC-^{19}F NMR technique a more useful qualitative detector. However, quantitation could still be difficult with the ^{1}H decoupled technique due to intensity

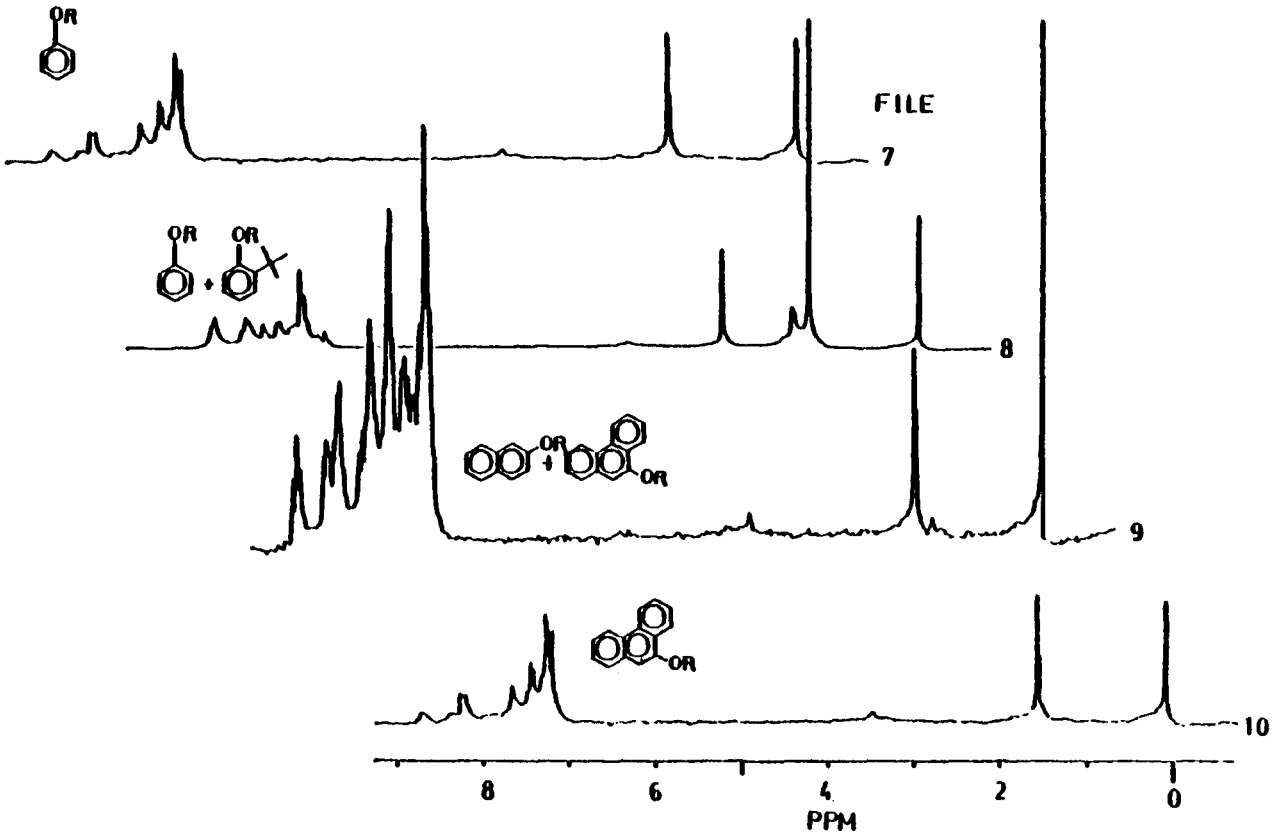

FIGURE 4.4 LC-^{1}H-NMR profiles of phenol derivatives (i.e. phenol, napthol, o-tertbutyl phenol, and 9-phenantherol). Files are 120 s wide. The same chromatographic solvent and file widths as in Figure 5.2 are used.

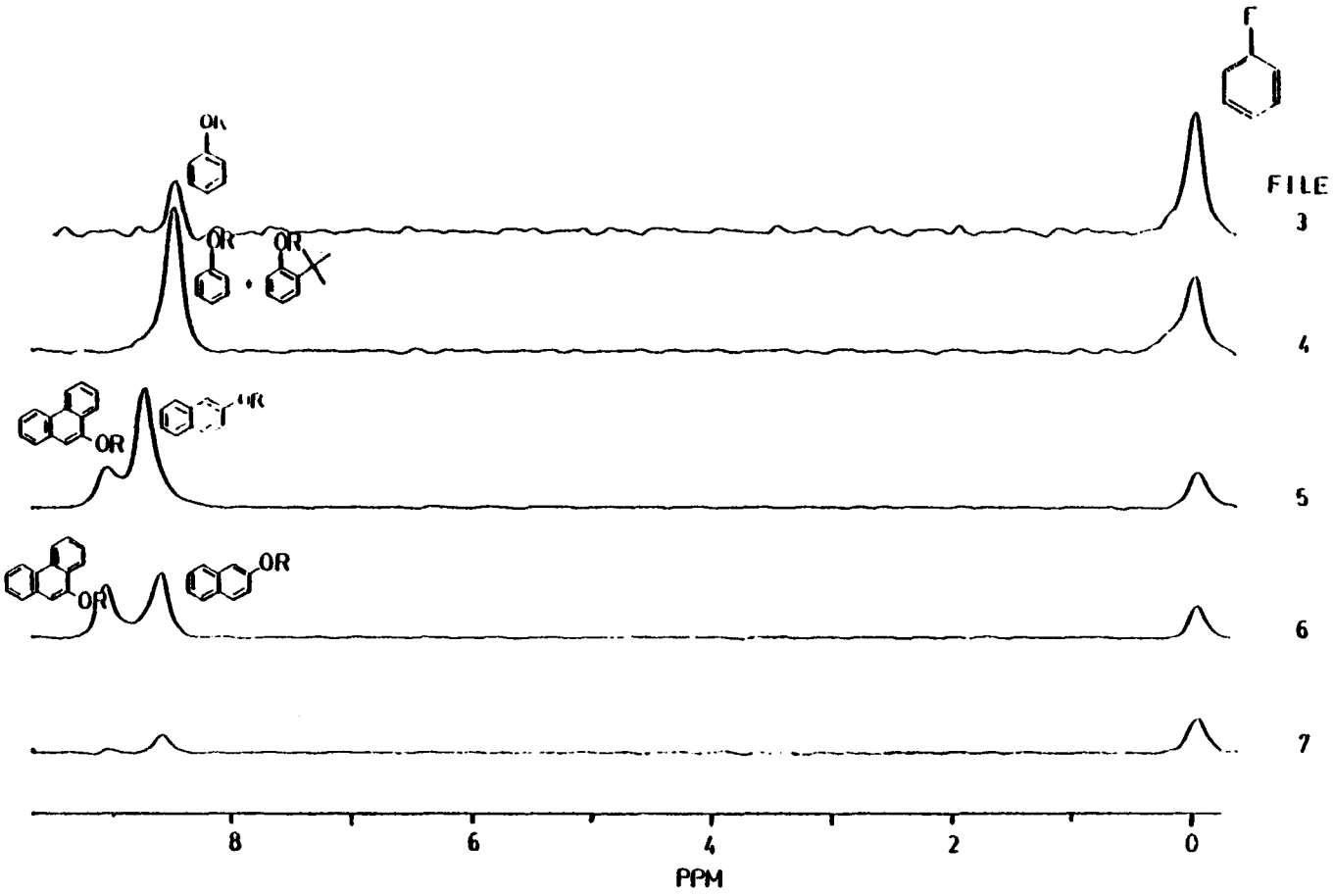

FIGURE 4.5 LC-^{19}F-NMR profile of phenol p-fluorobenzoates. Files are 100 s wide. The internal reference is fluorobenzene. The solvent is an 80:20 mixture of pentane:chloroform. The chromatographic column is a Whatman Magnum-9 PAC column with a flow rate of 0.5 ml/min.

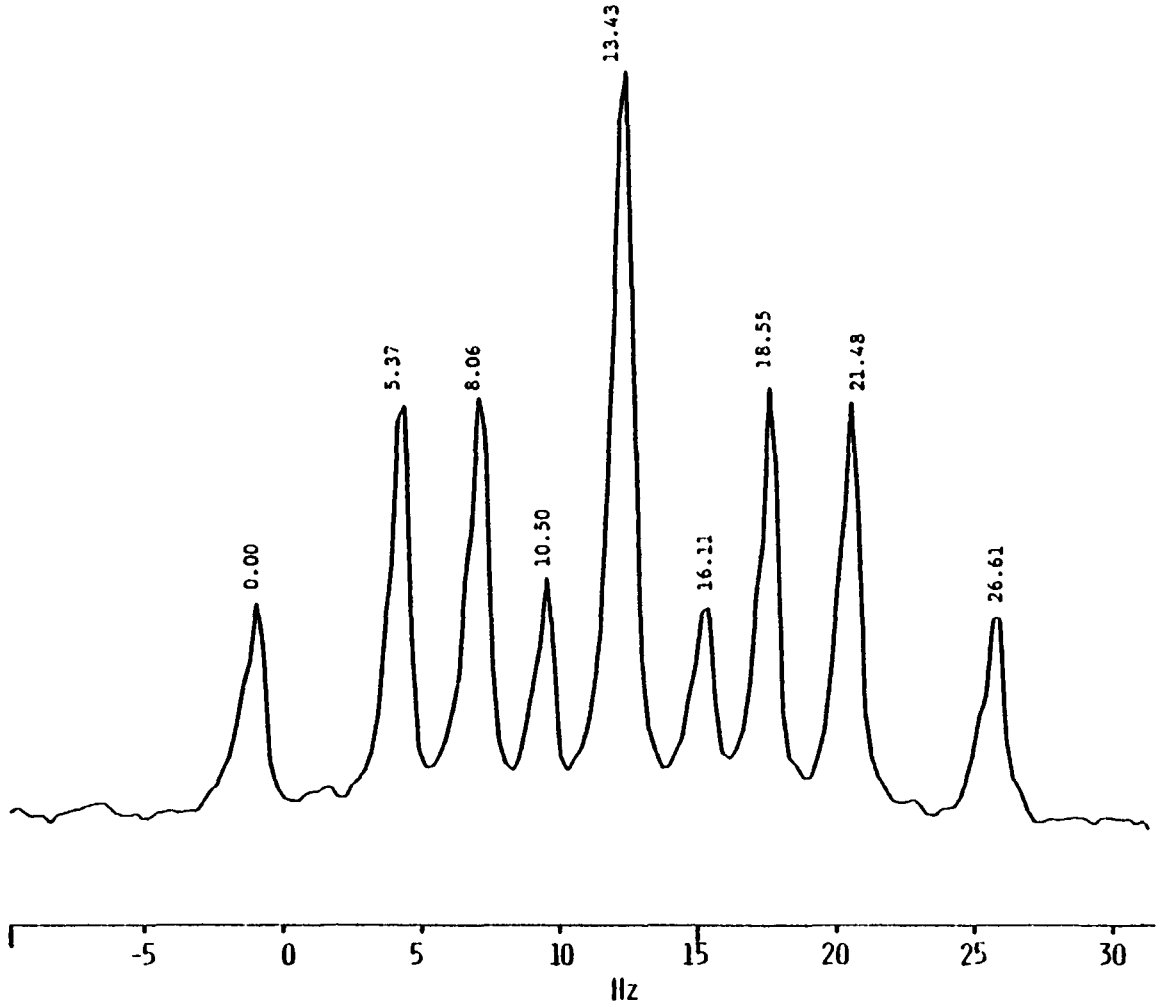

FIGURE 4.6 A typical multiplet for the ^{19}F nucleus of a p-fluorobenzoyl derivative due to ^{1}H-^{19}F spin coupling.

variations arising from different nuclear Overhauser effects.

Conclusions

This study has shown potential advantages of LC-^{19}F NMR for the analysis of complex molecules containing active hydrogen functional groups. In tandem with LC-^{1}H NMR, LC-^{19}F NMR provides another dimension in analyzing complex mixtures. By utilizing a ^{19}F derivatizing reagent one may initially analyze a number of functional groups (e.g., amines, thiols, carboxylic acids, hydroxyl groups, etc.) by LC-^{19}F NMR. The LC-^{1}H NMR profiles could then be used to provide a "finger print" for each type of chemical species with or without derivatization. The study has also shown that if the prederivatizing reagent contains ^{19}F nuclei then $^{n}J_{HF}$ coupling with neighboring protons reduces the effectiveness of the technique (i.e., sensitivity and spectral resolution) unless ^{1}H decoupling is employed.

CHATPER V

STUDIES OF SOLIDS USING CP/MAS NMR AND FLUORINE TAGGING REAGENTS

Introduction

The first half of this dissertation has dealt with characterization and applications of the fluorine tagging reagent, p-fluorobenzoyl chloride, in high resolution solution state NMR studies. It proved to be an effective tool for analysis of complex mixtures with molecules containing active hydrogen functional groups. This chapter emphasizes the role fluorine tagging reagents may play in analyzing solid systems. Fluorine tagging reagents will be used to derivatize acidic hydrogen sites in solid systems, with the derivatized solid then being analyzed by solid state NMR. Unlike the solution ^{19}F NMR studies where the substrates were characterized by isotropic chemical shifts in well defined ^{19}F chemical shift regions, the fluorine-tag will now be used to broaden solid state spectra of dilute nuclear spin systems (e.g. ^{13}C, ^{29}Si...).

An important broadening mechanism in solid state NMR is dipolar interactions between spin-1/2 nuclei (i.e. ^{1}H and ^{13}C). Dipolar coupling between ^{1}H and ^{13}C nuclei can be significantly reduced or even eliminated by using cross polarization/ magic angle spinning (CP/MAS) techniques, combined with high power proton decoupling. However, other spin-1/2 nuclei (e.g., ^{19}F or ^{31}P) with high natural abundance that may be present present in the solid system, can also contribute to line

broadening of the observed nucleus.

The purpose of this study is to show how dipolar line broadening may be advantageously used to analyze functional groups in solid systems. As discussed in previous chapters, solids that contain active hydrogen functional groups (e.g. amines, hydroxyls, or thiols) are derivatized with a fluorine containing reagent. It is expected that NMR resonances for those nuclei in the immediate proximity of the fluorine derivative will be broadened due to the ^{13}C-^{19}F dipole-dipole interactions. These studies are designed only to demonstrate the magnitude of the fluorine-carbon (or silicon) dipolar coupling. The dipolar coupling may include contributions from both intra-and/or intermolecular coupling interactions, as revealed by the broadening of ^{13}C resonances in simple model systems.

In this section nuclear spin interactions which broaden solid state spectra and fundamental techniques that are generally used to obtain solid state NMR spectra, will be briefly reviewed. Also, a review pertaining to the study of solid systems containing adsorbed or covalently bonded substrates, as studied by solid state NMR, is presented. In these investigations many characteristics of the solid system were obtained from chemical shift anisotropy, quadrupole and dipole interactions, and relaxation studies of the guest molecules with the solid.

5.1 Nuclear Spin Interactions in the Solid State - Sources of Line Broadening.

Several excellent monographs and reviews are now available which

cover both theoretical aspects of solid state NMR spectrsocopy and many specific applications in detail (81-90). Although the reference list is not exhaustive, it does provide a sound basis for those interested in the subject matter. Therefore, the material discussed here is not a comprehensive treatment of nuclear spin interactions in solids, but is intended to highlight those concepts utilized in studying the problem addressed in this chapter.

The general Hamiltonian for the principle interactions experienced by a nucleus with a magnetic moment (μ) and spin = I in the solid state is written as follows:

$$H = H_Z + H_D + H_{CS} + H_{SC} + H_Q \qquad (1)$$

where each Hamilitonian is defined as:

H_Z - The Zeeman interaction with the magnetic field

H_D - Direct dipole-dipole interactions with other nuclei

H_{CS} - Magnetic shielding of surrounding nuclei, yielding chemical shifts

H_{SC} - Spin-spin coupling (scalar couplings) to other nuclei

H_Q - Quadrupolar interactions which occur for nuclei with spin I > 1/2

Table 5.1 (85) compares the relative magnitudes of the individual interactions for the case of a ^{13}C spin in a 1.4 T field, in both solid and solution NMR. As indicated, high-resolution spectra are obtained for solution NMR because the rapid motion of molecules in solution effectively averages the dipolar and quadrupolar interactions to zero. In a similar manner the chemical shift interaction is also averaged to a single "isotropic" value. This leaves only the Zeeman and scalar

Table 5.1

^{13}C Nuclear Spin Interactions in a 1.4 Tesla Magnetic Field (85).

Hamiltonian	H_{Zeeman}	$H_{Dipolar}$	H_{Scalar}	$H_{Chemical\ Shift}$	$H_{Dipolar}$ from quadrupolar nucleus
Magnitude in Solution	15.1 MHz	0 kHz	~200 Hz	σ isotropic	0
Magnitude in Solids	15.1 MHz	~50 kHz	~200 Hz	up to 3 kHz	up to 1 MHz
		Removed by dipolar decoupling	Removed by scalar decoupling	Reduced to σ (isotropic) by magic angle spinning	Reduced, but may not be completely removed by magic angle spinning

coupling terms to significantly influence spectral line-broadening. In contrast, the relatively rigid order found for molecules in the solid state gives an orientation dependence to these NMR interactions. The decrease in molecular motion of the molecules in the solid lattice increases the effects of these interactions by several orders of magnitude (91).

5.1.1 Zeeman Interactions- H_Z

The Zeeman interaction occurs for all nuclei with odd atomic mass or odd atomic number (92). In a magnetic field $\vec{H}_0$ the normally degenerate magnetic spin energy levels become nondegenerate giving 2I + 1 energy levels (where I is the nuclear spin quantum number). These energy levels are separated by:

$$\nu = \frac{\gamma H_0}{2\pi} \qquad (2)$$

where γ is the magnetogyric ratio, ν is the Larmor precession frequency, and H_0 is the static magnetic field strength. Note that the higher the static magnetic field strength, the greater the separation of the energy levels. Hence, at higher fields, the greater energy difference between the quantized energy levels yields a corresponding increase in the spin population difference between them, improving the S/N (signal/noise ratio) of the spectrum. The interaction is linear with respect to the applied magnetic field and is given by the expression:

$$H_Z = -\gamma_I h \vec{H}_0 \vec{I}_Z = -g_N \beta_N \vec{H}_0 \vec{I}_Z \qquad (3)$$

where γ is the magnetogyric ratio, g_N the nuclear g factor, and β_N the Bohr magneton of the nucleus. Table 5.1 shows that the Zeeman interaction for a ^{13}C nucleus in a 1.4 Tesla magnetic field (~15.1 MHz) is, by far, the strongest interaction of the spin system. The magnitude of the largest of the other interactions is less than 1% as large as the Zeeman effect.

5.1.2 Scalar Coupling Interactions - H_{SC}

The Hamiltonian for the scalar interaction between a pair of spins $\vec{I}$ and $\vec{S}$ is given in equation 4

$$H_{CS} = \vec{I} \cdot \hat{J} \cdot \vec{S} \qquad (4)$$

where $\hat{J}$ is the second-rank coupling tensor (~200 Hz), as shown in Table 5.1 (85). This interaction is field independent and is generally several orders of magnitude smaller than the other line broadening interactions. Theory indicates scalar coupling arises from indirect spin-spin coupling between two spins due to their electronic interactions. This coupling occurs because a bonding electron spin tends to associate with the spin of a neighboring nucleus. The scalar interaction is exhibited in the NMR spectrum as J-coupling. J-coupling is routinely used in solution NMR for conformational analysis. However, it is rarely observed in solid state NMR because high power proton decoupling fields are used to reduce dipolar interactions and eliminate any scalar coupling, although in certain circumstances J-coupling has been used to determine the dynamics of guest molecules inclathrated into solid host lattices (94). The power required to decouple scalar

interactions is approximately 10 times less than that required to decouple dipolar interactions (95).

5.1.3 Dipole-Dipole Interactions - H_D

Dipolar interactions are a consequence of direct, through-space magnetic coupling between nuclei (96). The dipolar broadening may result from two sources: coupling of two nuclei with like spin (homonuclear dipolar coupling) or coupling between nuclei with unlike spins (heteronuclear dipolar coupling).

For a solid containing two unlike spins I and S the heteronuclear interaction can be written as:

$$H_{IS} = \frac{\delta_I \delta_S}{r^3} h^2 \vec{I} \bullet D \bullet \vec{S} \qquad (5)$$

where r is the distance between I and S (86-90). Each spin has components (Ix, Iy, Iz) and (Sx, Sy, Sz). In addition, D is the dipolar coupling terms given by:

$$D = \frac{1}{r^2} \begin{vmatrix} (r^2-3x^2) & -3xy & -3xz \\ -3xy & (r^2-3y^2) & -3yz \\ -3xz & -3yz & (r^2-3z^2) \end{vmatrix} \qquad (6)$$

in a Cartasian coordinate system. If r lies along z it is easily shown that the trace is zero and off-diagonal elements are zero. It is useful to cast Equation (5) in terms of a polar coordinate system and this equation can then be decomposed into six terms as follows:

$$H_{IS} = \frac{\delta_I \delta_S}{r^3} h^2 (A + B + C + D + E + F) \qquad (7)$$

where $A = \vec{I}_Z \vec{S}_Z (1-3 \cos^2 \phi IS)$ and expressions for the other terms (B-F) are found in standard texts (81, 86-90). Each of the other terms contain a spin factor and a geometric factor. However, the other terms (B-F) do not commute with a Zeeman operator. Therefore, the A term is the only one which influences the energy (to the 1st order) of an isolated two spin system.

Three major points may be inferred concerning equations 6 and 7:
1) For solution NMR, where molecules are tumbling rapidly, all angles θ are sampled. Therefore, averaging the $(1-3 \cos^2 \phi_{IS})$ term or $< 1-3 \cos^2 \phi_{IS}>$ is equal to zero and the interaction $H_{IS} = 0$.
2) The term $<1-3 \cos^2 \phi_{IS}>$ also vanishes if the angle ϕ_{IS} 54.7°. This has extremely important implications for solid state NMR studies where the rigidity of the sample does not permit an average isotropic value to be attained and the dipolar couplings produce broad signals. Mechanically spinning the sample at an angle 54.7° to the magnetic field H_o can reduce dipolar broadening.
3) Finally, the distance dependence term (r^{-3}) of the dipolar interaction indicates that only directly-bonded nuclei or nuclei in the immediate proximity of the perturbing dipole will be broadened. The magnitude of the r^{-3} dependence has been calculated by Lin and Ward (3) for ^{13}C-^{19}F dipolar interactions. For r=1Å the dipolar interaction is greater than 5.6×10^4 Hz but is only 8.8×10^2 Hz if r=4Å.

The Hamiltonian for the homonuclear dipolar interactions H_{II} and H_{SS} between two like spins are analogous to the heteronuclear

expression

$$H_{II} = \sum_{IS} \vec{I}_I \cdot \hat{D}_{II} \cdot \vec{I} \qquad (8)$$

$$H_{II} = \frac{\gamma I \gamma I}{r^3} h^2 (A + B + C + D + E + F) \qquad (9)$$

The magnitude of the dipolar interaction depends on the magnitude of the magnetic moments as reflected by the magnetogyric ratio (see eqn. 7 and 9). Therefore, the magnitude of the interaction is more important for spin 1/2 nuclei with large magnetic moments such as ^{1}H or ^{19}F. Homonuclear dipolar coupling is not as pronounced for nuclei such as ^{13}C, ^{29}Si, ^{15}N, ^{195}Pt, ^{199}Hg, etc. by virtue of the smaller magnetic moments and/or low natural abundance.

5.2 Narrowing the NMR Spectra of Solids

Aside from the Zeeman interaction in solids systems the other four anisotropic interactions may be reduced or eliminated by a number of experimental techniques. Rapidly spinning the solid sample at the magic angle, magic angle spinning (MAS), can reduce all the line broadening interactions discussed (97, 98). However, direct heteronuclear dipolar interactions are generally removed by high power decoupling (99), which also removes the isotropic and anisotropic parts of the scalar coupling interactions. Homonuclear dipolar interactions may be reduced by various pulse sequences such as the WAHUHA sequence (100). The three techniques are discussed in more detail below.

5.2.1. Magic Angle Spinning

Independently, Lowe (101) and Andrew (102, 103) have shown that manipulation of dipolar and chemical shift spin interactions could easily be achieved by rotating a sample about an axis which is tilted by an angle θ with respect to the magnetic field H_0. The angle, $\theta = 54°$ 44' 8" or ($\tan \theta = \sqrt{2}$), is called the magic angle. At this angle the second rank tensor interactions which generally dominate NMR anisotropies are averaged to zero. Pines found that intermediate effects would be observed if the angle θ deviated even slightly from the magic angle (104). Note, in each case, that only the trace of the second rank tensor interaction remains. Therefore, tensor interactions which have zero trace, like dipole-dipole interactions vanish, while the nonzero trace for chemical shift anisotropies remain, yielding the measureable isotropic chemical shift quantity.

5.2.2 Spinning Rates and Spinning Sidebands

In polycrystalline samples where all angles of θ are sampled, the trace of the second rank tensor for the anisotropic terms will not be zero. The broadening due to these interactions may be reduced by MAS, but they will not be completely removed (100, 105). The anisotropic interactions are attenuated by the presence of molecular motion, being zero for isotropic motion, as in solution. Therefore, mechanically rotating the whole sample, (maximum speeds of ~8K Hz have been reported for modified Andrew and Lowe rotors (106-109)) while not approaching the

frequency of molecular motions, does reduce the broadening considerably. The power of the MAS technique has been illustrated by a number of studies (110-114). Two of the more interesting studies are the investigation of $K^+PF_6^-$and $K^+AsF_6^-$(110, 111) using solid state ^{19}F MAS NMR spectroscopy. Static ^{19}F NMR spectra for the two compounds showed a broad resonance of ~15 KHz. The same spectra accumulated under MAS conditions showed sufficient resolution to observe the doublet for scalar J_{PF} coupling (743 Hz) for the PF_6^- ion and a quartet for the J_{AsF} coupling. The quartet arises because arsenic is a quadrupolar nuclei with (I=3/2, 100% natural abundance). In these examples the homonuclear and quadrupolar interactions were small enough to be efficiently attenuated by MAS. Furthermore, isotropic chemical shift differences and scalar coupling were large enough to allow chemical shift and coupling constant data to be determined from the two ^{19}F spectra.

Typically, MAS rates are in the range of 2-5 kHz for most commerical instruments. These spinning rates are not adequate to efficiently eliminate dipolar proton-carbon interactions which are 10-40 kHz. Therefore, when the spinning frequency is less than the frequency spread of the interaction being removed, sidebands result (115). Characteristically, the isotropic central peak of the sideband is not narrowed as the spinning rate is increased, and the sideband spectrum intensities roughly "map out" the envelope of the static spectrum. The appearance of sidebands leads to a loss in spectra sensitivity and confusion in assigning spectra. Typically, these sidebands can be removed by using pulse sequences developed to cancel the rotational

echoes. Two of which are the Phase Adjustment Pulse Sequence (PASS) (116) and Total Supression of Sideband Sequence (TOSS) (117).

For the 1.4 Tesla electromagnet used in this study MAS can efficiently reduce the chemical shift anisotropy interaction which may be as large as 3 kHz, (Table 5.1). Spinning rates used in these experiments were typically 2 kHz. These spinning rates are also sufficient to remove the dipolar interactions of nuclei with small magnetogyric ratios (e.g. ^{13}C). The ^{13}C-^{13}C dipolar interactions may be considered negligible because the low natural abundance (1.1%) of the ^{13}C isotope reduces the probability that two ^{13}C nuclei would be close enough to give homonuclear dipolar interactions of significant magnitude (i.e. recall that the dipolar interaction has the $1/r^3$ dependance). However, the most efficient technique to remove dipolar interaction is by high power decoupling, as discussed below.

5.2.3. Dipolar Decoupling and Heteronuclear Dipolar Interactions

Decoupling is a double resonance technique involving two radio frequency (r.f.) sources (100). One r.f. (H_1) source is used to perturb signals of the nucleus being studied. The other r.f. source (H_2), strongly irradiates the entire chemical shift range of the nucleus being decoupled (broad-band decoupling). Irradiation by the H_2 field effectively saturates the Zeeman splitting of the decoupled nucleus.

In the samples under investigation, there are two major sources of heterogenous dipolar broadening interactions due to coupling between ^{13}C-^{1}H and ^{13}C-^{19}F. The magnitude of the dipolar coupling will be

similar because the ^{1}H and ^{19}F nuclei each have 100% natural abundance and similar magnetogyric ratios, $\gamma_{^{1}H}$ = 12.83 MHz/Tesla and $\gamma_{^{19}F}$ = 11.93 MHz/Tesla, respectively, in a 1.4 Tesla magnetic field.

The magnitude of dipolar couplings in solids may be as high as 50 kHz (Table 5.1). These interactions can easily be removed by a high power (H_2) r.f. field. Typical proton decoupling field strengths require 100 watts of power (118). In principle one should be able to decouple ^{13}C-^{19}F dipolar interactions in a manner similar to ^{13}C-^{1}H decoupling. However, Yannoni and co-workers (119, 120) have indicated there is significant experimental difficulty in removing the heteronuclear (C-F) dipolar broadening. The problem arises from the width of the ^{19}F chemical shift range. As stated earlier, effective dipolar decoupling requires that the decoupling field be of sufficient strength so that all spins causing dipolar broadening experience the effective H_2 field. This is easily achieved for the proton case due to its small chemical shift range and small shielding anisotropies. However, the ^{19}F chemical shift range is twenty times greater than the ^{1}H range. The result is that larger decoupling fields are needed to remove ^{13}C-^{19}F dipolar interactions. To illustrate this point, in a 1.4 Tesla magnetic field, Yannoni and co-workers (119) found the nonaxial ^{19}F powder pattern for poly(tetrafluoroethylene) to be ~8 kHz. The ^{1}H powder pattern for the protonated analogue, polyethylene, was ~270 Hz. The ^{13}C CP/MAS, ^{1}H decoupled spectrum for polyethylene gave ^{13}C signals of ~5 Hz at (35-40 kHz) decoupling power. In sharp contrast the ^{13}C

linewidths for poly(tetrafluoroethylene) were 50-70 Hz in the ^{13}C CP/MAS ^{19}F decoupled spectrum using the same decoupling power.

5.3. Effects of Long Relaxation Times in Sensitivity of ^{13}C Spectra

One factor which contributes to the difficulty of obtaining a solid-state C-13 spectrum is long spin-lattice relaxation times (T_1) (the rate at which carbon magnetization is reestablished along $\vec{H}_0$ after application of a 90° H_1 pulse). Low natural abundance of the ^{13}C isotope (1.1%) dictates that numerous accumulations must be taken to attain a reasonable signal/noise (S/N) ratio. However, relaxation times of carbons in different chemical environments may range from milliseconds to hundreds of seconds. Thus, with a pulse delay of $2T_1$'s between accumulations, one ^{13}C spectrum could require days to acquire. The next section will briefly review the general relaxation characteristics of ^{13}C-nuclei in the solid state experiment.

5.3.1. General Characteristics of Relaxation Times

Three types of relaxation times are invariably discussed in NMR (121):

a) T_1 (spin lattice relaxation time) characteristic of the first order relaxation process by which perturbed nuclear spins return to equilibrium with their surroundings (the lattice). In the rotating coordinate system it is indicative of the relaxation of the magnetization M_z component back to the z or H_0-axis, (vida supra).

b) T_2-(spin-spin relaxation time) accounts for the process by which spins come to equilbrium with each other. In the rotating coordinate system the M_{xy} component of the magnetization decays with a time characterized by T_2.

c) $T_{1\rho}$ (T_1 in the rotating frame) during the spin lock experiment in the rotating frame, H_1 plays the role of the fixed field. Thus, the magnetization vector M tends to relax in the the direction of H_1 (normally along the y axis), which is analogous to spin-lattice relaxation. This relaxation is called $T_{1\rho}$. For most liquids $T_{1\rho} \approx T_2$.

The common factor between each of these relaxation times is their dependence on the correlation time of the molecular motion and the magnitude of the relaxation mechanism. (e.g. dipole-dipole, quadrupole, CSA, scalar coupling, etc.). These relaxation mechanisms (87) are the same interactions which serve to broaden solid state spectra. The relaxation rate for each mechanism may be written (122) as,

$$R_{im} = \frac{1}{T_{im}} = E_c^2 \, f_{im} \, (\tau_c) \qquad (10)$$

or if more then one mechanism is involved

$$R_{im} = \frac{1}{T_i(obs)} = \sum_m \frac{1}{T_{im}} \qquad (11)$$

where E_c is the magnitude of the specific relaxation interaction and f_{im} (τ_c) is determined by the molecular motion. The notation (im) describes the relaxation time (T_1, T_2) and the corresponding relaxation mechanism.

5.3.2 Spin Diffusion in Solid Systems

The previous discussion of $T_1(^1H)$ relaxation in a solid system was based on the assumption that the ^{13}C nuclei were coupled to "static" or rigid proton magnetic moments. In reality the proton magnetic moments

are a rapidly fluctuating dynamic system. These fluctuations are the result of rapid simultaneous transitions of dipolar-coupled protons having antiparallel moments (83). The interaction can be described in classical terms (88). Consider a dipole with a moment ($\vec{\mu}_1$) that precesses around a magnetic field ($\vec{H}_0$) at its Larmor frequency. The dipole then possesses a static component along the field, $\vec{H}o$, and a rotating component in a plane perpendicular to the field. The static component of $\vec{\mu}_1$ can then generate a small field at the site of another dipole ($\vec{\mu}_2$) oriented relative to $\vec{H}o$. The physical explanation is that a strong coupling between the spins leads to frequent "flip-flops" between them, causing a random but rapid modulation of the local field reducing the efficiency of interactions that broaden spectral linewidths. This process, known as spin diffusion, is characteristic of coupled nuclei with the same precession frequency. It does not imply physical movement of the nuclei, as is the case for diffusion processes in solution-state NMR.

The diffusion rate (k_{HH}) is roughly equal to the homogeneous proton line width ($\Delta\nu_{HH}$)$\approx(\pi T_2)^{-1}$. For organic molecules $\Delta\nu_{HH}$ is typically 10-50kHz. More importantly, in solid state ^{13}C NMR, the proton spin state will fluctuate at this rate and average the ^{13}C-^{1}H interaction to

$$\Delta\nu_{CH} \quad (\Delta\nu_{CH}/\Delta\nu_{HH}) \tag{12}$$

Since $\Delta\nu_{HH} > \Delta\nu_{CH}$ for most organic solids, the ^{13}C line width is reduced.

In relation to this work the ^{19}F nucleus should be just as efficient in relaxing the ^{13}C-nuclei by spin diffusion since $\Delta\nu_{FF} > \Delta\nu_{CF}$. Abragam

and Kambe (123) have shown that ^{19}F spin-diffusion can efficiently inter act with neighboring inorganic nuclei. Using second moment analysis, they found that linewidths for KF (^{39}K) and AgF (^{109}Ag) were reduced by a factor of 0.12 for width at half height, due to ^{19}F spin diffusion. Spin diffusion is also important when considering the cross-polarization (CP) phenomena. Cross-polarization is a double resonance technique which allows the ^{13}C and ^{1}H (or ^{19}F) nuclei to interact while processing at the same frequency in the rotating frame (124).

5.4. Cross Polarization - Spin Temperature

Spin temperature is a concept often used in nuclear magnetism to illustrate the transfer of magnetization from an abundant spin reservoir (^{1}H nuclei) to a rare spin reservoir (e.g., the ^{13}C nuclei). The relative populations of the two spins are given as,

$$N^{1}_{H} \gg N^{13}C \qquad (13)$$

where N is the number of spins (88, 125, 126). Each spin system is coupled to a common lattice with spin-lattice relaxation times of $T_1(^{1}H)$ and $T_1(^{13}C)$ respectively, and by the cross relaxation time $T_{1_H 13_C}$.

Once the organic solid is placed in the magnetic field $\vec{H}o$, the proton spins quickly (<100μs) reach internal equilibrium within the field by spin diffusion. This is approximately equal to T_2 since $\Delta\nu_{HH}\ (\approx T_2)^{-1}$. The proton spins in a sense, make up a thermal reservoir with a temperature T_H, and their Zeeman spin levels are populated according to a Boltzmann distribution. After several $T_1(^{1}H)$'s the protons reach thermal

equilibrium with the lattice with temperature T_L. At this point the proton magnetization expression may be written as

$$M_o(^1H) = \frac{C_H H_o}{T_L} \tag{14}$$

which is the high temperature approximation of Curies' Law, where C_H is the Curie constant.

$$C_H = \frac{N_H \gamma_H^2 \hbar^2}{4k} \tag{15}$$

In a similar manner, the carbon magnetization may be written as

$$M_o(^{13}C) = \frac{C_{13_C} Ho}{T_{13_C}} \tag{16}$$

where the Curie constant for ^{13}C is,

$$C_{13_C} = \frac{N_{13_C} \gamma^2_{13_C} \hbar^2}{4k} \tag{17}$$

where h and k are the Plank and Boltzmann constants, respectively. Because $M_o(^1H)$ is large, compared to $M_o(^{13}C)$, $T_L = T_H$ must be small. Therefore the proton spins constitute a "low temperature" reservoir. Conversely, $M_o(^{13}C)$ being small implies T_{13_C} is large, constituting a a "hot" ^{13}C spin system.

The two spin reservoirs are brought together by irradiating the carbon magnetization (on resonance) during the first part of the proton spin lock period then adjusting the field amplitude so that

$$\frac{\gamma_{13_C}}{2\pi} H_1(^{13}C) = \frac{\gamma_{^1H}}{2\pi} H_1(^1H) \tag{18}$$

While "matched" at the same frequency the ^{13}C and ^1H dipole moments

interact by heteronuclear spin diffusion with a cross relaxation time of T_{CH} which is usually much shorter than $T_1(^{13}C)$. The ^1H and ^{13}C spin reservoirs come to equilibrium at a constant spin temperature. Therefore, since the carbon reservoir temperature (Tc) has been lowered by,

$$Tc = T_H = T_L \frac{H_1(^1H)}{H_0} \tag{19}$$

there is a corresponding rise in the magnitude of $M_0(^{13}C)$. The M_0 (^{13}C) is enhanced roughly by a factor of four.

5.4.1 Cross Polarization - Hartmann - Hahn Condition for Double Resonances

The Hartmann-Hahn condition (86, 127) for the ^1H-^{13}C system can be easily derived from equation 18, that is

$$\frac{H_1(^1H)}{H(^{13}C)} = \frac{\gamma(^1H)}{\gamma(^{13}C)} \tag{20}$$

This is the result of an observation by Hartman and Hahn (128) who found that magnetic fields have negligible effects on nuclei unless the alternating H_1 frequency is close to the precession frequency. That is, given two alternating fields, for the general case $H_1(I)$ and $H_1(S)$, at precession frequencies ω_I and ω_S, resonance conditions for I and S are

$$\begin{aligned} \omega_I &= \gamma_I H_1 \ (I) \\ \omega_S &= \gamma_S H_1 \ (S) \end{aligned} \tag{21}$$

There is little interaction between the two spin systems since they

precess at different frequencies. However, equation 21 implies that the precession frequencies may be matched by adjusting the respective H_1 fields or

$$\gamma_I H_1(I) = w_I = w_S = \gamma_S H_1(S) \qquad (22)$$

which reduces to equation 20. Instrumentally, one approaches the Hartmann-Hahn match for ^{13}C by simply adjusting the H_1 field control to achieve maximum signal intensity on a standard hexamethylbenzene sample.

5.4.2 Cross Polarization - The Procedure

Spin interactions using the cross polarization technique were reviewed briefly in the previous section (124). The physical characteristics of the pulse sequence will now be discussed. Figure 5.1 illustrates the single-contact time (CP) experiment which was used throughout the course of this work. The figure can roughly be divided into four general regions.

The first region is the preparation of the I spins (i.e. ^1H). During the "preparation" period the I spins equilibrate in the magnetic field $\vec{H}o$ by spin-lattice relaxation. This occurs before the first pulse is initiated (e.g. placing the sample in the magnetic field) and generally requires a time period of $5T_1(I)$'s. Other techniques that have been used to polarize the I spins are optical (129, 130) or microwave (131, 132) polarization. I spins may also be polarized using quadrupolar nuclei which have short spin-lattice relaxation times (133, 134).

The next region in Figure 5.1 is the "hold" period. In this step a 90° pulse is applied to the proton magnetization by $H_1(I)$ followed by a

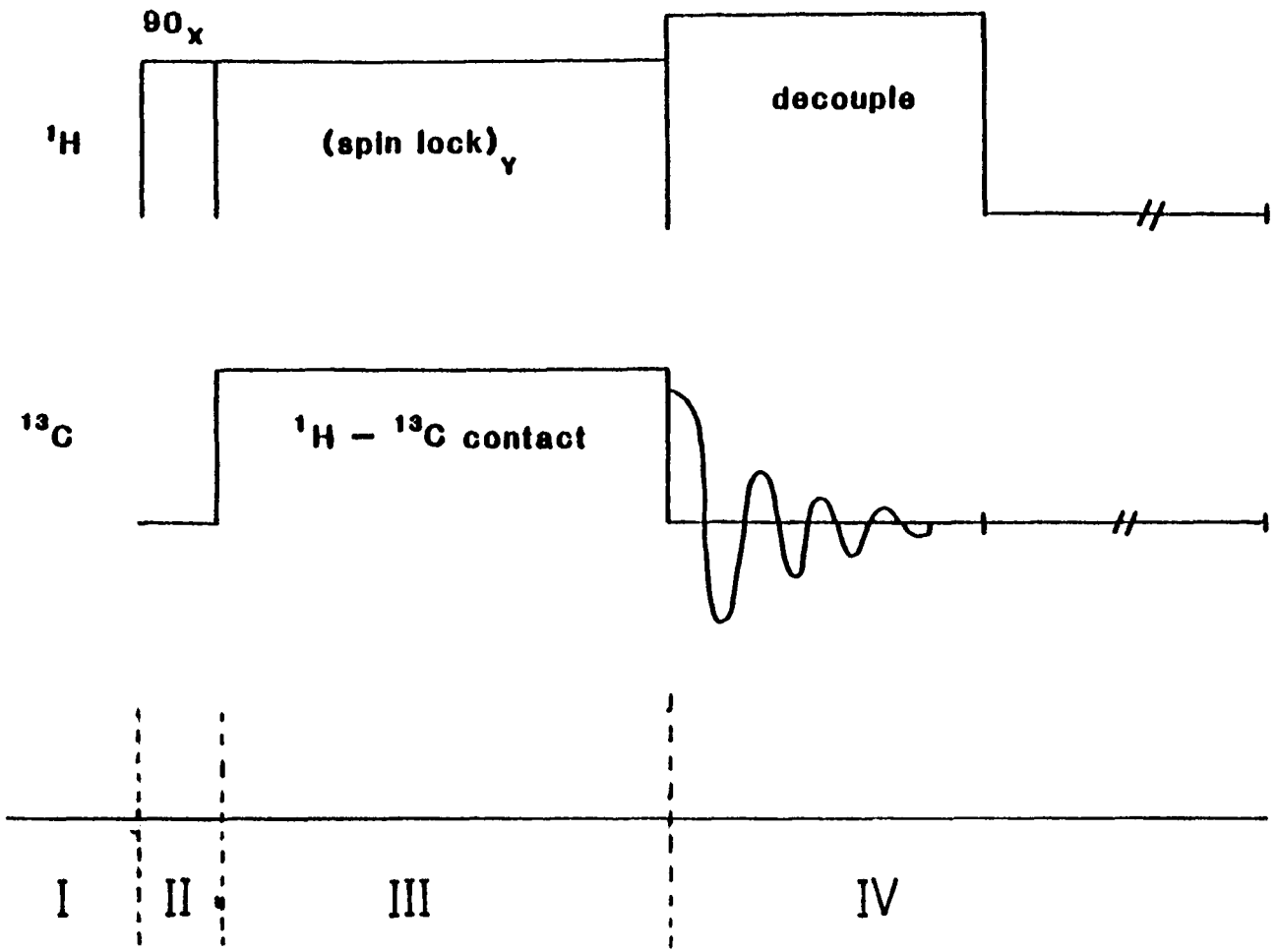

Figure 5.1 Single-contact spin-lock cross polarization (CP) rf pulse sequence illustrating the four regions of the pulse sequence: equilibration of ^{1}H spins (I); initiation of ^{1}H spin lock (II); transfer of spin polarization from ^{1}H to ^{13}C spin systems (III); and observation period (IV).

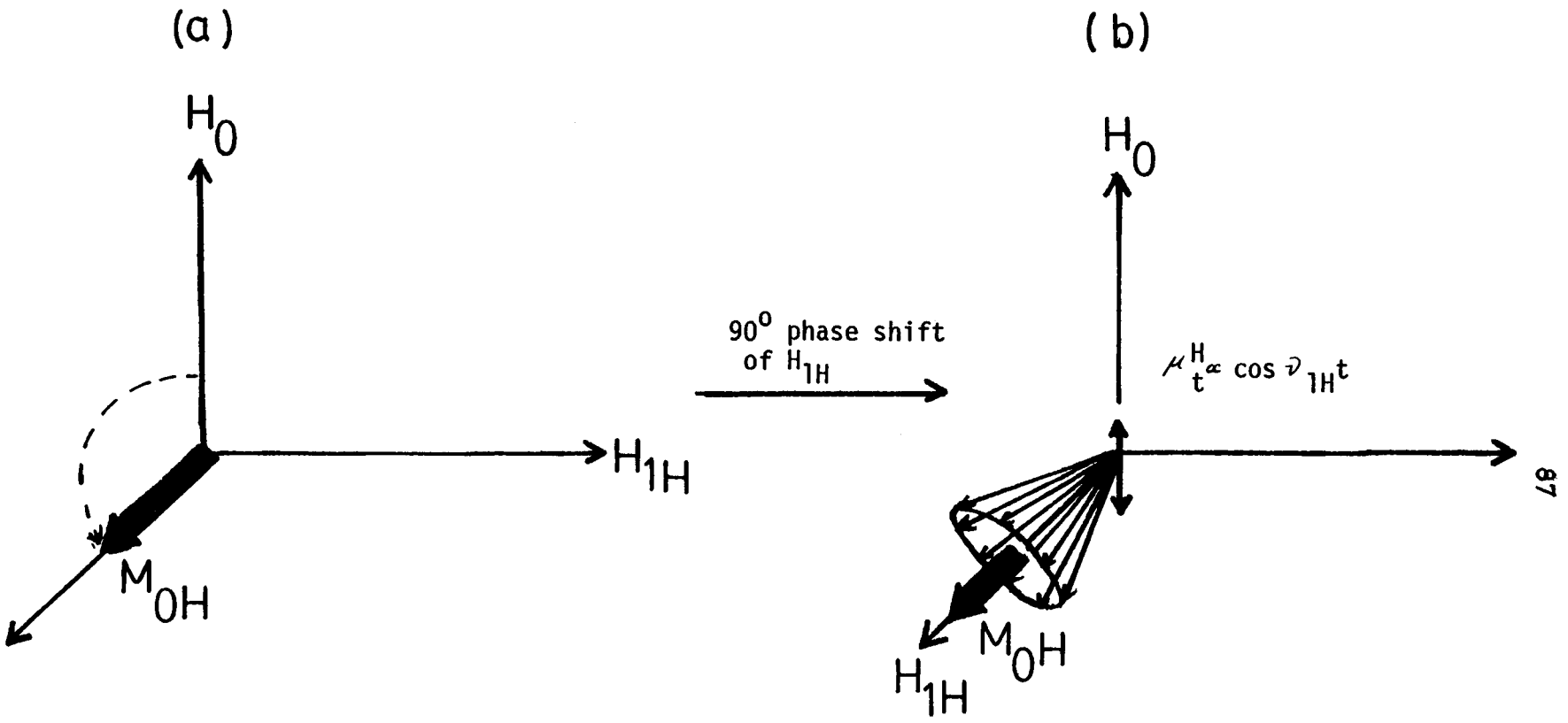

Figure 5.2 Proton spin locking dynamics viewed in the rotating frame at resonance $\nu_0 = (\gamma/2\pi)H_0$: (a) just after the $\pi/2$ pulse and (b) after the 90^o phase shift of the rf field. Precession of individual proton moments around H_{1H} results in an oscillatory component along the z axis.

90° phase shift of the $H_1(I)$ field. A phase shift of the $H_1(I)$ field aligns it along the same axis with M_I. M_1 now precesses about $H_1(I)$, or is spin-locked along H_1 (Figure 5).

In the third region the transfer of spin polarization from the I to the S spin systems occurs. At this point the $H_1(S)$ field is turned on and the amplitude of $H_1(S)$ adjusted so that the Hartmann-Hahn matching conditions are achieved.

Finally, the S spin signal is observed in the final region. The $H_1(I)$ spin may be continued from the spin-lock step to achieve continuous I-spin decoupling of the FID as indicated in Figure 5.1. However, one may turn the decoupler off to obtain coupled S spectra, or use a gated spin decoupling technique, just as in solution NMR.

Instrumental artifacts (signals) often appear in a CP solid state spectrum because of long receiver recovery times which allow transmitter feed through (83, 135). A modified version of the CP experiment reduces these spectral artifacts. The technique calls for a 180° phase shift of the $\pi/2$ proton pulse every other spin-lock sequence. Therefore $\vec{M}_0(I)$ is alternately spin-locked parallel and antiparallel to H_0 (I). The $\vec{M}_0(S)$ which follows $\vec{M}_0(I)$, is also reversed every CP sequence while the $H_1(S)$ retains the same phase. By alternately adding and subtracting the ^{13}C FID's, r.f. transients are subtracted out, while the carbon FID's are coherently added.

Generally, $^{1}H/^{13}C$ cross polarization is utilized extensively for studying organic compounds. However Yannoni and coworkers (136) have shown that $^{19}F/^{13}C$ CP experiments are extremely useful when studying

fluorinated organic compounds (e.g. fluoropolymers), enhancing carbon magnetization by a factor related to $\delta^{19}F/\delta^{13}C$ (see below). Another, useful variation of the CP experiment is monitoring $^{1}H/^{29}Si$ nuclei.

5.5 Signal Enhancement in Solid State CP/NMR

Once the cross polarization experiment has been completed, the proton-decoupled free induction decay (FID) time-domain signal is acquired in a conventional manner, stored, and transformed to the frequency domain by a high speed computer (124). The entire sequence is repeated until an adequate signal-to-noise (S/N) ratio has been obtained. The process increases signal intensities of dilute spins (S) in two ways: 1) S-spin magnetization is increased due to polarization to a larger I-spin magnetic moment and 2) more accumulations may be taken, because $T_1(S)$ is normally reduced in the CP experiment due to spin interactions of the I and S spins. The sensitivity that may be gained in the CP experiment over the more conventional 90° pulse experiment, where CP is not used, is approximately:

$$(S/N)_{CP} \approx (S/N)_{\circ} (\gamma_I/\gamma_S) (T_{1S}/T_{1I})^{1/2} \qquad (23)$$

where $(S/N)_{\circ}$ is that S/N ratio attained without cross-polarization.

5.6 Quantitation of CP/MAS NMR Studies

Quantitative work in solid state NMR is obtained only if all dilute nuclei are given adequate time to equilibrate with the spin-locked reservoir of abundant spins, which decays in $\sim T_{1\rho}(I)$. Therefore $T_{1\rho}(I)$ should be greater than the longest T_{IS}. The rate of cross polarization

$(T_{IS})^{-1}$ for a series of S spins can be significantly different. An estimation of the cross-polarization rate under Hartmann-Hahn matching conditions is

$$T_{IS}^{-1} \sim \Delta\nu_{IS}^2/\Delta\nu_{II} \qquad (24)$$

Cross polarization rates depends on the distance of the I-S nuclei, by a factor r_{IS}^{-6}. For the case of C-H interactions in organic molecules, Vanderhart et.al. (137) have shown that carbons isolated by more than 0.35 nm from protons would have their signal intensities significantly attenuated. Thus, carbons with no bonded protons will cross polarize more slowly than protonated carbons. In order for quantitative work in CP experiments to be valid, the following experimental condition must hold

$$T_{1\rho}\ (^1H) > \text{Contact time} > 3\ T_{CH}\ (\text{of longest } ^{13}C) \qquad (25)$$

5.7 Relaxation Measurements in the CP Experiment

There are several variations to the basic single contact, spin-lock, cross-polarization experiment previously described. All are designed to yield information regarding the interactions of the I and S spin systems being investigated. There are seven basic parameters one may site which characterize the interactions between two spin systems, they are:

$$T_1(S),\ T_1(I),\ T_2(S),\ T_2(I),\ T_{1\rho}(S),\ T_{1\rho}(I),\ T_{SI}$$

These relaxation times give information about the molecular motion of a

solid sample over a wide range of frequencies. Three of the relaxation times (T_{SI}, $T_{1\rho}(S)$, and $T_{1\rho}(I)$) are typically reported in the literature. These may be obtained directly from the single contact CP experiment with little modification of the sequence. They are reviewed below.

As discussed previously, T_{CH} represents the cross relaxation time or that time needed for ^{1}H and ^{13}C nuclei to reach an efficient state of polarization. The relaxation time relies on the strength of the ^{1}H-^{13}C dipolar coupling. For most organic molecules the T_{CH} is typically between 0.5 to 5.0 ms. (100, 138). Optimum T_{CH} values are obtained by varying the contact time over several experiments until the maximum signal intensity for a given carbon is observed. A plot of peak amplitude vs. contact time provides the measured T_{CH} values.

The carbon $T_{1\rho}$ experiments measure the loss of carbon magnetization in the rotating frame as a function of the time that the proton H_1 spin lock field is turned off (100, 139). The pulse sequence in Figure 5.3 is simply the single contact CP experiment with variable decoupling times. Values of carbon $T_{1\rho}$ are typically 0.1-0.8 ms. and are obtained by plotting the log of signal intensity versus the delay time. Carbon $T_{1\rho}$ values are an indicator of molecular motions that occur on a 10 kHz time scale. $T_{1\rho}$ is directly proportional to the local field strength. Therefore, measurements in the 10 kHz time scale are obtained because the magnitude of typical H_1 fields are approximately 10 kHz.

Like carbon $T_{1\rho}$ values, proton $T_{1\rho}$ measurements also reflect molecular motions that occur in the 10 kHz region. $T_{1\rho}$ (^{1}H) is measured using the pulse sequence illustrated in Figure 5.4. In this single

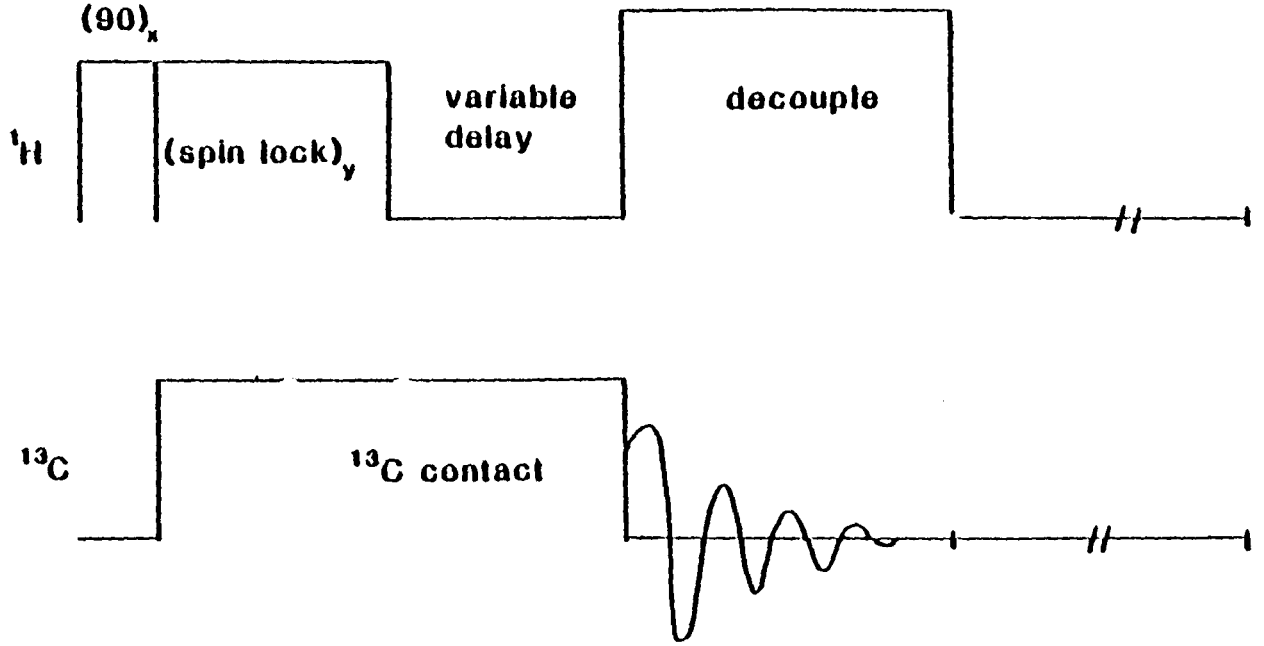

FIGURE 5.3. Pulse sequence for carbon-13 $T_{1\rho}$ measurements.

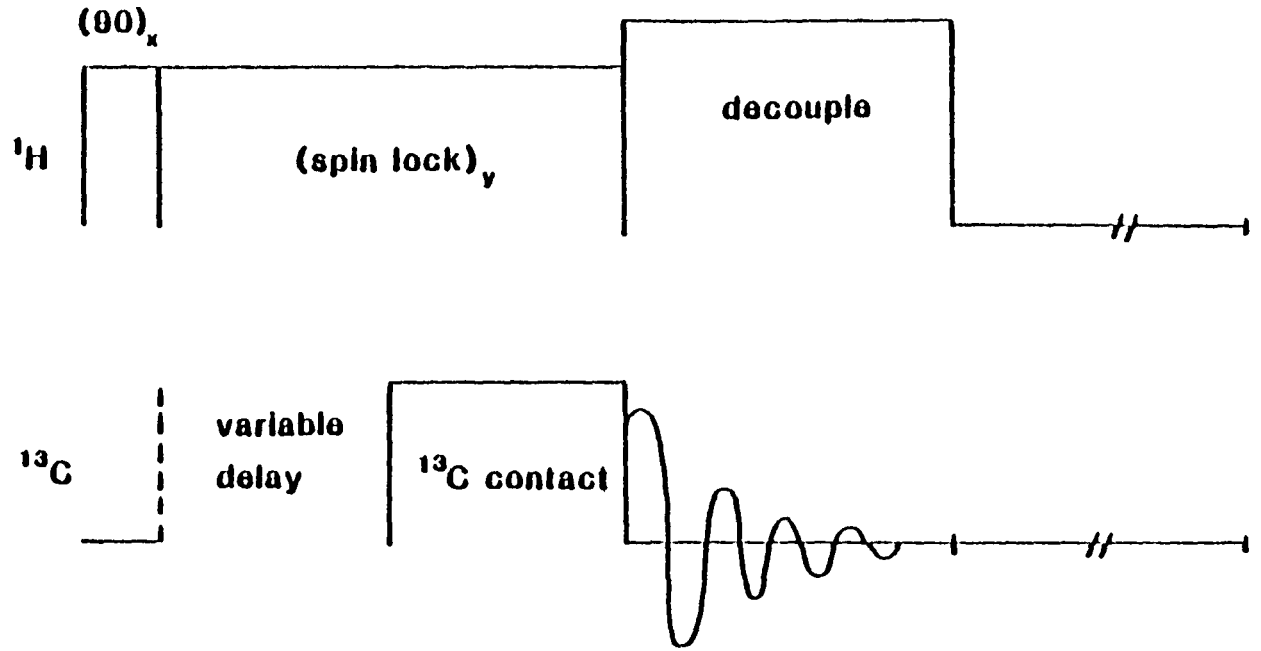

FIGURE 5.4 Pulse sequence for measuring proton $T_{1\rho}$

contact CP experiment the time that ^{1}H-^{13}C contact pulse is initiated is varied. $T_{1\rho}$ (^{1}H) values are obtained from the slope of the plot, $I_{^{13}C}/I_{max}$ versus delay time.

5.8 Studying Immobilized Substrates on Complex Solid Supports by CP/MAS NMR

Active sites within solids (i.e. Bronstead or Lewis acid/base sites) play an important role in many areas of chemistry, such as; catalysis, chromatographic separations, peptide synthesis, and reinforced polymer composites (140). Cross polarization/magic angle spinning (CP/MAS) techniques have provided considerable insight into the characteristics of these solid systems. But, perhaps more importantly, characteristics of the adsorption site may be obtained by either covalently bonding or adsorbing organic molecules onto the active site, then studying their interactions with the solid system (141).

In this section we review solid state NMR techniques which have been used to study inorganic (i.e. silica and alumina) and organic (i.e. biologically related) materials. Many of the studies involve the reaction of a guest molecule with the active sites of the solid system, then studying the interaction of the guest-host adduct by solid state NMR.

5.9 Reactions of Solid Materials

There have been a variety of techniques used to derivatize active sites on solids. For hydroxyl groups on silica surfaces, the site is

typically silylated with a chloro-or alkoxy-substituted silane as indicated in equations 26 and 27 (142-145).

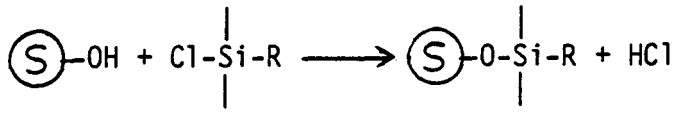

(26)

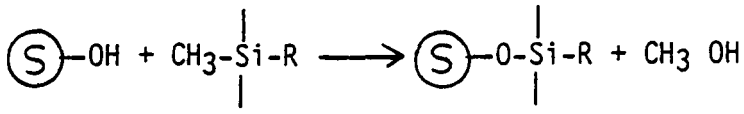

(27)

Polymer supported catalysis have recently been studied using ^{31}P CP/MAS (146, 147). The polymer support was a cross-linked polystyrene and was functionalized by direct (Grignard) reaction of the polymer with a phosphine ligand, equation 28. A variety of transition metal catalysts were added by ligand exchange (equation 28 and 29).

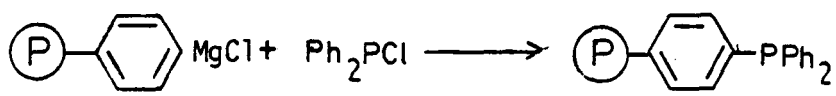

(28)

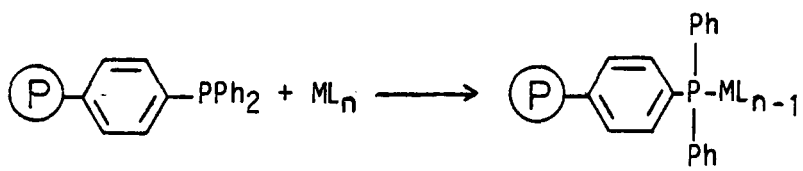

(29)

Functional groups on organic solids (i.e. coal or biological samples) were often derivatized by silylation (20) or acetylation (36).

5.10. Solid State ^{13}C NMR of Substrates Attached to Inorganic Surfaces

Solid state ^{13}C NMR spectra of substrates adsorbed onto solids directly reflect the adsorbates motional freedom. Therefore, the chemical shift anisotropy (CAS) interactions yield considerable information concerning the system under investigation. If the solid state ^{13}C spectrum of an adsorbate has a large CSA, this could suggest decreased motion of the adsorbate and may imply interaction with the active site on the solid. Conversely, substantial motional freedom can isotropically average the CSA, this reflects little interaction with an active site. Several studies have been made of relatively mobile and rapidly diffusing adsorbates (148-157). High resolution and solid state NMR spectra obtained for the adsorbates were comparable.

One example was an elegant study of chemisorbed methanol on magnesium oxide. Gay (158) demonstrated how chemical shift anisotropy can be used to probe the interaction between the surface and the adsorbed species. He found that when adsorbed methanol covered less than half a monolayer on the magnesium oxide a rigidly bound methoxide-like species existed with a shift anisotropy ($\Delta\sigma = \sigma\parallel - \sigma\perp$ = 63ppm). This implied some interaction between the solid and adsorbate. At higher coverages a more motionally free methanol species with a sharp isotropic peak at σ = 49ppm was observed. This indicated negligible

solid-adsorbate interactions.

Vaughan and co-workers (159, 160) studied adsorbed ^{13}CO (^{13}C-enriched) on Rh dispersed on Al_2O_3. Three different types of Rh-^{13}CO configurations were found and characterized by their different relaxation times and chemical shift anisotropies.

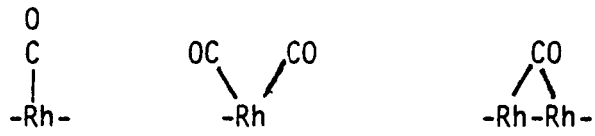

Similar studies have included adsorption of $^{13}CO_2$ onto the zeolite, mordenite (161), and benzene adsorbed on charcoal at 77°K (162). In each case chemical shift anisotropy studies showed a rigidly held species (anisotropically rotating molecule) and a relatively freely rotating species which gave an isotropic signal.

The dynamics and preferred orientations of organic molecules bound to various solids may also be studied by solid state ^{13}C NMR. Work with pyrolytic graphite (163) and sedimented clays (164), two highly oriented surfaces, have shown that it is possible to deduce surface orientations of adsorbed molecules by knowing the chemical shift tensor elements of the carbons in the adsorb molecule with respect to the variation of the orientation of the substrate surface in the magnetic field.

Slotfeldt-Ellingson and Resing (165) have studied the motion of phenyl groups covalently bonded to surfaces of silica gel by solid state ^{13}C NMR. At room temperature motional freedom of the functional

group kept the plane of the phenyl ring parallel to the surface. At 77°K the anisotropy patterns indicated the phenyl groups were nearly rigid and inclined at an angle θ with respect to the surface. In a similar study Maciel and Sindorf (166) reported the molecular motions of n-alkyl silanes bonded to a silica surface. The work examined how ^{13}C relaxation measurements could be used to study motional dynamics of substrates bonded to silica gel.

5.10.1. Studying Molecular Cavities in Solids by ^{129}Xe NMR

An ingeneous application of chemical shift anisotropy patterns to the study of molecular cavities in solids has been reported by Ripmeester (167, 168) and others (169). They have measured the ^{129}Xe spectra of xenon gas inclathrated into a variety of solid systems. The ^{129}Xe nucleus (spin = 1/2, natural abundance = 26.24%, NMR frequency = 24.91 MHz) was characterized by a large chemical shift range. The isolated atom, being spherically symmetrical showed no chemical shift anisotropy. However, the atom was very sensitive to the asymmetry of its immediate environment as reflected by its large chemical shift range. Thus the atom was used as a very sensitive probe to examine the interior shapes of solid materials.

To demonstrate the possibilites of this technique Ripmeester (167, 168) inclathrated ^{129}Xe atoms into β-quinol and β-phenol crystals. The β-quinol clathrate is a single asymmetric cage that can hold a single Xe atom. The β-phenol clathrate contains two interior regions, one will hold a single Xe atom while a larger one will hold two Xe atoms. The

solid state ^{129}Xe spectrum (for β-quinol) showed a single symmetrical CSA pattern. The ^{129}Xe spectrum for the β-phenol clathrate revealed a series of three signals corresponding to the three inclathrated Xe atoms (168).

5.10.2 Solid State ^{29}Si NMR of Inorganic Systems

Silicates, alumino silicates, and zeolites are widely used as catalysts, catalyst supports, molecular sieves, and ion exchange resins (170). Important advances in understanding the properties of these materials have been made in recent years due to applications of ^{29}Si MAS NMR techniques (171). Typically, the ^{29}Si MAS NMR studies of these solid compounds use simple 90° pulse sequences with MAS. This is because there are no hydrogen atoms in these systems, therefore, high-power decoupling and cross-polarization are not needed (170). The NMR results accurately reflect the local environments of the ^{29}Si atoms in both silicates and aluminosilicates (172-181). The ^{29}Si signals of zeolites are very sensitive to the atoms attached to the oxygens of the SiO_4 tetrahedron (i.e., ^{27}Al). Thus, the ^{29}Si spectrum of zeolites typically contain five peaks corresponding to the five Si/Al combinations: Si(4Al), Si(3Al, 1Si), Si(2Al, 2Si), Si(1Al, 3Si), and Si(4Si) (177-181). These signals are rather broad with linewdiths of 10-20 ppm.

One possible explanation for the line broadening is the dipolar coupling between the ^{29}Si and ^{27}Al nuclei. The ^{27}Al nucleus is a quadrupolar nucleus, therefore, the interaction will not be averaged to

zero by MAS. When the ^{27}Al nucleus is removed from the ^{29}Si nucleus by at least one atom (e.g., ^{29}Si-O-^{27}Al) the magnitude of the interaction is dramatically attenuated (180). One technique used to improve the resolution ^{29}Si spectra is to chemically dealuminate the zeolite samples. Fyfe and co-workers (181) have applied this technique successfully with a number of zeolite samples. The improved resolution allows more accurate quantitative Si/Al measurements to be made over the five ^{29}Si spectral regions.

5.10.3 ^{29}Si CP/MAS NMR of Inorganic Systems

Recently, Maciel and Sindorf (182-184) have reported direct investigation of active sites on silica-gel surfaces using $^{1}H/^{29}Si$ CP/MAS techniques. The significance of these studies was that only ^{29}Si nuclei in the immediate proximity of protons were observed in the solid state ^{29}Si spectrum. The silicon atoms in the interior of the solid were discriminated against because the silicon magnetization was cross-polarized from the proton spin system. Therefore, only those nuclei attached to or near the surface hydroxyl groups were observed as indicated by the $T_{(SiH)}$ values. Maciel and Sindorf (182) observed and assigned three characteristic peaks in the ^{29}Si-CP/MAS NMR spectrum of silica gel structures 1, 2, and 3 below. They confirmed these assignments by studying the dependence of the ^{29}Si spectral intensities of each signal with respect to contact times (T_{SiH})

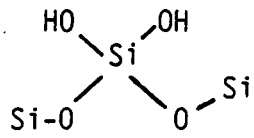

(1)

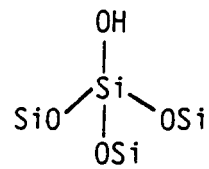

(2)

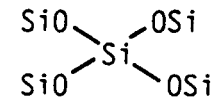

(3)

	1	2	3
δSi	-90.6 ppm	-99.8 ppm	-109.3 ppm
T_{SiH}	2.3 ms	2.9 ms	12.7 ms

Maciel and Sindorf have also studied active sites on silica gel by derivatizing those sites with methylchlorosilane reagents and studying the results with ^{29}Si CP/MAS (184). They observed separate ^{29}Si signals for both the surface silica sites and the attached silanes. In a similar study Maciel and co-workers (185, 186) reported the total concentration of all acidic sites (i.e., Bronsted and Lewis acid sites) on silica-alumina surfaces using ^{13}C and ^{15}N CP/MAS NMR. Their studies have shown that it possible to gain semiquantitative estimates of the active surface sites on silica solids. Other nuclei have also been used as probes (i.e., ^{31}P) to study solid systems and a plethora of reports have appeared in the literature.

5.10.4 ^{31}P CP/MAS NMR Studies of Solid Systems

The ^{31}P nucleus is attractive for surface characterization studies since it has 100% natural abundance and exhibits a large chemical shift

range. As indicated earlier, phosphorus groups can be covalently bound to either silica or polymer catalytic supports. These groups are then allowed to react with a number of metal catalysts. Fyfe and co-workers (146, 147, 187, 188) have shown that ^{31}P CP/MAS experiments provide a direct and convenient technique for characterizing these catalytic systems. Principle sources of information come from chemical shift anisotropy and scalar coupling parameters ($^{J}31P\text{-}M$). Scalar coupling is a particularly sensitive parameter if the metal is ^{195}Pt, because $^{J}31P\text{-}^{195}Pt$ > 3000 Hz. Non-equivalent metal sites are easily detected by the ^{31}P chemical shift.

^{31}P-MAS NMR has also been used to study acidic sites on catalytic systems (141, 189, 190) in a manner similar to previously described studies (185, 186). Bronsted acid sites on zeolites were characterized by chemisorbing trimethylphosphonium ions onto the active sites. The ^{1}H decoupled ^{31}P MAS NMR spectrum revealed two types of acidic OH sites. However, a rare phenomena was observed in the ^{1}H coupled solid state ^{31}P spectrum. Specifically, $^{1}H\text{-}^{31}P$ J-coupling from the $[(CH_3)_3P\text{-}H]^+$ complex provided direct evidence that the acidic OH site has been successfully complexed.

To date, no ^{19}F tagging reagents have been used as a probe to study acidic sites on inorganic catalytic supports. However, various reports of ^{19}F incorporated into biological and organic compounds have been studied by solid state NMR.

5.11 Effects of the ^{19}F Nucleus in Solid State ^{13}C NMR of Organic Compounds

The effects of ^{19}F-^{13}C dipolar interactions are very apparent in ^{1}H-decoupled ^{13}C solid state spectra (191, 192). Unless directly decoupled (119, 120) as previously discussed, the ^{19}F-^{13}C intra-and/or intermolecular dipole-dipole coupling significantly contributes to ^{13}C line broadening. In the two cases cited, ^{13}C signals were broadened due to intermolecular dipolar coupling and could be eliminated by ^{19}F decoupling. However, in cases where the fluorine atom is directly bound to ^{13}C atom (intramolecular dipolar coupling), ^{19}F decoupling is not as effective due to the large ^{19}F CSA, as previously indicated (193).

Solid fluorine polymers (i.e. poly(tetrafluoroethylene) have been studied by ^{19}F and ^{13}C solid state NMR (3, 193-195). These ^{19}F solid state studies were concerned with determining ^{19}F chemical shifts (193) and reducing homonuclear ^{19}F-dipolar coupling by multiple-pulse techniques (194, 195). Also, fluorine-19 decoupling (119, 120) and ^{19}F-^{13}C cross-polarization studies (119) have been pursued in the solid state for several polymer systems. Ward and Lin (3) have reported measurements of the degree of mixing, at the molecular level, between poly(vinylidene fluoride) and three non-fluorinated vinyl polymers using solid state ^{13}C CP/MAS NMR. Their study depended upon the ^{13}C-^{19}F intermolecular dipole interaction to attenuate the ^{13}C signals of the nonfluorinated polymers. By knowing the degree of attenuation of the ^{13}C peak intensity, they were able to calculate the extent of the polymer mixing process.

Fluorine spin-labels have also been useful in studying biological compounds in the solid state. Hull and Sykes (196) incorporated fluorotyrosines into alkaline phosphatase proteins. Dipolar T_1 and line-width data, chemical shift anisotropy linewidths, and NOE enhancements obtained from solid state ^{19}F NMR allowed them to derive the overall tumbling correlation time (τ_c) for alkaline phosphatase and establish limits on the internal mobility of the tyrosine residues. Gent, Ho, and co-workers (197, 198) incorporated 8,8'-difluoromyristate, a fluorinated fatty acid, into the phospholipids of the bacteria Escherichia coli (E. coli). They were able to draw some conclusions on the molecular motions and orientations of the fatty acids by using the known chemical shift tensor in the ^{19}F labelled compound. However, ^{13}C and ^{15}N spin labels are most commonly used when studying solid biologic and organic compounds. Investigations using solid state NMR and one or both probes are opening exciting new areas of the study in biology and agriculture.

5.11.1 ^{13}C and ^{15}N - Enriched Probes in Solid State NMR

An exciting new area currently under investigation by solid state NMR spectroscopists is using the technique to study "intact" biological systems such as soybean seeds (199), corn seeds (200), cellulose (201), or even live animal tissue (202). To improve carbon or nitrogen sensitivity in these experiments the organism is typically exposed to an environment where enriched carbon-13 and/or nitrogen-15 compounds are present. This is a particularly useful technique when investigating

plant material, because plants can easily be exposed to ^{13}C-enriched $^{*}CO_2$ or ^{15}N-enriched nitrates from fertilizers (203-207) to yield doubly labelled proteins in plant material. When both labelled precursors are used Schaefer, et. al. (207) has shown that double cross-polarization experiments can be performed. In this technique ^{1}H polarization is first transferred to the ^{15}N system, the second contact is made between the ^{15}N and ^{13}C systems. The purpose of the first polarization between ^{1}H-^{15}N is to improve sensitivity in the ^{15}N spin system and the second is to detect ^{13}C-^{15}N dipolar coupling.

Recently, Henriches and Linder (208) have shown how ^{13}C spin diffusion could be used to determine intermolecular structures in solids. Spin diffusion times in unenriched ^{13}C samples are long (10-100 s) because internuclear distances between ^{13}C nuclei are large. Isotopic ^{13}C-enrichment shortens the distance between ^{13}C nuclei and shortens diffusion times. The technique offers a means by which relative orientations of neighboring molecules may be determined.

Pfeffer, et. al. (4) have shown ^{13}C-enrichment techniques can be used as a technique for making resonance assignments in solid state ^{13}C NMR spectra of organic compounds. By using ^{13}C-enriched compounds, Pfeffer captitalized upon the carbon-carbon dipolar interaction observed in the system. The carbon-carbon dipolar interactions are homogeneous (209) and do not break into spinning sidebands as observed in inhomogeneous interactions, i.e. chemical shift anisotropy. Instead, the broadening induced by the dipolar interaction will not spin out, even at very high spin rates and those carbons in the immediate proximity of the enriched ^{13}C nucleus are significantly broadened.

Experimental

Preparation of 1-Adamantyl Benzoates

The benzoate derivatives of 1-Adamantanol were prepared by a method similar to that reported by Kaiser and Woodruff (210). The tetrahydrofuran (THF) was dried by storage over lithium aluminum hydride and was used directly after distillation. 1-Adamantanol and the benzoyl chlorides were used directly, as obtained (from Aldrich Chem. Co), without further purification. All acid chlorides were stored in a desiccator over $CaSO_4$ to reduce the possibility of contact with moisture.

To a solution of 0.020 mol of 1-Adamantanol (Aldrich Chem. Co., mw = 152.24) in 30 mL of anhydrous (THF) was added, over several minutes, 8.8 mL (0.022 mol) of 2.7 M n-butyllithium in hexane (Aldrich Chem. Co.) under nitrogen. After stirring ~30 min. the appropriate benzoyl chloride solution (0.022 mol in 15 mL THF) was added dropwise. Addition of the acid chloride solution routinely required 5-10 min. The resulting solution was brought to reflux for 1 hr., cooled to 0°C in an ice bath and hydrolyzed with 25 mL of distilled water. The aqueous phase was extracted with three 30 mL portions of ethyl ether, and the combined organic phases were dried over anhydrous $MgSO_4$. The excess solvent was removed *in vacuo*. The crude solid product was usually yellow/orange in color. The product was purified by recrystallization from methanol, this yielded white crystals for all 1-adamantyl benzoates. On occasion the products were further purified by dissolving the solids in hot methanol, adding a trace of carbon black, with

subsequent hot filtration. After recrystallization the crystals were separated from the mother liquor by vacuum filtration. The crystals were dried and stored in a desiccator.

1-Adamantyl benzoate: mp 67.0 -67.5°C; ^{1}H NMR ($CDCl_3$) δ = 7.99 (2H,m); 7.50 (1H, m); 7.64 (2H, m); 2.26 (6H, m); 2.22 (3H, m); 1.71 (6H, m). ^{13}C NMR (ppm $CDCl_3$) 165.50; 132.32, 129.48; 128.20; 81.02; 41.60; 36.39; 31.05.

1-Adamantyl p-fluorobenzoate: mp 67.0 -68.0°C; ^{1}H NMR (CDl_3) δ 7.99 (2H, m); 7.07 (2H, t, J=8.7 Hz); 2.24 (9H, m); 1.71 (6H, m). ^{13}C NMR (ppm $CDCl_3$) 165.51 (d, J^{1}_{CF} = 252.42 Hz); 164.44; 131.92; (d, J^{3}_{CF} = 9.13 Hz); 128.50; 115.18 (d, J^{2}_{CF} = 21.24 Hz); 81.32; 41.59; 36.35; 31.04.

1-Adamantyl 2,6-difluorobenzoate: mp 81.0 -81.5°C; ^{1}H NMR ($CDCl_3$) δ 7.34 (1H, m); 6.90 (2H, t, J=8.08 Hz); 2.22 (9H, m); 1.71 (6H, m). ^{13}C NMR (ppm $CDCl_3$) 160.78 (d, J^{1}_{CF} = 254.02 Hz, J^{3}_{CF} = 7.91 Hz); 160.14; 131.54 (t, J^{3}_{CF} = 10.52 Hz); 111.74 (d, J^{2}_{CF} = 22.12 Hz); 83.54; 41.53; 36.24; 31.09.

1-Adamantyl m-fluorobenzoate: mp 66.5 -67.0 °C; ^{1}H NMR ($CDCl_3$) δ 7.77 (1H, m); 7.65 (1H, m); 7.36 (1H, m); 7.20 (1H, m); 2.25 (9H, m); 1.71 (6H, m).
^{13}C NMR (ppm, $CDCl_3$) 162.49 (d, J^{1}_{CF} = 248.07 Hz); 164.17; 134.36; 129.70 (d, J^{3}_{CF} = 7.43 Hz); 125.10; 119.36 (d, J^{2}_{CF} = 21.26 Hz); 232.56 (d, J^{2}_{CF} = 23.05 Hz); 81.57; 41.33; 36.18; 30.89.

1-Adamantyl p-trifluoromethylbenzoate: mp 132.5 -133.5°C; ^{1}H NMR ($CDCl_3$) δ 8.09 (2H, d, J=8.01 Hz); 7.67 (2H, d, J=8.34 Hz); 2.26 (9H, m); 1.72 (6H,m).

^{13}C NMR (ppm $CDCl_3$) 163.95; 135.19; 129.65; 125.02; 121.61; 81.82; 41.20; 36.03; 30.79.

1-Adamantyl pentafluorobenzoate: mp 85.0 -86.0°C ^{1}H NMR ($CDCl_3$) δ 2.24 (9h, m); 1.72 (6H, m).

^{13}C (ppm $CDCl_3$) 157.43; 147.62, 147.48 147.39, 145.20, 142.62, 142.56, 142.41, 142.17, 140.48, 140.17, 140.07, 139.80, 135.45 (m, characterizes aromatic carbons coupled to fluorine), 85.23; 41.44; 36.08; 31.07.

Preparation of Sterol Derivatives

Pyridine (Fisher Scientific) was distilled over barium hydroxide, with the first and last fractions (~10%) being discarded. The main fraction of pyridine was retained and stored over KOH pellets. The steroids (Aldrich Chem. Co.) and acid chlorides or anhydrides were used without further purification. Cholesteryl benzoate 1; cholesteryl p-fluorobenzoate 2; cholesteryl pentafluorobenzoate 3; testosterone benzoate 4, and testosterone pentafluorobenzoate 5 were prepared according to the procedure described in chapter one of this thesis.

Preparation of Cholesteryl trifluoroacetate 6

Cholesteryl trifluoroactate was prepared by adding 15 mL of trifluoroacetic anhydride (Aldrich Chem. Co. mw = 210.03; d = 1.487) to 2.0g (0.005 mol) to cholesterol and refluxing for 12 hrs. under a nitrogen atmosphere. To this solution 0.610 g (0.005 mol) of

4-dimethylamino pyridine (Aldrich Chem. Co.) was added as the tertiary amine base catalyst. Upon cooling, the reaction mixture was poured into a separatory funnel, ice chips were added, and diluted with 20 mL of 6N HCl. The aqueous phase was extracted with three 20 mL portions of ethyl ether. The organic phases were combined, washed with three 30 mL portions of 10% $NaHCO_3$, and once with 30 mL of distilled water. The organic phase was dried over anhydrous $MgSO_4$ and then removed in vacuo. The white solid obtained was recrystallized from a solution of 1% ethyl acetate in benzene.

Carbon-13 NMR was used to check the purity of all steroid derivatives prepared. The ^{13}C chemical shifts were assigned on the basis of a previous report by Reich, et. al. (211). The assignments are given in Table 5.2, where the numbering system for the steroid system was:

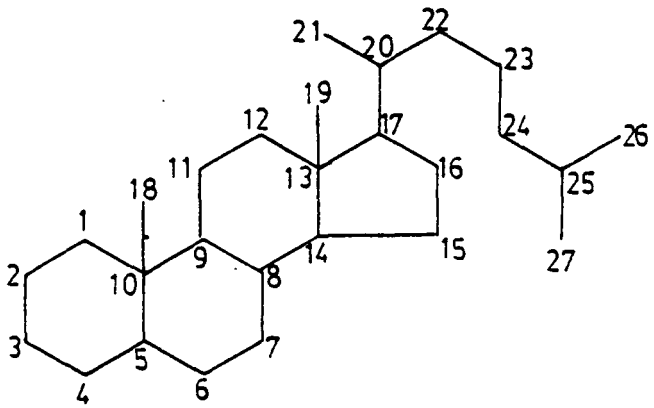

Derivatization of Coal with Benzoyl and Pentafluorobenzoyl Chloride

A Western Virginia bituminous coal (United Coal Co., Bristol, TN) was derivatized with benzoyl and pentafluorobenzoyl chloride using the following technique: Approximately 1.5 g of coal was added to 25 mL

Table 5.2

The Chemical Shift Assignments for the ^{13}C Spectra of Derivatized Steroids

Carbon	1	2	3	4	5	6
1	37.04	37.06	36.94	35.74	35.71	36.82
2	3.91	31.92	31.92	33.93	33.87	31.92
3	74.56	74.79	78.63	199.13	199.16	78.75
4	42.34	42.31	42.37	123.98	124.01	42.37
5	139.63	139.54	139.02	170.81	170.49	138.55
6	122.78	122.84	123.31	32.76	32.65	123.84
7	39.54	39.57	39.57	31.53	31.44	39.57
8	38.21	38.22	37.87	35.57	35.40	37.52
9	50.07	50.08	50.08	53.78	53.66	50.08
10	35.81	35.77	35.83	38.66	38.57	35.83
11	21.09	21.06	21.06	20.61	20.49	21.11
12	28.27	28.06	28.00	36.79	36.57	28.06
13	27.90	27.51	27.35	42.92	42.78	27.13
14	56.72	56.74	56.74	50.34	50.08	56.73
15	22.58	22.57	22.51	23.65	23.49	22.57
16	28.04	27.88	27.53	27.68	27.40	27.30
17	56.17	56.15	56.21	82.98	85.32	56.27
18	11.87	11.89	11.88	12.32	12.03	11.89
19	19.38	19.36	19.25	17.46	17.37	19.25
20	36.19	36.18	36.23			36.24

Table 5.2 (cont.)

The Chemical Shift Assignments for the ^{13}C Spectra of Derivatized Steroids

Carbon	1	2	3	4	5	6
21	18.75	18.72	18.74			18.78
22	36.19	36.65	36.59			36.61
23	24.29	24.30	24.27			24.32
24	39.76	39.73	39.74			39.75
25	28.04	28.20	28.26			28.23
26	22.83	22.81	22.75			22.81
27	23.85	23.86	23.84			23.92

anhydrous pyridine. The mixture was stirred vigorously under a nitrogen atmosphere, while heating to 110°C. After 30 min. 0.01 mol of the appropriate acid chloride was slowly added and this mixture was refluxed under nitrogen for 48 hrs.

Upon cooling 20 mL of distilled water was added to the reaction vessel in order to quench any excess acid chloride. This mixture was stirred for two additional hrs. The liquid portion of the mixture was then removed by gravity filtration and the remaining solid washed with three 20 mL portions of $CHCl_3$ and three 20 mL portions of ethyl ether. The derivatized coal was then dried in a vacuum oven at 160°C for 24 hrs. The initial and final weights of the solid coal material, along with net gain (or loss) of the material are summarized in Table 6.3.

Derivatization of Silica Gel with Fluorine Tagging Reagents

Silica Gel was derivatized with a number of tagging reagents for the purpose of observing ^{29}Si-^{19}F dipolar coupling interactions. The silica gel used was flash chromatography silica gel (Baker Scientific Supplies) with an average particle diameter of 40 microns (μm). Locke, et. al. (212) reported that the surface area of silica gel is approximately $50m^2$/ g. Previous studies (213) have also shown that 5.2 hydroxyl groups per $100Å^2$ are present on typical silica gel surfaces. Using these numbers one can show there are ~6.478 mmole of surface hydroxyl groups per gm of silica gel. Prior to any reaction all silica gel samples were dried in a vacuum oven at 160°C for 24 hrs.

Table 5.3

Initial and Final Weights of Derivatized Western Virginia Coal

Weight (grm)	Benzoyl Chloride	Pentafluorobenzoyl
	(MW = 140.57)	(MW = 230.52)
initial	1.64751	1.63688
final	1.66248	1.67111
net gain	0.0150	0.03423
percent increase	0.91%	2.09%[1]

[1] Note that the molecular weight of pentafluorobenzoyl chloride is 1.64 times greater than the mw of benzoyl chloride. Taking this correction into account percent increase in wt. of pentafluorobenzylated coal is 1.27% relative to benzylated coal.

Preparation of Silica Gel Benzoate and Pentafluorobenzoate Derivatives

Typically 3.0-3.5 g was used in each experiment. The silica gel, contained in its reaction flask, was placed on a vacuum line equipped with a reflux condenser, the reaction vessel was evacuated, and a nitrogen atmosphere admitted. The appropiate acid chloride was added (~10 mL) and the mixture stirred vigorously while being heated until the acid chloride refluxed over the silica gel. Refluxing was continued for 4 hrs under N_2, after which time the excess acid chloride was vacuum distilled from the silica gel (at 0.005 mm Hg). After drying the samples were stored in a vacuum desiccator until analyzed.

Preparation of Silica Gel 1,1,1-Trifluoroethyl ethers

Silica gel 2,2,2-trifluoroethyl ethers were prepared by a procedure similar to that reported by Koller and Dorn (60). A mixture containing 30 mL of 2,2,2-trifluorodiazoethane (0.2 M in CH_2Cl_2) and 1 gm silica gel was prepared and stirred vigorously under a N_2 atmosphere. Tetrafluoroboric acid (20 µL) was added as an acid catalyst. The reaction was carried out at atmospheric pressure on a vacuum line system so that the progress of the reaction could be monitored by the evolution of nitrogen gas (as observed by a manometer connected to the system). After the reaction was complete, excess 2,2,2-trifluorodiazoethane and methylene chloride were distilled from the solid silica gel. The silica gel was dried further in a vacuum oven (160°C, 24 hr) and stored in a vacuum desiccator.

Preparation of Diluted Fluorine-Tagged Solid Samples

One of the first problems encountered in this project was that ^{13}C-signals in the solid state NMR spectra were attenuated by contributions from intra- and intermolecular ^{13}C-^{19}F dipole-dipole interactions, vide infra. In an attempt to separate the two interactions a series of dilution studies was carried out where attempts were made to isolate the fluorinated sample in an inert or noninteracting solid matrix.

Dilution of 1-Adamantyl Pentafluorobenzoate Samples in hexamethylbenzene

Hexamethylbenzene (0.806 g, 0.0050 mol) and 1-adamantyl pentafluorobenzoate (0.226 g, 0.00065 mol), a ratio of approximately 80:20 w/w, were dissolved in 15 mL ethyl ether. The components were allowed to slowly recrystallize at room temperature. After 3 days the solvent was separated from the solid by vacuum filtration. The white solid was air dried and stored in a desiccator. The recovered solid materials weight was 0.943 g, 91 percent of initial starting material.

Dilution of 1-Adamantylpentafluorobenzoate in Sulfur

1.001 g of sulfur and 0.1257 g of 1-Adamantyl pentafluorobenzoate were weighed into a 25 mL round bottom flask. The sulfur: 1-adamantyl pentafluorobenzoate ratio was approximately 90:10 w/w. The solid mixture was stirred with a magnetic stir bar as the temperature in the flask was slowly raised to the melting point of sulfur (~122°C). The melt was stirred for 3 min. at this temperature, allowed to cool, and stored in a desiccator.

Preparation of Thiourea: 1-AdamantylPentafluorobenzoate Inclusion Complexes

Urea and thiourea clathrates of alkyl molecules have been well characterized (214). X-ray crystal studies have shown that the diameter of the channels thiourea can make around a guest molecule are ~15.8Å. Thiourea has been shown to be useful when isolating adamantane, and its derivatives, in organic preparations (215). Thus, thiourea clathrates of 1-adamantyl pentafluorobenzoates have been made in an effort to isolate the fluorinated molecules. These complexes were prepared by dissolving 3.00 g (0.039 mol) of thiourea (Aldrich Chem.) in 30 mL hot methanol. Once the thiourea was in solution, 0.35 g (0.001 mol) of 1-adamantyl pentafluorobenzoate was added and dissolved. The solution was then stirred for ~10 min. and allowed to cool to room temperature. Crystals slowly form over a 3-4 day period. The mother liquor was filtered from the solid via a Buchner funnel and the solid washed twice with 20 mL portions of cold methanol. It was then dried in a desiccator. The same technique was also used to prepare thiourea clathrates of 1-adamantyl p-fluorobenzoate and 1-adamantyl p-trifluoromethylbenzoate.

Instrumentation

The solid state carbon-13 NMR spectra were acquired at 15.0 MHz using a JEOL FX-60 spectrometer. All spectra were obtained using high-power proton decoupling, magic angle spinning, and cross-polarization sampling conditions. The matched spin-lock cross-polarization condition was attained with appropriate contact and pulse repetition

times. The strength of the high power proton decoupling field was 33 kHz (7.75 G). All MAS experiments were carried out utilizing Kel-F bullet type rotors and a spinning rate of 1.6-2.0 kHz. Samples were hand packed, each rotor would hold ~0.6 grm of sample.

The Hartmann-Hahn condition and magic angle were adjusted using the aromatic and alkyl signals of hexamethylbenzene (HMB). The Hartmann-Hahn condition was optimized when maximum signal intensities were attained for HMB. The magic angle was set when the alkyl and aromatic signals of HMB were of equal intensity. Spinning rates were also calibrated using the spinning sidebands of HMB. All ^{13}C spectra were externally referenced to liquid tetramethylsilane (TMS) ($\delta^{13}C$ = 0.00 ppm), based on the substitution of HMB as the reference and assigning 132.3 and 16.9 ppm to the ^{13}C chemical shifts of the aromatic and aliphatic signals of HMB, respectively. In some cases cured silicon rubber was used as the reference, $\delta^{13}C$ = 1.87 ppm relative to TMS. A plug of the appropiate reference was placed at the bottom of the rotor for each sample.

Typically, spectra were obtained by using a contact time of 2 ms and a pulse repetition time of 1.0-2.0 s. All spectra contained 1K data points using zero filling to attain a total of 4K points. A spectral width of 8000 Hz and acquisition time of 64 ms were used for all accummulations.

Carbon-13 spectra were also collected on a Nicolet NT-200 spectrometer, operating at 50.1 MHz, located at the Colorado State University (CSU) Regional NMR Facility. Typically spectra were obtained

using a contact time of 2.0 msec, pulse repetition time of 2.00 sec., and an acquisition time of 10.0 ms.

Silicon-29 spectra were also obtained on the Nicolet NT-200 at the CSU NMR Facility. The ^{29}Si NMR were acquired at 29.75 MHz. Spectra were obtained using a contact time of 10 ms and a pulse repetition time of 0.5-1.05 s. The spinning rates were 2.0-2.3 kHz. The ^{29}Si chemical shifts were referenced with respect to liquid TMS with larger numbers corresponding to lower shielding.

$T_{1\rho}$ Measurements'

$T_{1\rho}$ values for the carbon-13 nuclei in 1-adamantyl benzoate were measured using the single contact cross polarization procedure described previously (216). The ^{13}C $T_{1\rho}$ study was obtained using the pulse diagram illustrated in Figure 5.3 where variable delay times were used for ^{1}H decoupling. A plot of intensity versus delay time was made and ^{13}C $T_{1\rho}$ values were calculated from the slope of the decay curve. The ^{1}H $T_{1\rho}$ experiments for 1-adamantyl benzoate were carried out using the pulse sequence illustrated in Figure 5.4. In this experiment the ^{1}H-^{13}C contact time was varied. A plot of ln I/Io versus contact time was made and ^{1}H $T_{1\rho}$ values calculated from the slope.

Results and Discussion

^{13}C-^{19}F Dipolar Interactions in 1-Adamantyl Benzoate Model Systems

General Description of Spectra.

Previous studies (see Background Section) have shown that the behavior of guest molecules either absorbed or covalently bonded to a solid can best be studied by solid state NMR techniques. Several groups have used dipolar interactions to study various properties of the solids. Specifically, Pfeffer (4) monitored ^{13}C-^{13}C dipole interactions to obtain resonance assignments in solid state ^{13}C NMR spectra. The effectiveness of his technique was overshadowed by the preparative work needed to incorporate ^{13}C-enriched nuclei in the molecules studied. Also, Ward and Lin (3) measured the degree of mixing in fluorinated and hydrogen containing polymer systems (e.g., mixtures of polyvinylidene fluoride and methyl methacrylate). In this work coupled fluorine-19 attenuation of carbon-13 peak intensities indicated the extent of the mixing process.

The purpose of the research undertaken by this author was to illustrate that a large percentage of the same information Pfeffer's technique (4) yielded may be obtained by utilizing a less complex labelling experiment, that is, one that proceeds by a routine reaction which introduces a ^{19}F tag onto the active solid site. Based on the work of Ward and Lin (3), we chose to study the ^{13}C-^{19}F dipolar inter-

action which attenuates ^{13}C signals of nuclei in the proximity of the tagging group. To observe the principle characteristics of this reaction, fluorinated derivatives of a simple model compound, 1-adamantyl benzoate, were studied. The choice of 1-adamantyl benzoate derivatives as the model compound(s) is readily appreciated by examining Figures 5.5a and 5.5b. The symmetrical adamantyl portion of the molecule (C_{3v} symmetry) produces a simple four-line pattern that is well resolved in both the solution and solid state ^{13}C NMR spectra. Also, one finds the ^{13}C carbonyl signal well removed from any overlapping resonances in both spectra. The only ^{13}C-signals not completely resolved in the solid state ^{13}C spectrum (Figure 5.5b) are those signals for the aromatic carbons.

However, in the absence of ^{19}F decoupling, solid state ^{13}C-NMR signal intensities of 1-adamantyl fluorobenzoates are attenuated by ^{13}C-^{19}F dipolar coupling. The extent of attenuation depends upon the internuclear distances between the fluorine-19 and carbon-13 nuclei (4). Figures 5.6a and 5.6b provide one example. The 1-adamantyl trifluoromethylbenzoate signals are attenuated due to intermolecular ^{13}C-^{19}F dipolar coupling between neighboring 1-adamantyl p-trifluoromethyl benzoate molecules. The high resolution ^{13}C-NMR spectrum (Figure 5.6a) is included for reference. Spectrum 5.6b was obtained under the same pulse conditions as the 1-adamantyl benzoate spectrum (Figure 5.6b) to illustrate the spectral changes induced by the fluorine spin label.

Sample calculations involving the number of accumulations and the residual S/N ratios for 1-adamantyl p-trifluoromethylbenzoate and

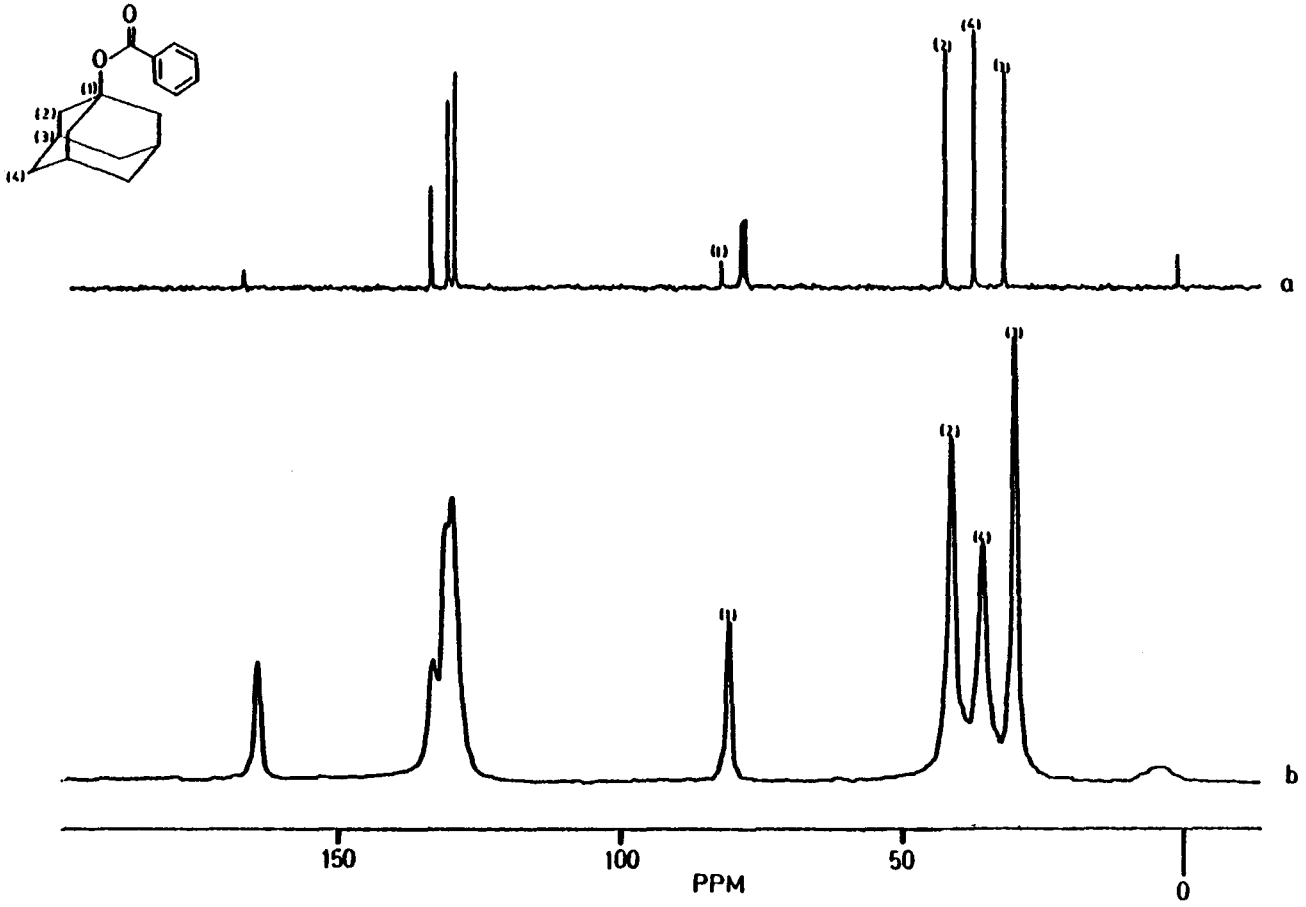

FIGURE 5.5 The 50.10 MHz proton noise decoupled ^{13}C-NMR spectrum of 1-adamantyl benzoate (a) and 15.0 MHz solid state ^{13}C CP/MAS NMR spectrum of 1-adamantyl benzoate (b). The chemical shift assignments for the adamantane ring carbons have been made in each spectrum. Spectrum (b) was obtained from 4000 FID accumulations of a single-contact cross polarization pulse sequence with a contact time (CT) of 2.0 ms and pulse repetition time of 2.0 s. Unless otherwise noted all ^{13}C CP/MAS spectra contained 1K FT data points with zero-filling to a total of 4K points. Also, no spectral linebroadening was applied.

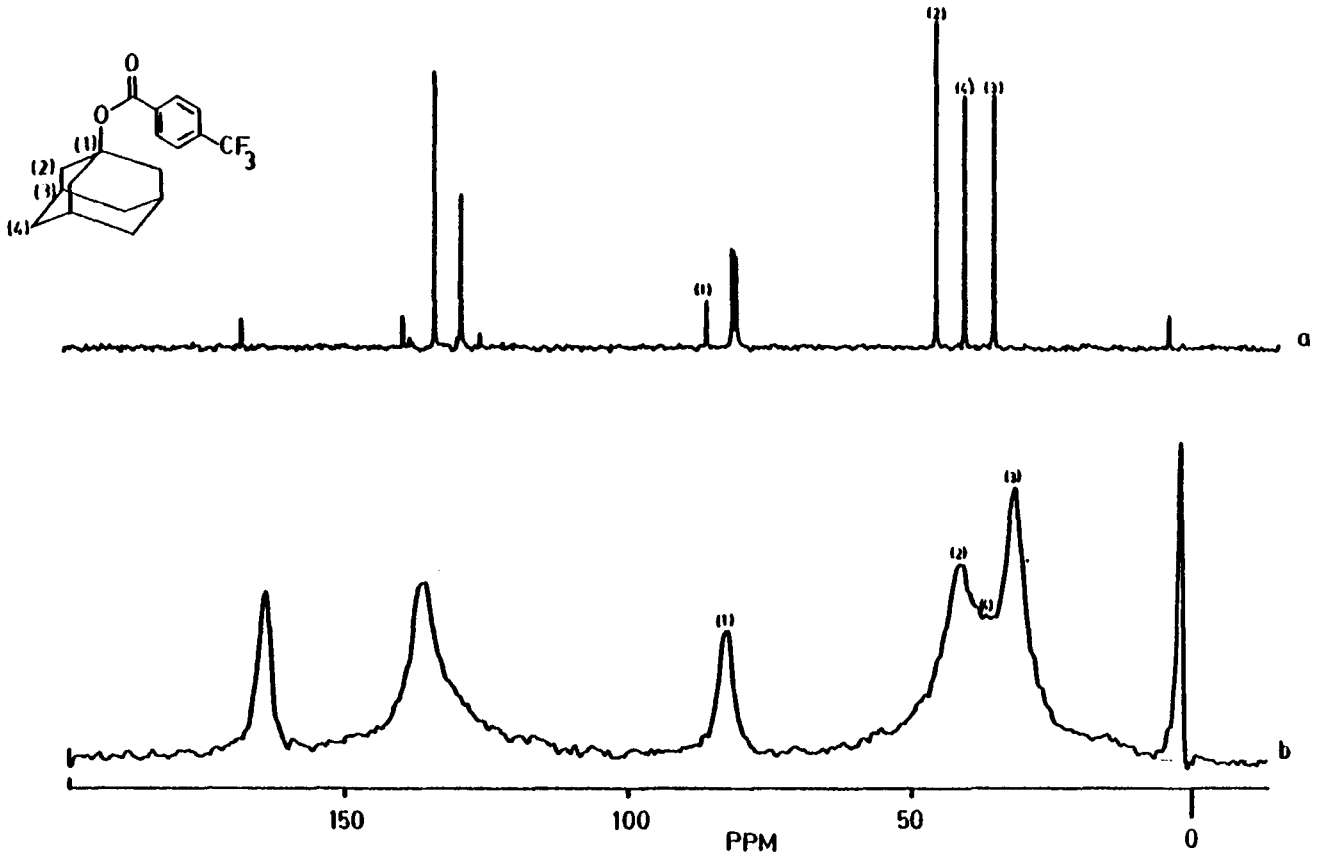

FIGURE 5.6 The 50.10 MHz proton noise decoupled ^{13}C-NMR spectrum of 1-adamantyl p-trifluoromethylbenzoate (a) and the 15.0 MHz solid state ^{13}C CP/MAS NMR spectrum of 1-adamantyl p-trifluoromethylbenzoate (b). Chemical shift assignments for the adamantane ring carbons have been made in each spectrum. Spectrum (b) was obtained from 4000 FID accumulations by a single-contact cross polarization pulse sequence with a CT = 2.0 ms and pulse repetition time = 2.0 s.

1-adamantyl pentafluorobenzoate are found in Table 5.4. The calculations were based on the following assumptions (217):

i) The absolute signal-to-noise is directly proportional to the number of nuclei (moles of sample) and to the square root of the number of accumulations. The sample weight was relatively constant for all samples.

ii) The data handling capabilities of the NMR computer is not limited as the number of scans increases.

iii) Instrument noise is assumed to remain constant during the course of the experiment.

The results are illustrated graphically in Figure 5.7. Thus, for any given carbon in the fluorine tagged molecules the ratio of expected S/N to observed S/N will provide the percentage of attenuation that is ascribed to ^{19}F in the immediate vicinity of that carbon.

As found in Table 5.4 (and Figure 5.7) the S/N for the entire ^{13}C CP/MAS spectrum of 1-adamantyl p-trifluoromethylbenzoate is reduced versus values obtained from the 1-adamantyl benzoate ^{13}C CP/MAS spectrum. The S/N ratio for the carbonyl signal is reduced by 60 percent, while the S/N for the adamantane ring carbons are attenuated almost 80 percent. Though the ^{19}F-nuclei are well removed from the adamantane ring system, the ^{13}C-signals corresponding to the alkyl carbons are also attenuated. This implies that ^{13}C-signals for the adamantyl ring and carbonyl carbons are attenuated due to intermolecular ^{13}C-^{19}F dipole coupling. However, this coupling may be modulated by complex molecular motion in the solid.

The solid state ^{13}C CP/MAS spectrum of 1-adamantyl pentafluorobenzoate (Figure 5.8) illustrates the extent of signal attenuation from

Table 5.4

Measured Signal-to-Noise S/N Ratios for Selected 1-Adamantyl Benzoate Derivatives

Samples		Benzoate	p-Trifluoromethyl Benzoate	Pentafluorobenzoate
Approx. sample wgt. (mg) ± 20 mg		600	600	600
Number of accumulations		4000	4000	4000
Measured signal/noise (S/N) Ratio	carbonyl	46.2	18.1	-
	quaternary (C-1)	61.9	13.4	1.9
	methylene (C-2)[1]	45.3	6.9	0.9
	methine (C-3)[1]	58.2	9.7	0.8
	methylene (C-4)[1]	31.1	5.0	1.2
Residual S/N %	carbonyl	1.00	0.39	
	quaternary	1.00	0.22	0.03
	methylene	1.00	0.15	0.02
	methine	1.00	0.17	0.01
	methylene	1.00	0.16	0.04
		1.00		

[1] S/N ratios were normalized to one carbon for C-2 and C-4 methylene signals and the C-3 methine signal.

^{13}C CP/MAS S/N RATIOS FOR 1-ADAMANTYL FLUORINATED DERIVATIVES

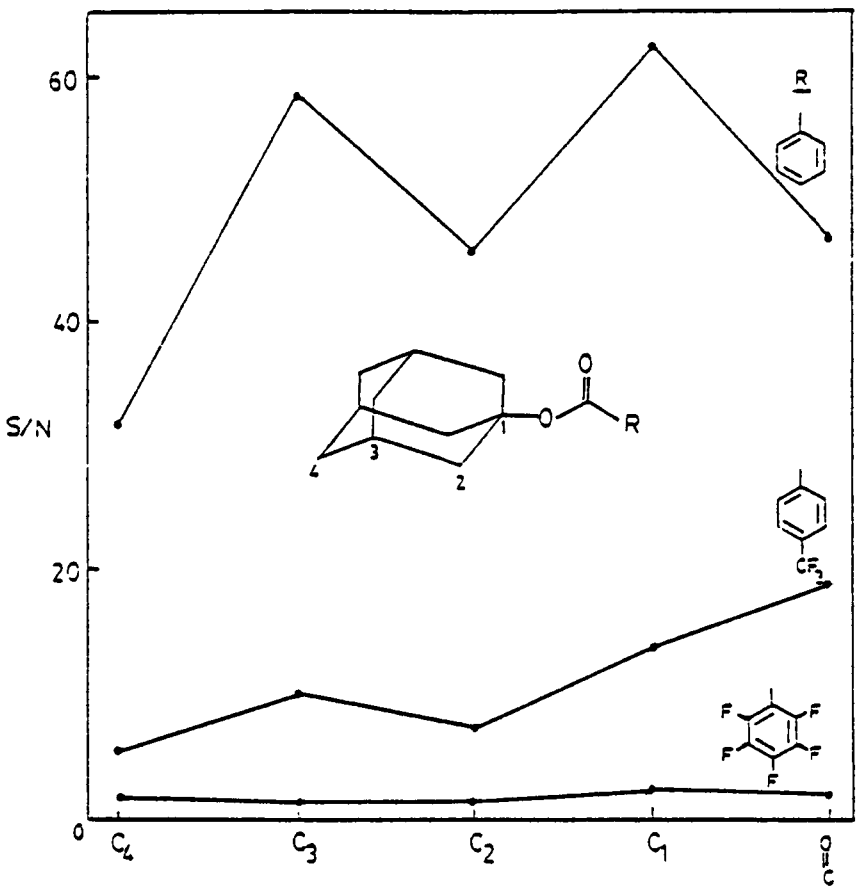

FIGURE 5.7 Dependence of ^{13}C CP/MAS S/N ratios for adamantane ring and carbonyl signals on the number of ^{19}F-nuclei present in the molecule.

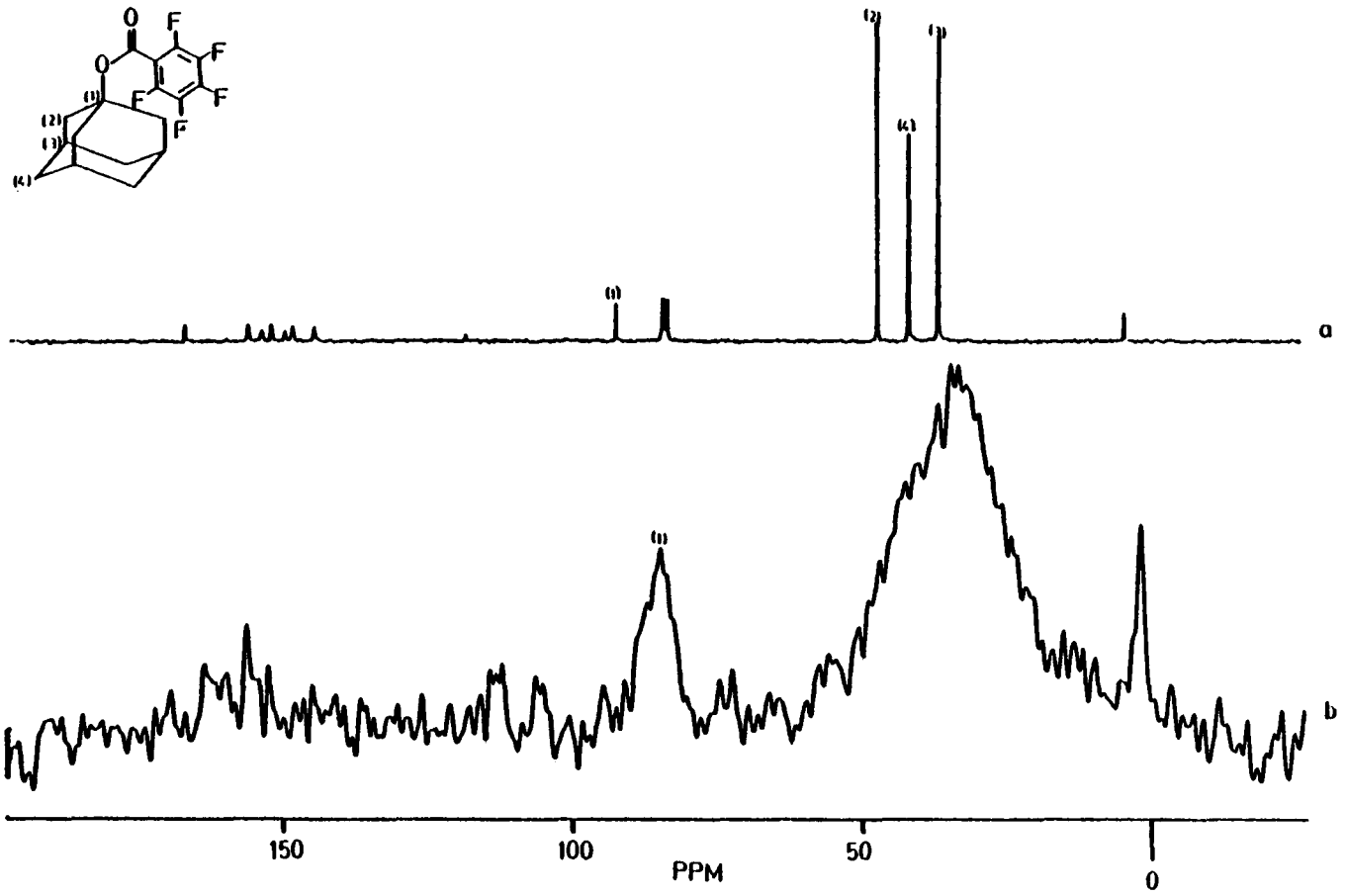

FIGURE 5.8 The 50.10 MHz proton noise decoupled ^{13}C-NMR spectrum of 1-adamantyl pentafluorobenzoate (a) and the corresponding 15.0 MHz solid state ^{13}C CP/MAS NMR spectrum. Chemical shift assignments for the adamantane ring carbons have been made in spectrum (a). Spectrum (b) was obtained from 4000 FID accumulations of a single-contact cross polarization pulse sequence with CT = 2.0 ms and pulse repetition time = 2.0 s.

both inter-and intramolecular ^{13}C-^{19}F dipolar coupling. Those signals for carbons directly bonded to a fluorine nucleus (i.e., the aromatic ring carbons) are totally eliminated by intramolecular ^{13}C-^{19}F coupling. The carbon signal for the adjacent carbonyl nucleus is also strongly attenuated. However, the S/N for all adamantyl alkyl carbon-13 signals in the spectrum have also been reduced by ~95%, when compared with the 1-adamantyl benzoate spectrum, Table 5.4 and Figure 5.7. Again this implies extensive intermolecular ^{13}C-^{19}F dipolar interactions. In this case, the ^{13}C-^{19}F coupling may again be modulated by anisotropic molecular motion within the system (i.e., rotation of the aromatic and adamantyl rings about their respective C_{2v} and C_{3v} symmetry axis).

Three other 1-adamantyl fluorobenzoate samples were examined. The compounds were 1-adamantyl p-fluorobenzoate, 1-adamantyl m-fluorobenzoate, and 1-adamantyl 2,6-difluorobenzoate. The solid state ^{13}C CP/MAS NMR spectra of these compounds are presented in Figure 5.9a, 5.9b, and 5.9c, respectively, and the S/N data summarized in Table 5.5. The S/N values in Table 5.5 were compared to those obtained for 1-adamantyl benzoate. One finds in Table 5.5 that the decrease in S/N for the carbonyl and adamantane ring alkyl carbon signals was very similar for each of the three compounds. The most striking difference is between the residual S/N ratios for the carbonyl signal of the 1-adamantyl p-fluorobenzoate and 1-admantyl 2,6-fluorobenzoate cases. In the former case, the carbonyl signal intensity was reduced ~50 percent whereas in the latter case the signal was attenuated ~90 percent. This illustrated that intramolecular ^{13}C-^{19}F dipole coupling

Table 5.5

Measured Signal-to-Noise S/N Ratios for 1-Adamantyl Fluorobenzoates

Samples		1-Adamantyl Benzoate	1-Adamantyl p-Fluorobenzoate	1-Adamantyl m-Fluorobenzoate	1-Adamantyl 2,6-Difluoro- benzoate
Approx. sample wgt. (mg) ± 20 mg		600	600	600	600
Number of accumulations		4000	4000	4000	4000
Measured signal/noise (S/N) Ratio	carbonyl	46.2	20.3	14.8	3.1
	quaternary (C-1)	61.9	10.6	15.0	12.8
	methylene (C-2)[1]	45.3	5.7	8.3	8.2
	methine (C-3)[1]	58.2	9.9	14.9	15.7
	methylene (C-4)[1]	31.1	6.7	8.5	8.7
Residual S/N %	carbonyl	1.00	0.44	0.32	0.08
	quaternary (C-1)	1.00	0.17	0.24	0.21
	methylene (C-2)	1.00	0.12	0.18	0.18
	methine (C-3)	1.00	0.17	0.25	0.27
	methylene (C-4)	1.00	0.21	0.27	0.28

FIGURE 5.9

The solid state 15.0 MHz ^{13}C CP/MAS NMR spectra for 1-adamantyl p-fluorobenzoate (a), 1-adamantyl m-fluorobenzoate (b), and 1-adamantyl 2,6-difluorobenzoate (c). Chemical shift assignments for the adamantane ring carbons have been made in each spectrum. Each spectrum was obtained from 4000 FID accumulations by a single-contact cross polarization pulse sequence with a CT = 2.0 ms and pulse repetition time = 2.0 s.

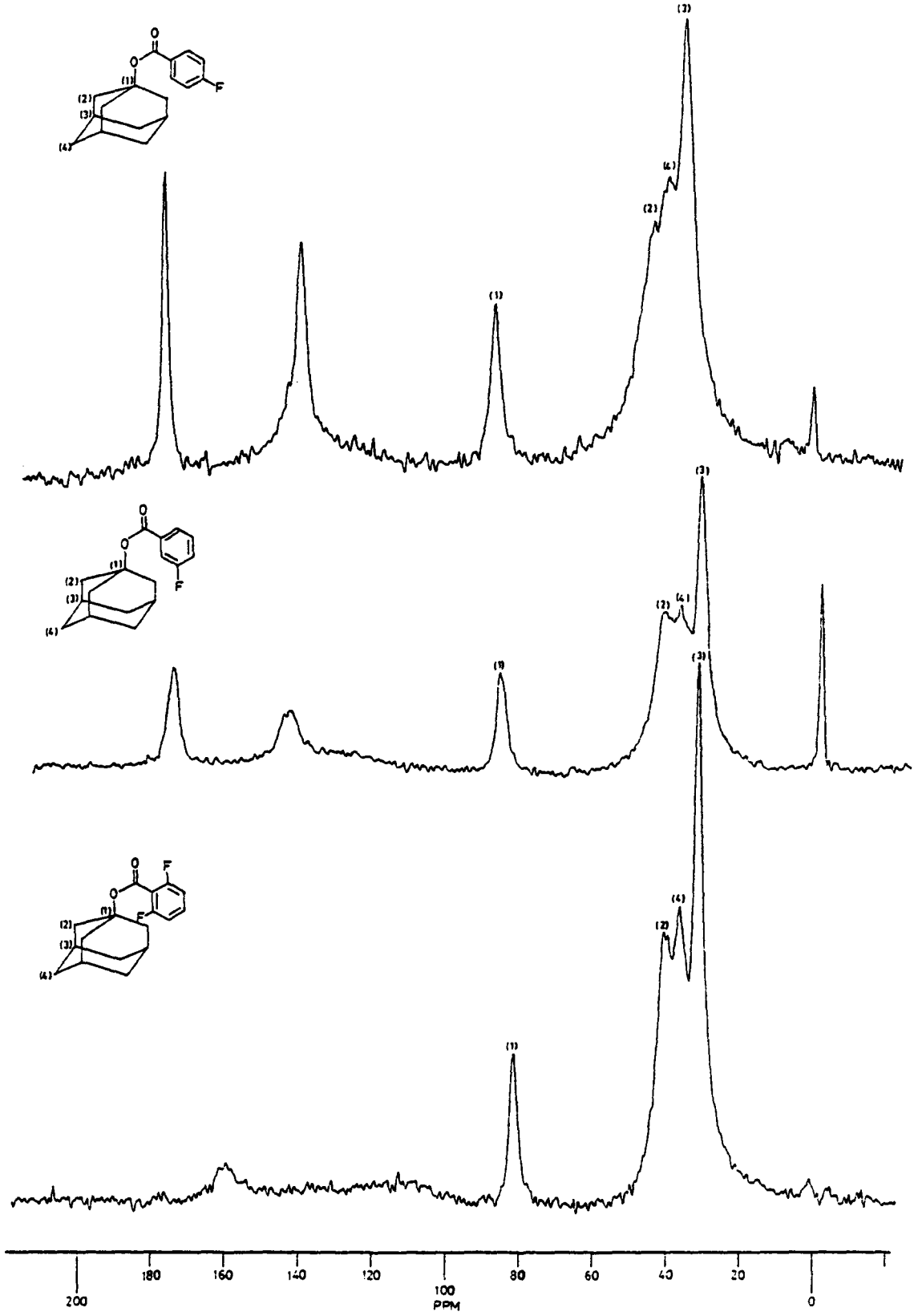
O
O
F
(1)
(2)
(3)
(4)
200
180
160
140
120
100
80
60
40
20
0
PPM

was the prominent interaction at this carbon site, for the 1-adamantyl 2,6-difluorobenzoate compound. The effects of the ^{13}C-^{19}F intramolecular interactions fall-off rapidly, as noted by the rise in S/N for the quaternary and other carbon signals in the ^{13}C CP/MAS 1-adamantyl 2,6-difluorobenzoate spectrum.

The slight increase in S/N for the ^{13}C NMR signals for the adamantyl ring carbons in the 1-adamantyl m-fluorobenzoate and 1-adamantyl 2,6-difluorobenzoate spectra versus the 1-adamantyl p-fluorobenzoate spectrum may be attributed to more effective motional averaging of the ^{13}C-^{19}F coupling by rapid rotation of the aromatic ring. Maciel et. al. (185) have shown that rapid rotation of an aromatic ring (i.e., pyridine) about its C_{2v} axis can average dipole coupling in certain solid systems. At the time, they were studying the characteristics of pyridine adsorbed onto silica/alumina surfaces by solid state ^{15}N and ^{13}C NMR. They also found that the position of the carbon nuclei on the aromatic ring was important. For rotation about the C_{2v} axis the carbon para to the pyridine nitrogen atom was least effective in averaging ^{13}C-^{1}H dipolar coupling, while the ortho and meta carbons were more efficient in averaging the ^{13}C-^{1}H dipolar coupling.

For the cases being considered, rotation of the aromatic and adamantyl ring systems about their respective C_{2v} and C_{3v} axes reduce ^{13}C-^{19}F dipole coupling (i.e., improve S/N values) for the 1-adamantyl m-fluorobenzoate and 1-adamantyl 2,6-difluorobenzoate compounds. In the 1-adamantyl p-fluorobenzoate case the position of the ^{19}F nucleus is unchanged by rotation of the aromatic ring about the C_{2v} axis. There-

fore, the parafluoro group is less effectively motionally averaged in comparison with the fluoro group in the ortho or meta position. This, allows stronger dipolar coupling interactions to persist (i.e., lower S/N values). However, because the values for the three compounds are very similar, this implies that rotation of the admantane ring about its C_{3v} axis is more effective in reducing ^{13}C-^{19}F dipole coupling than aromatic ring rotation.

As found in the previous section, the interpretation of the data concerning the attenuation of ^{13}C signals by ^{13}C-^{19}F intermolecular dipole interactions depends upon the molecular mobility of the 1-admantyl benzoate system. Therefore, a series of relaxation studies has been performed on 1-adamantyl benzoate to determine $T_{1\rho}$ (^{1}H), and $T_{1\rho}$ (^{13}C) relaxation parameters.

Relaxation Studies - $T_{1\rho}$ (^{1}H) Measurments

Proton $T_{1\rho}$ values for 1-adamantyl benzoate were calculated from the dependency of the ^{13}C CP intensities ln (I/I_{ρ}) for different contact times (Figures 5.10 - 5.12) and are presented in Table 5.6. For the sample, the $T_{1\rho}$ values obtained from the carbonyl and four adamantyl ring carbon ^{13}C resonance peaks are relatively the same. A total of fifteen spectra (data points) were used to determining the $T_{1\rho}$ value (Figure 5.10). The average proton $\langle T_{1\rho} \rangle$ value for the molecule was 51.12 ms. Typically in a molecular system (i.e., polymers) $T_{1\rho}$ (^{1}H) values reflect motional processes which were most efficient in relaxing the entire molecule. In this case, the complex rotation of the

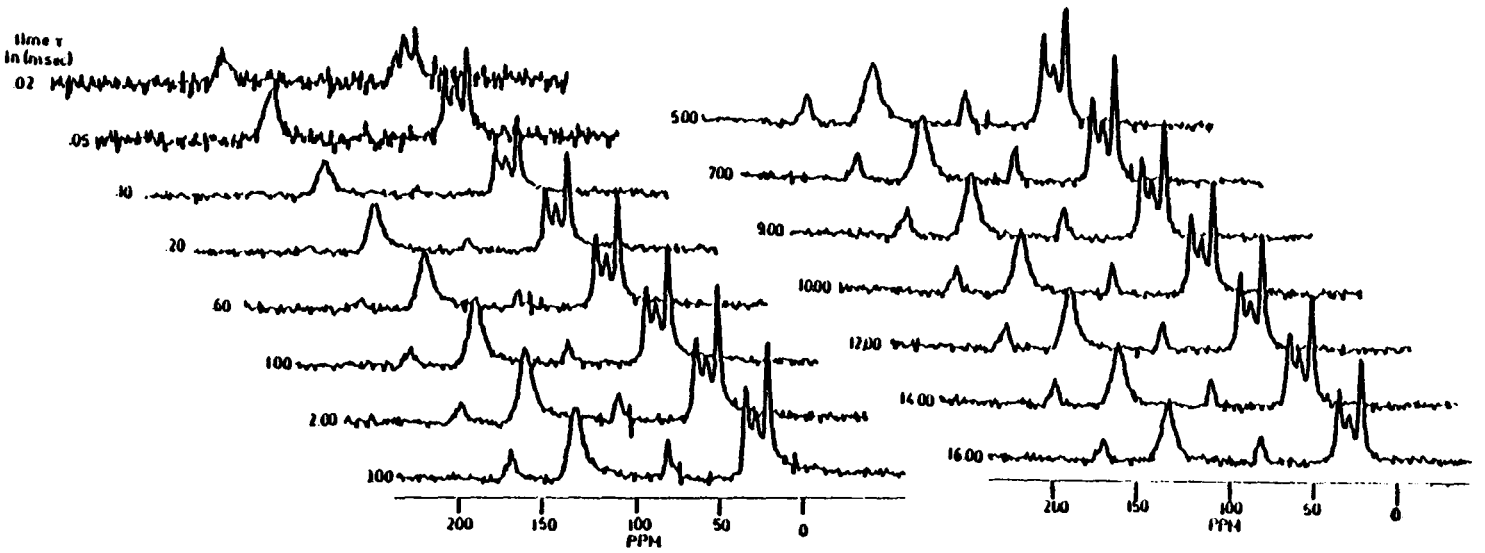

FIGURE 5.10 CP/MAS ^{13}C spectra of 1-adamantyl benzoate obtained at increasing contact times (ms).

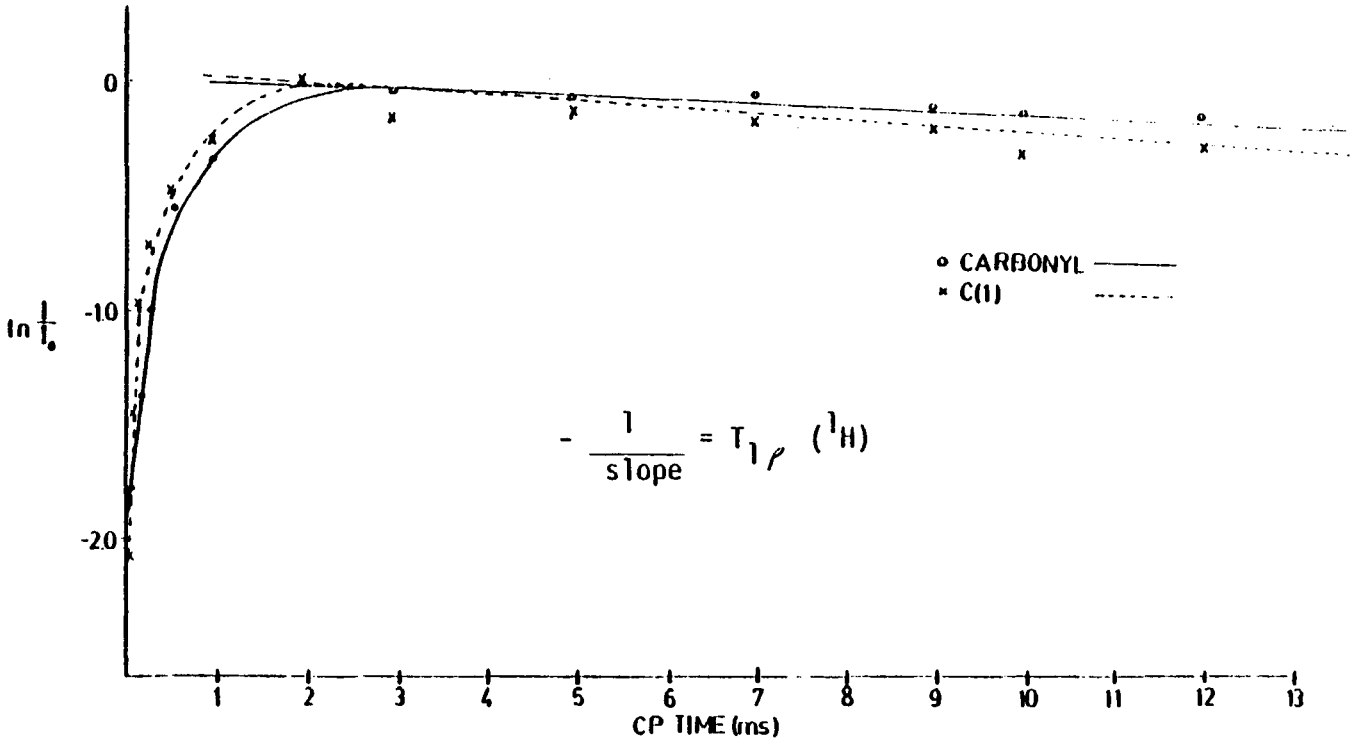

FIGURE 5.11 Proton $T_{1\rho}$ data for the carbonyl and quaternary C(1) carbon of 1-adamantyl benzoate. The $T_{1\rho}$ values were calculated from the latter portion of the ln I/I_0 versus CP time curve.

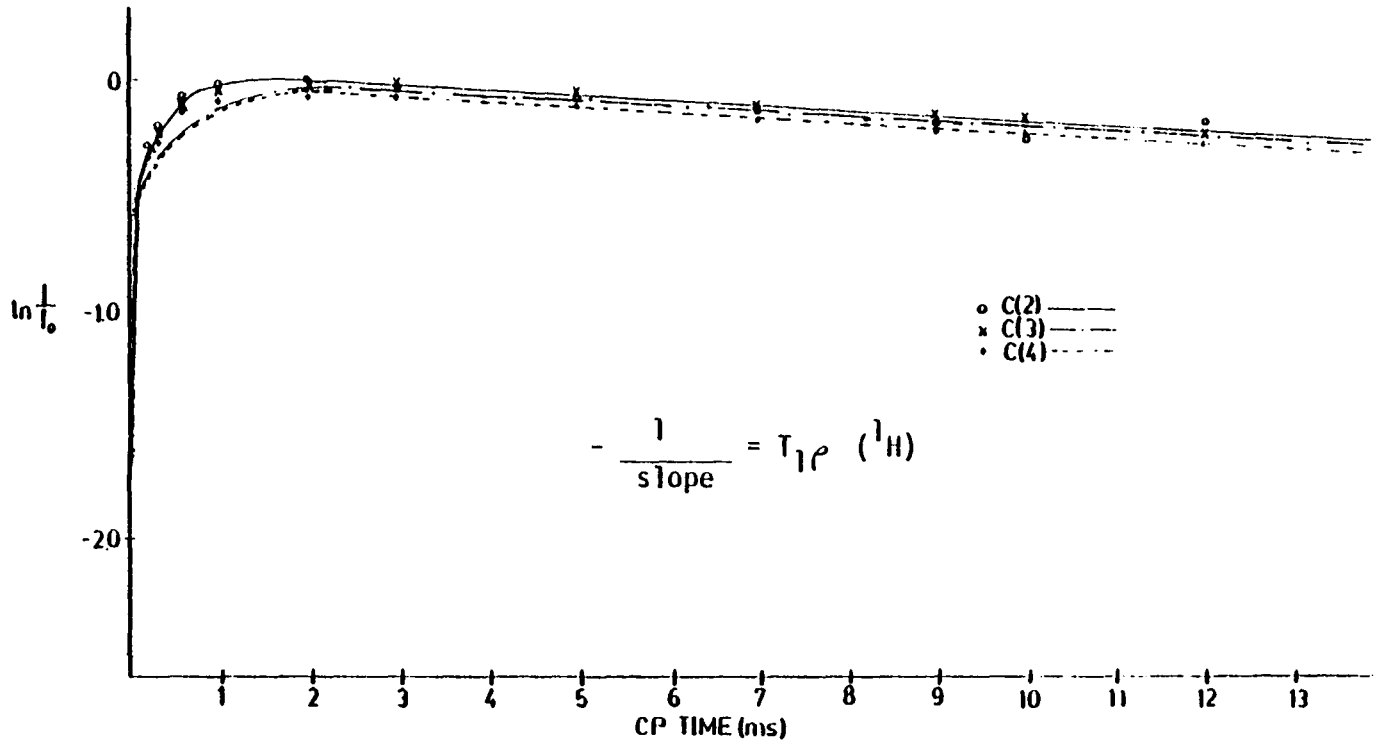

FIGURE 5.12 Proton $T_{1\rho}$ data for the methylene (i.e. C(2) and C(4)) and methine C(3) carbons of 1-adamantyl benzoate. The $T_{1\rho}$ values were calculated from the latter portion of the ln I/I_0 versus CP time curve.

Table 5.6

Relaxation Values for Selected Carbons of 1-Adamantyl Benzoate

Carbon	(C-1) quaternary	(C-2) methylene	(C-3) methine	(C-4) methine	carbonyl
$T_{1\rho}$ $(^{1}H)_{(MS)}$	47.50	46.11	50.36	54.24	55.28
$T_{1\rho}$ $(^{13}C)_{(MS)}$	86.24	18.06	20.70	22.18	184.50

adamantyl and aromatic rings have been sufficiently rapid as to average slower relaxation processes (i.e. relaxation of the nonprotonated quaternary and carbonyl carbons). As will be seen in the next section $T_{1\rho}$ (^{13}C) values reflect a more accurate value for the relaxation of individual carbons in the molecule.

Relaxation Studies - $T_{1\rho}$ (^{13}C) Measurements

In Table 5.6 the ^{13}C NMR $T_{1\rho}$ values are presented for the 1-adamantyl benzoate sample. The $T_{1\rho}$ values were calculated from the plot of ln I versus different delay times (Figure 5.13 and Figure 5.15) for the carbonyl and adamantyl ring carbons. The carbon $T_{1\rho}$ data are reported in Table 5.6. The values are calculated from the initial portion of the plot of ln I versus delay time (approximately 0.1 -0.8 ms) curve. This is done because $T_{1\rho}$ (^{13}C) values are dependent on the homogeneity of the proton and carbon H_1 fields (e.g., during the spin lock period). Also, spin-spin (T_2) and spin lattice (T_1) processes begin to contribute to molecular relaxation at longer delay times (87). These factors cause nonlinearity in the plots at long delay periods.

The $T_{1\rho}$ (^{13}C) values for the protonated adamantyl ring carbons were very similar ≈18-22 ms, suggesting that some degree of molecular motion was present within the system. The $T_{1\rho}$ (^{13}C) values for the aromatic ring carbons were slightly longer with $T_{1\rho}$ (^{13}C) ≈ 30 ms. However, the $T_{1\rho}$ (^{13}C) values for the two ring systems imply they were rotating at similar rates. Conversely, the quaternary (C-1) and carbonyl carbons have much longer $T_{1\rho}$ (^{13}C) values, 86.24 ms and 184.50 ms, respectively, impling less molecular motion. This was anticipated on the basis of

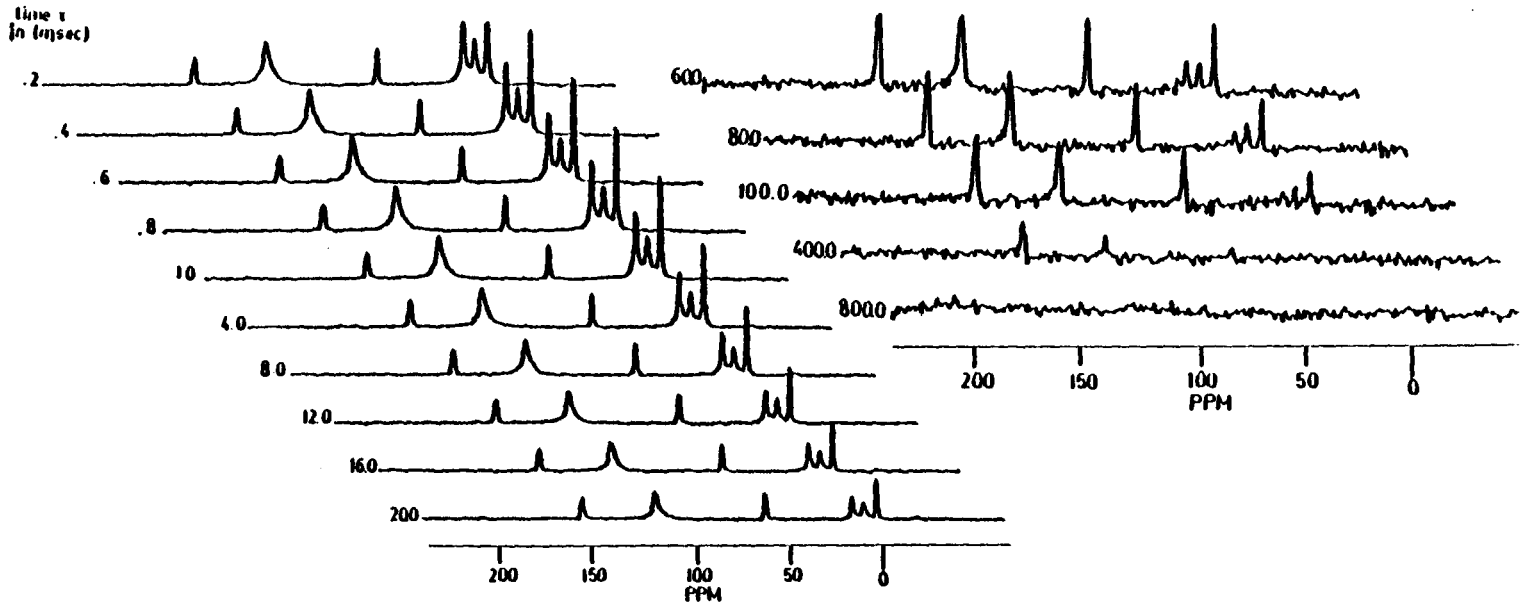

FIGURE 5.13 CP/MAS ^{13}C spectra of 1-adamantyl benzoate obtained at increasing ^{1}H decoupler delay times.

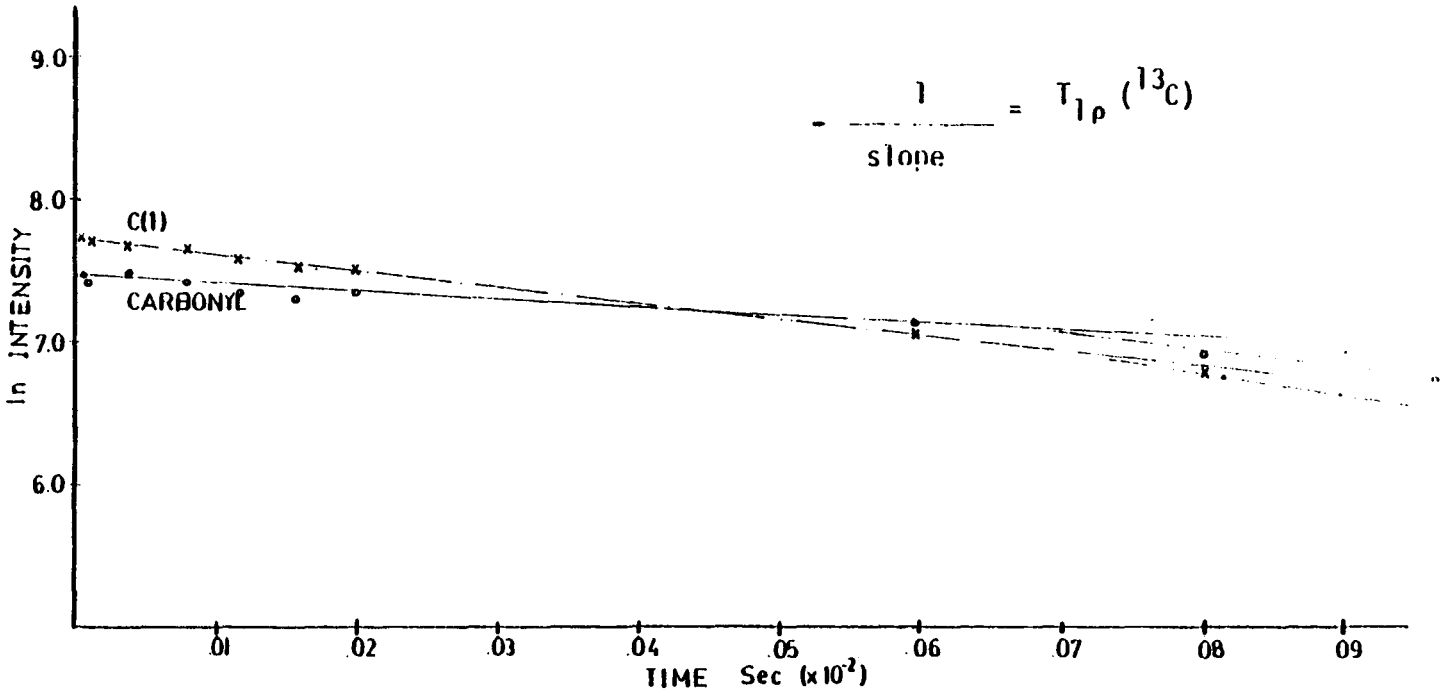

FIGURE. 5.14 Carbon $T_{1\rho}$ data for the carbonyl and quaternary C(1) carbon of 1-adamantyl benzoate. The carbon $T_{1\rho}$ values were obtained from the initial part of the ln Intensity versus time decay curve.

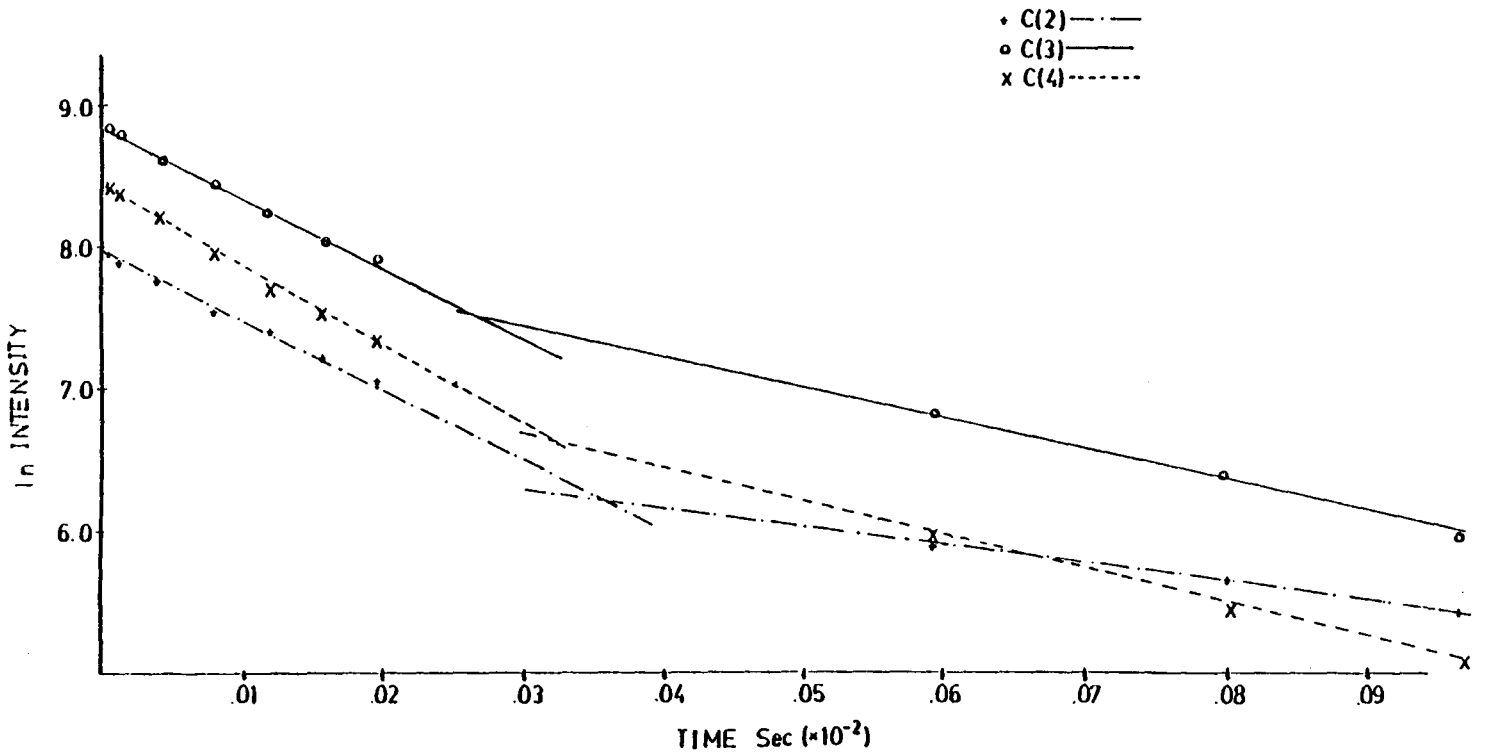

FIGURE 5.15 Carbon $T_{1\rho}$ data for the methylene (i.e., C(2) and C(4)) and methine C(3) carbons of 1-adamantyl benzoate. The carbon $T_{1\rho}$ values were obtained from the initial part of the ln Intensity versus time delay curve.

previous reports (220, 221). The $T_{1\rho}$ (^{1}H) and $T_{1\rho}$ (^{13}C) data together are consistent with the hypothesis that different motional processes for the aromatic and adamantyl rings are present in this system. More importantly, the motion of the two rings may be sufficient to modulate the intermolecular ^{13}C-^{19}F dipole coupling.

Line Broadening in the Solid State ^{13}C CP/MAS Spectra of 1-Adamantyl Fluorobenzoate

By comparing the solid state ^{13}C CP/MAS spectra of 1-adamantyl fluorobenzoates to 1-adamantyl benzoate one finds that linewidths for the ^{13}C-spectra are usually broader for the ^{13}C CP/MAS spectra of the 1-adamantyl fluorobenzoates. The linewidths were measured at the half-height (ν 1/2) for the carbonyl and adamantyl ring alkyl carbon signals and are summarized in Table 5.7. As indicated some of the linewidth measure-ments are only rough approximations. In certain cases resolution was poor for the adamantyl C-2, C-3, and C-4 carbon signals (see Figures 5.6 -5.9) and line shapes were estimated from only the top portion of the signal.

The principle source of line broadening is ^{13}C-^{19}F dipolar coupling. The observation that the linewidths increase by factors of only 2-4 (considering ^{13}C-^{19}F dipolar coupling can be as large as 10^4 Hz) is further evidence that the molecule has either: 1) components of anisotropic motion to reduce this coupling and/or 2) the residual ^{13}C-^{19}F dipolar coupling must be less than the sample spinning speed

Table 5.7

Linewidths of Carbonyl and Adamantane Ring Carbons in 1-Adamantyl Benzoates

R	^{13}C linewidth measured at 1/2 hgt (Hz)				
	carbonyl	1	2	3	4
Benzoate	17.74	15.92	22.13	16.93	27.34
p-Fluorobenzoate	25.03	39.92	134.38[1]	70.31	182.80[1]
p-Trifluoromethylbenzoate	38.85	40.72	121.93	74.51	237.93[1]
m-Fluorobenzoate	47.15	40.32	104.03[1]	55.19	133.80[1]
2,6-Difluorobenzoate	80.84	40.32	118.24[1]	47.83	128.87[1]
Pentafluorobenzoate in Thiourea	-	36.59	44.41	37.20	52.81
Pentafluorobenzoate	-[2]	-[2]	-[2]	-[2]	-[2]

1. Line shapes estimated from very small point of original peak.

2. Values could not be determined, due to insufficient spectral resolution.

(~2.0 kHz). In addition, scalar ^{13}C-^{19}F coupling could be a factor influencing these linewidths, this has been observed in other work (220).

Other sources of broadening may also contribute to the linewidths observed in this study (221). An insufficient proton decoupling field (H_2) would also broaden ^{13}C-linewidths. However, linewidths for 1-adamantyl benzoate were ≈20 Hz, which is excellent for the JEOL FX60 instrument (i.e., factory specifications require 18 Hz resolution on a standard hexamethylbenzene (HMB) sample). A second major source of line broadening would arise from the inability to accurately set the magic angle. Standard adamantane and HMB samples were checked prior to each experiment to insure good spectra resolution and establish the position of the magic angle. However, small discrepancies in rotor design, etc. can change the magic angle setting between samples (81, 132, 171, 172), producing broader linewidths.

Isolation of 1-Adamantyl Fluorinated Benzoates in Solid Matrices

It is important to realize that magic angle spinning (MAS) can reduce chemical shift anisotropies and decouple weak dipolar interactions (e.g., for those interactions have strengths (in the 0.1 -1 kHz range) lower than that of the spinning frequency (222, 223). However, as indicated above, MAS has not completely removed the ^{13}C-^{19}F dipolar coupling present.

Since MAS did not completely average the intermolecular ^{13}C-^{19}F dipolar coupling interactions and ^{19}F decoupling was not available, an attempt was made to separate intra-and inter-molecular dipolar interactions by isolating the fluorinated 1-adamantyl benzoate derivative in a noninteracting solid matrix. The three different isolation techniques studied are discussed below.

The first attempts at isolating 1-adamantyl pentafluorobenzoate in a solid matrix employed co-crystallization with hexamethylbenzene. Hexamethylbenzene was chosen as the host lattice because it exhibits only two ^{13}C resonances which do not overlap with the ^{13}C signals from the adamantyl sample. However, there was little useable information contained in this spectrum. One explanation is that even at a 20% concentration, 1-adamantyl pentafluorobenzoate was not effectively isolated by the HMB and that intramolecular dipole coupling interactions continued to attenuate ^{13}C signals.

Mixtures of 10:80 w/w ratio of 1-adamantyl pentafluorobenzoate: sulfur were also studied. An advantage in using sulfur is the absence of interferring resonances in the ^{13}C-spectrum. As indicated in Figure 5.16b the 1-adamantyl pentafluorobenzoate was apparently diluted to some extent since the C-3 and C-4 signals of the admantane ring appear to be better resolved. This was an improvement over the undiluted 1-adamantyl pentafluorobenzoate spectrum (Figure 5.16a), which revealed one broad envelope for ^{13}C-signals in the alkyl region of the spectrum. The absence of totally resolved peaks suggests that the mixture was not

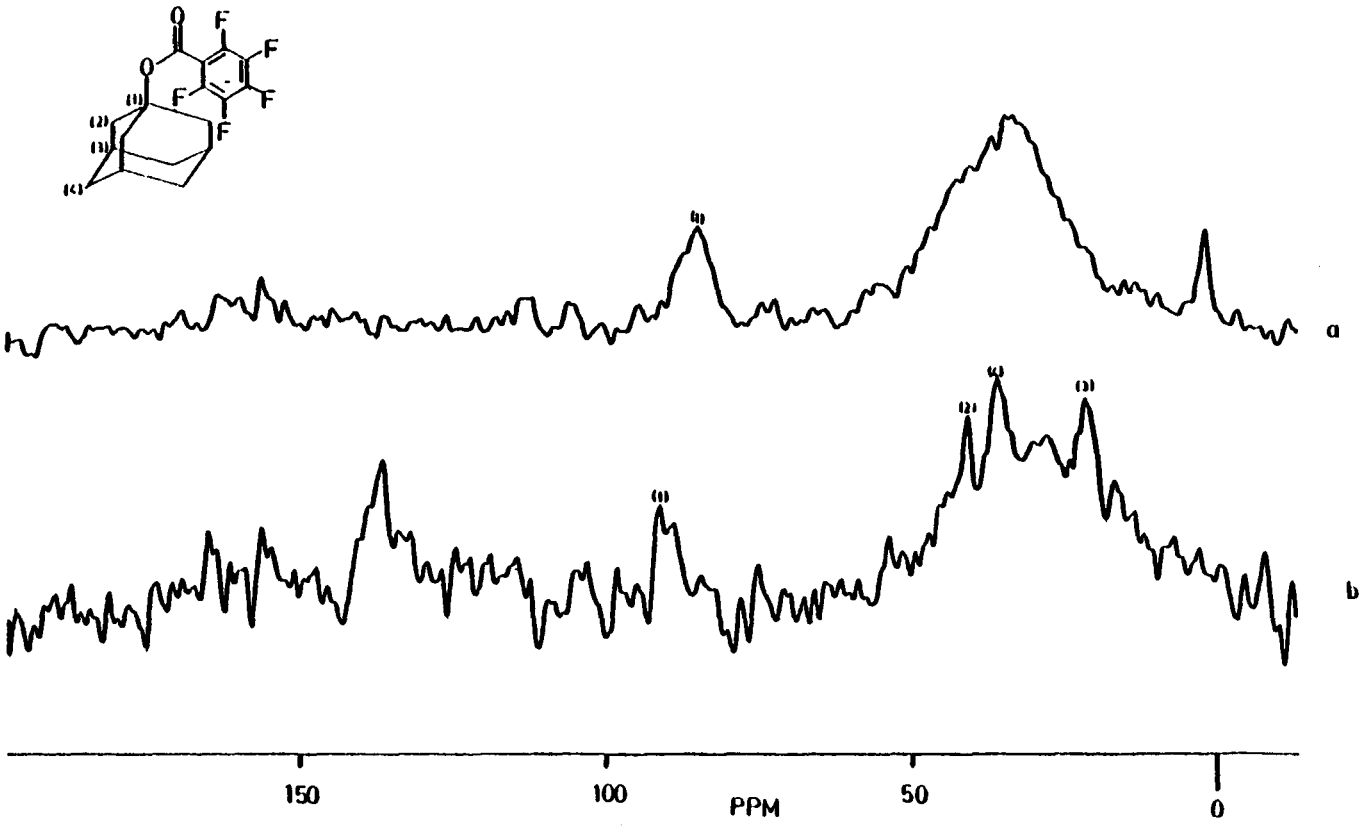

FIGURE 5.16 The 15.0 MHz ^{13}C CP/MAS spectrum of 1-adamantyl pentafluorobenzoate (a) and the corresponding spectrum of 1-adamantyl pentafluorobenzoate diluted in sulfur (b). Spectrum (a) was obtained from 4000 FID accumulations with a CT = 2.0 ms and pulse repetition time = 2 sec. Spectrum (b) was obtained under similar pulse conditions but required 24000 FID accumulations. Each spectral FID was exponentially apodized approximately 10 Hz.

totally homogeneous. There may have been crystalline regions where 1-adamantyl pentafluorobenzoate was not completely diluted in the matrix.

Typically, urea is used to inclathrate n-alkanes but not cyclic alkanes. However, thiourea inclusion complexes of normal and cyclic alkanes have been used in various NMR studies for several years (214). Attempts were made to isolate 1-adamantyl fluorobenzoates in thiourea inclusion complexes.

Thiourea is known to form hexagonal unit cells the channels of the cell being α_o = 15.8 A and c_o = 12.5 A (214). Figure 5.17b and 5.17c illustrate the ^{13}C CP/MAS spectrum of the thiourea/1-adamantyl p-fluorobenzoate inclusion complex obtained at 15.0 and 50.1 MHz, respectively. Although the results obtained from the two instruments are consistent, the spectral resolution and sensitivity of the 50.1 MHz ^{13}C CP/MAS spectrum (Figure 5.17c) is superior to the 15.0 MHz spectrum.

Both spectra reveal that once isolated in the thiourea inclusion complex the intermolecular ^{13}C-^{19}F dipolar interactions are significantly reduced. As expected, signals for every unique ^{13}C nucleus in the molecule are observed, excluding the ^{13}C-signal corresponding to the carbon directly attached to the ^{19}F nucleus.

It has also been shown that more than one molecule can be held in the thiourea inclusion channel, suggesting that the molecules are held in a head-to-toe type configuration (214). Therefore, the p-fluoro group may still potentially interact with at least one other 1-adamantyl

FIGURE 5.17

The 15.0 MHz ^{13}C CP/MAS spectra of 1-adamantyl p-fluorobenzoate (a) and the corresponding thiourea solution complex obtained at 15.0 MHz (b) and 50.1 MHz (c). Spectrum (a) was obtained from 4000 FID accumulations with a CT = 2.0 ms and pulse repetition time = 2.0 s. Spectra (b) and (c) were obtained under similar pulse conditions. However, spectrum (b) was the result of 24000 FID accumulations and spectrum (c) 5000 accumulations. No exponential linebroadening was used to reduce S/N in any of the given spectra.

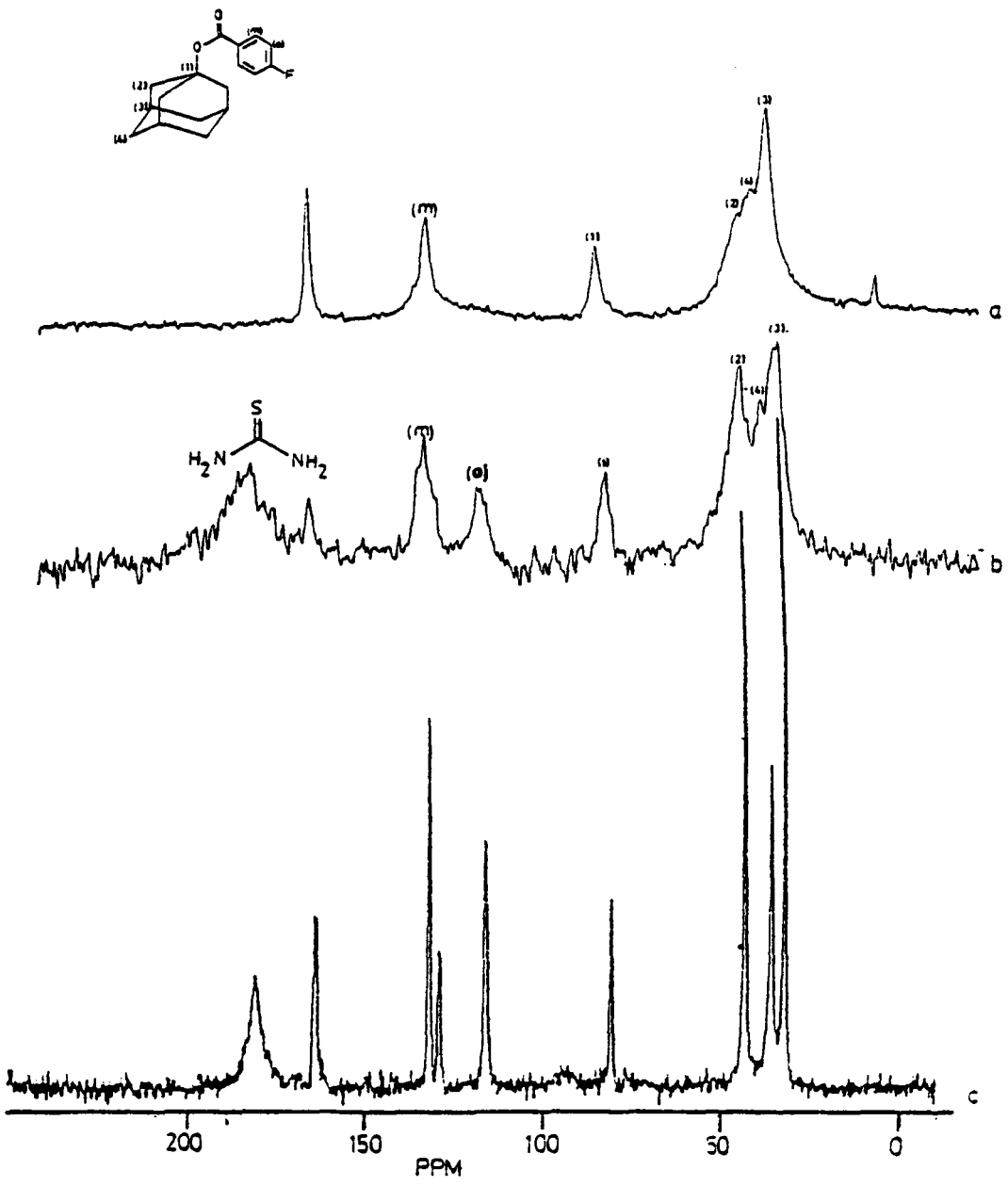
a
b
c
200
150
100
50
0
PPM

p-fluorobenzoate molecule. By integrating the quantitative solution ^{13}C spectrum, obtained under gated-coupling pulse conditions (80), the ratio of thiourea to 1-adamantyl p-fluorobenzoate is found to be ~ 19:1 (i.e., approximately one 1-adamantyl p-fluorobenzoate molecule per 3 thiourea unit cells) which is consistent with previous studies of similar complexes (214).

Thiourea inclusion complexes of 1-adamantyl pentafluorobenzoate have also been prepared. Figure 5.18a, 5.18b, and 5.18c compares the 15 MHz ^{13}C CP/MAS spectra of the uncomplexed 1-adamantyl pentafluorobenzoate, the corresponding thiourea inclusion complex and the reference spectrum for 1-adamantyl benzoate. Again, the intermolecular dipolar interactions are apparently reduced for the 1-adamantyl pentafluorobenzoate in the thiourea complexes (Figure 5.18a and 5.18b). The carbons directly bound to ^{19}F nuclei are not observed (Figure 5.18b) due to direct ^{13}C-^{19}F dipolar coupling. The carbonyl signal has also been significantly attenuated. However, comparing the ^{13}C alkyl regions of 1-adamantyl pentafluorobenzoate and 1-admantyl benzoate (Figures 5.18b and 5.18c respectively), one observes similarities in the two spectra that indicate the ^{13}C-^{19}F intermolecular interactions have been reduced.

The spectrum for the thiourea/1-adamantyl pentafluorobenzoate inclusion complex offers the opportunity to explore the distance dependence of the dipole-dipole interaction. If one assumes that

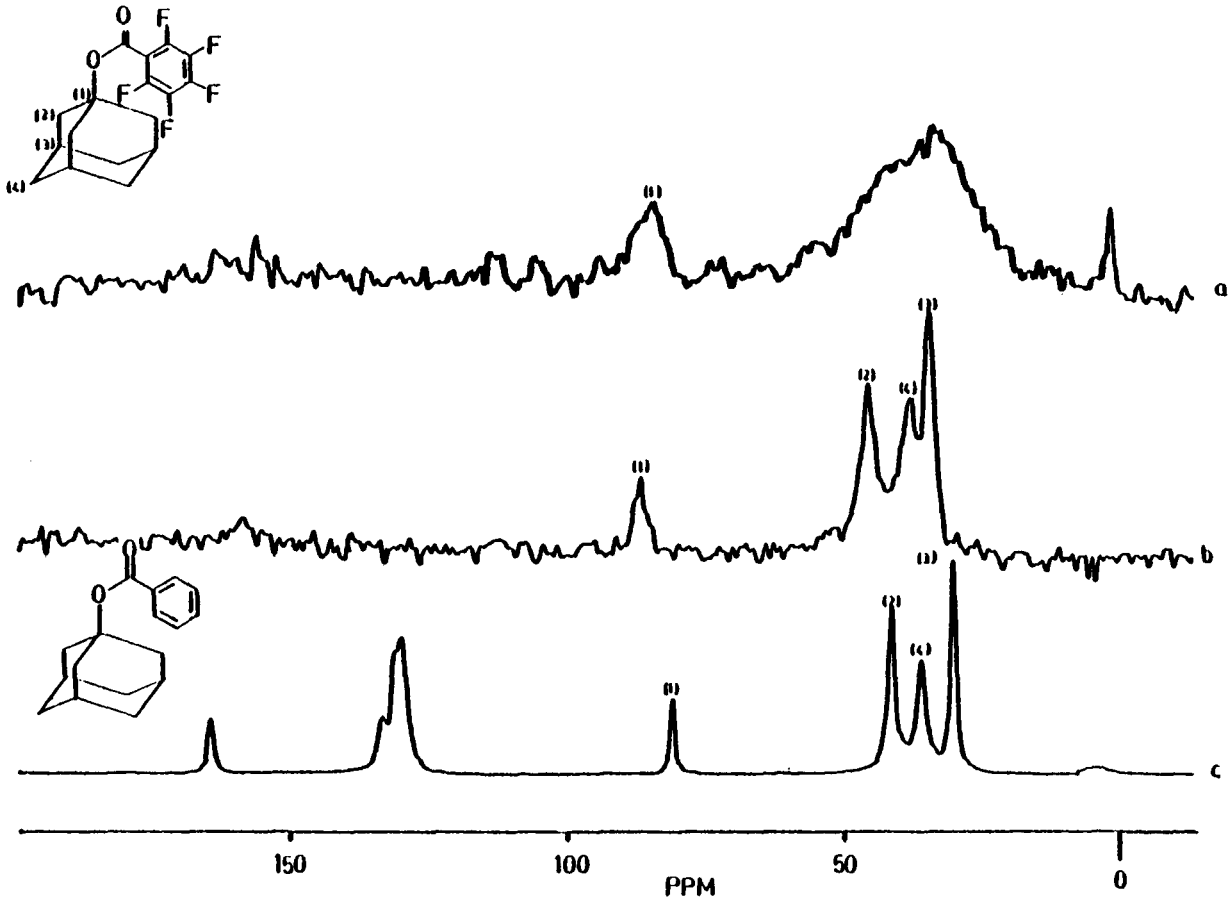

FIGURE 5.18 The 15.0 MHz ^{13}C CP/MAS spectra of 1-adamantyl pentafluorobenzoate (a), the corresponding thiourea inclusion complex (b), and 1-adamantyl benzoate (c). Spectra (a) and (c) were obtained from 4000 FID accumulations with a CT = 2.0 ms and pulse repetition time = 2.0 sec. Spectrum (b) was obtained under similar pulse conditions, but was the result of 36,000 FID accumulations.

signal-to-noise is proportional to r^{-3}, that is:

$$D_{^{13}C^{19}F} \propto \frac{1}{r^3} \qquad (30)$$

By plotting the S/N intensity versus $1/r^3$ (Å) a linear curve should be obtained. The distance values were obtained by building a Dreiding model of the 1-adamantyl pentafluorobenzoate molecule and directly measuring distances. The conformation used for this calculation is illustrated in Figure 5.19. Using a conversion factor of ≈1.5Å per 4 cm (distance of a sp^3 C-H bond), distances in Å were calculated, (Table 5.8). Also, only those (r) values from the ortho aromatic fluorine atom to the carbons on the adamantane ring were used in this calculation. While this is a "sledge-hammer and chisel" technique used to measure this dependence the S/N versus $1/r^3$ plot (Figure 5.19) is fairly good (Correlation Coefficient = 0.7945).

The initial distance measurements were taken utilizing the more stable molecular conformation, (e.g., with the adamantane and aromatic ring being separated at a maximum distance). A second set of measured distances were obtained where the two rings were in closest proximity (Table 5.9). The average r values for the longest and closest measurements were calculated and the S/N versus "averaged" $1/r^3$ values were plotted. This curve gave an even better linear correlation (Correlation Coefficient = 0.9509) (Table 5.9, Figure 5.20), illustrating that the dipolar coupling term <u>is</u> dependent on the distance between interacting nuclei.

FIGURE 5.19

The experimental ^{13}C CP/MAS S/N values for 1-adamantyl pentafluorobenzoate thiourea complex as a function of estimated r^{-3} values.

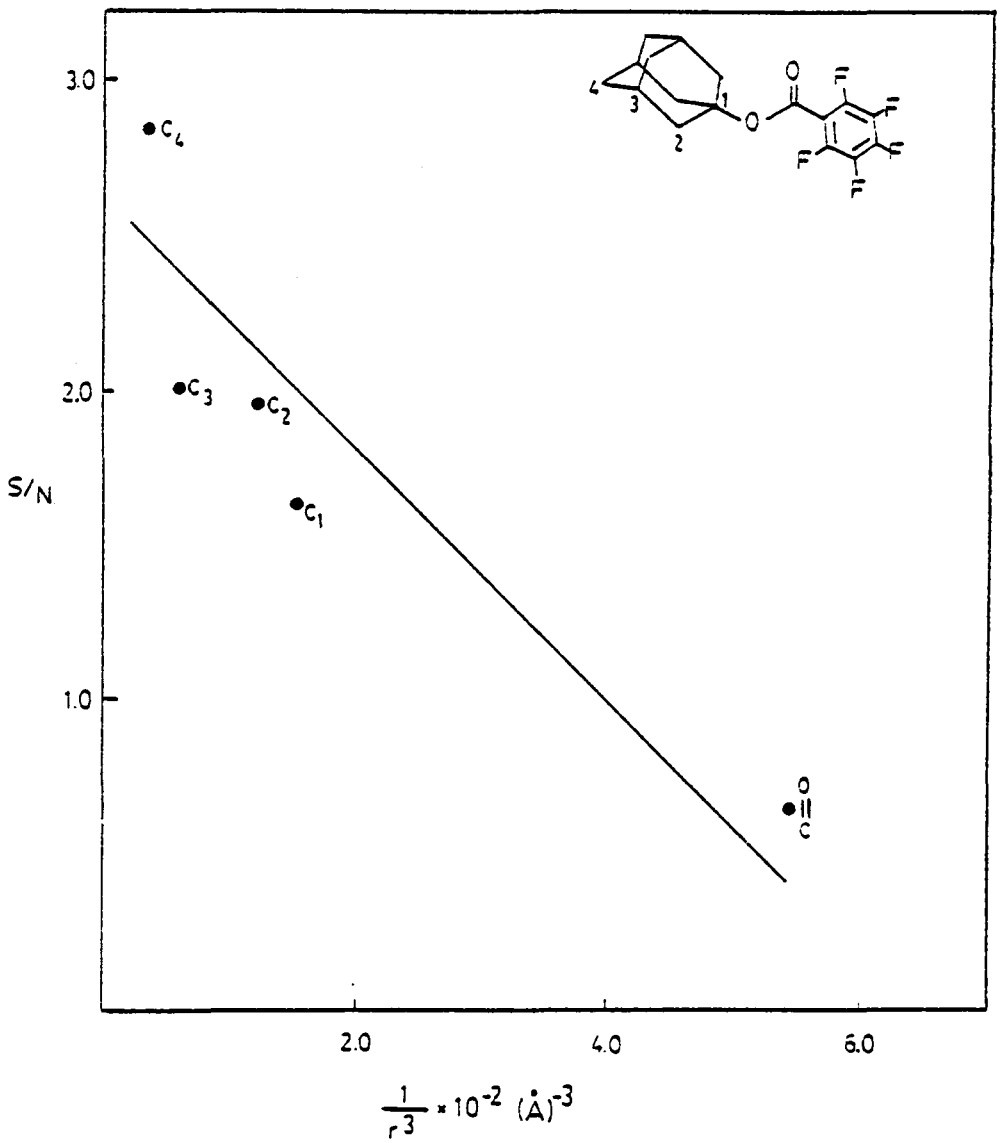

Table 5.8

S/N and $1/r^3$ Values for Thiourea/1-Adamantyl Pentafluorobenzoate Inclusion Complex

Carbon	measured distance from ortho-^{19}F nuclei (cm)	conversion to A	$1/r^3 \times 10^{-2}$	calculate S/N
quaternary (C-1)	7.265	2.77	4.70	1.60
methylene (C-2)[1]	4.740	1.81	16.86	1.94
methine (C-3)[1]	7.960	3.04	3.56	1.97
methylene (C-4)[1]	9.400	3.69	2.15	2.85
carbonyl	6.905	2.64	5.43	0.639

[1] r^{-3} values reflect that the adamantane and aromatic ring were separated by the greatest possible distance.

FIGURE 5.20

The experimental ^{13}C CP/MAS S/N values for 1-adamantyl pentafluorobenzoate/thiourea complex as a function of revised r^{-3} values.

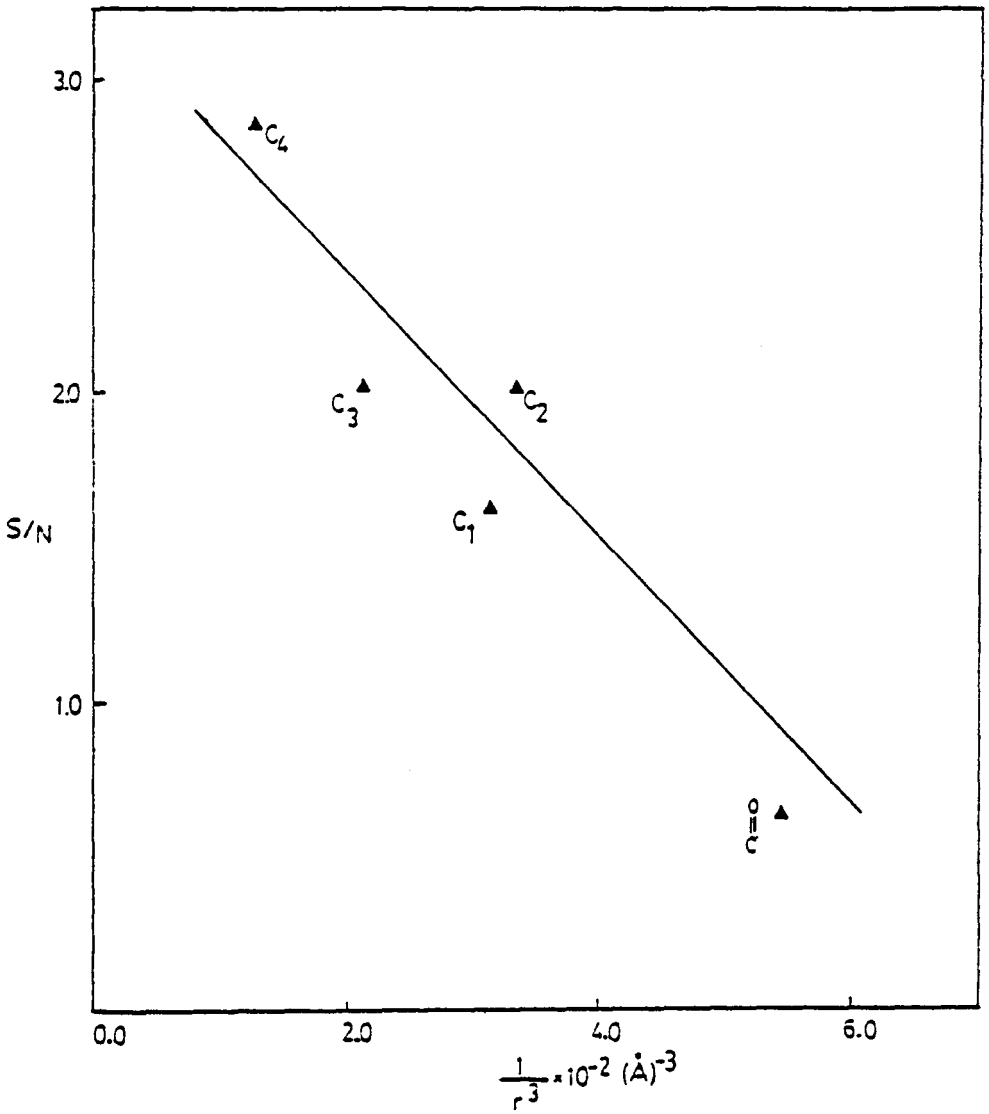

Table 5.9

S/N and Revised $1/r^{3}$[1] Values for Thiourea/1-Adamantyl Pentafluorobenzoate Inclusion Complex

Carbon Type	quaternary (C-1)	methylene (C-2)	methine (C-3)	methylene (C-4)	carbonyl
calculated S/N	1.60	1.94	1.97	2.85	0.639
$1/r^{3} \times 10^{-2}$ values (largest ring separation)	4.70	5.43	3.56	2.15	5.43
$1/r^{3} \times 10^{-2}$ values (closest ring separation)	1.48	1.17	0.52	0.44	5.43
Average $1/r^{3}$[1] $\times 10^{-2}$ values	3.09	3.30	2.04	1.30	5.43

[1] r^{-3} values are the average of measurement between the closest and the furthest approach of the adamantane and aromatic ring systems.

Solid State ^{13}C CP/MAS NMR of Fluorinated Steroid Derivatives

The previous section dealt with "diluting" fluorinated derivatives of small molecules (and thus the intermolecular dipolar interactions) in chemically and magnetically inert matrices. Another technique used to isolate the ^{13}C-^{19}F dipolar interaction was to simply derivatize larger molecules with fewer active sites. The 15.0 MHz ^{13}C spectrum of testosterone benzoate (Figure 5.21a) indicated good resolution for many signals of the steroid, even in the overlapping alkyl region. However, every carbon signal in the ^{13}C spectrum for the testosterone pentafluorobenzoate was extensively attenuated by ^{13}C-^{19}F dipolar interactions.

These observations were very consistent with those found for the 1-adamantyl fluorobenzoates. In the 1-adamantyl fluorobenzoates, rotation of the adamantane ring about its C_{3v} axis was thought to average ^{13}C-^{19}F dipole interactions. In the testosterone benzoate we find no corresponding rotational axis for the testosterone portion of the molecule. Although the aromatic ring may still rotate abouts its C_{2v} symmetry axis this did not appear to be sufficient in significantly reducing the ^{13}C-^{19}F dipolar coupling. The results again served to show the importance in the ability of anisotropic motion to modulate the intermolecular ^{13}C-^{19}F dipolar coupling.

Similar results were also found for a series of cholesteryl derivatives. The ^{13}C CP/MAS spectrum for cholesteryl pentafluorobenzoate, like the testosterone pentafluorobenzoate ^{13}C solid state

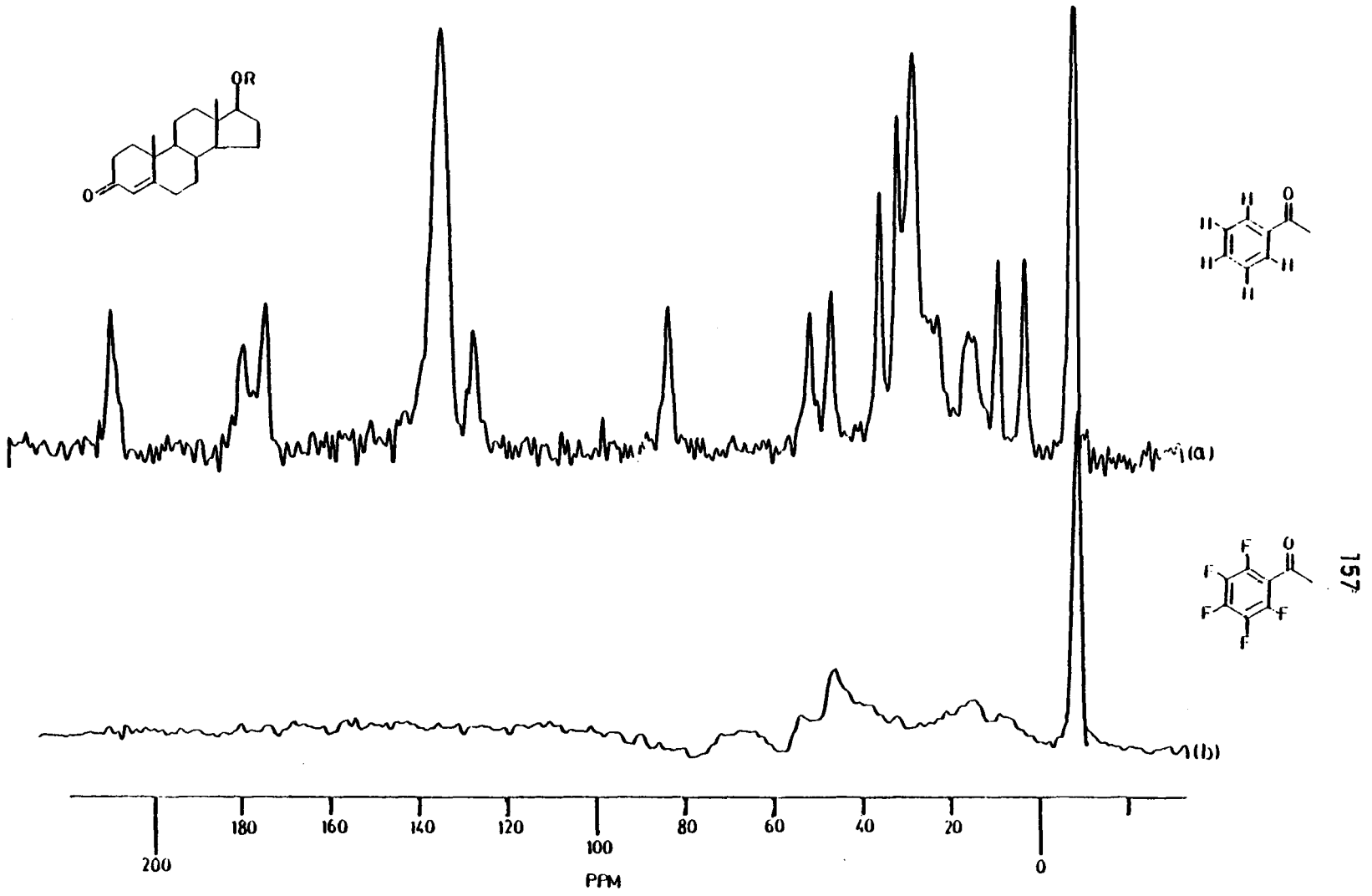

FIGURE 5.21 The 15.0 MHz ^{13}C CP/MAS spectra for testosterone benzoate (a) and testosterone pentafluorobenzoate (b). Both spectra were obtained from 5000 FID accumulations with a CT =.2.5 ms and pulse repetition time = 2.0 sec.

spectrum, also indicated extensive signal attenuations due to ^{13}C-^{19}F dipolar interactions (Figure 5.22a and 5.22b). However, in the case of cholesteryl benzoates, anisotropic motion from the alkyl side chain (carbons 20-27) may have been rapid enough to partially modulate the ^{13}C-^{19}F dipole coupling. This motion was not possible for the testosterone pentafluorobenzoates.

Two additional cholesterol derivatives were prepared, cholesteryl p-fluorobenzoate and cholesteryl trifluorobenzoate; the ^{13}C CP/MAS NMR spectra are shown in Figure 5.23a and 5.23b. Comparing these spectra to the solid state ^{13}C spectrum for cholesteryl benzoate (Figure 5.22a) it was apparent that several peaks had been attenuated due to dipolar coupling with the ^{19}F nuclei. However, the intense peaks that remained were used to "map out" the regions of the cholesterol molecule that are only weakly dipolar coupled to ^{19}F nuclei. The carbons which exhibited a prominent peak in the solid state NMR are labelled with an asterisk in Figure 5.23.

The principal regions of non-interaction for the ^{19}F nuclei in cholesteryl trifluoroacetate appear to be along the bridging carbons of the A-B ring junction (including carbons 4, 5, 10, 18) and along the bridging carbons of the C-D ring junction (e.g., carbons 8, 12, 13, and 19). In the cholesteryl p-fluorobenzoate system the lower portion of the A-B ring system which includes carbons 2-6, appears to have weaker residual ^{13}C-^{19}F dipolar interactions.

As to why these particular regions are less susceptable to inter- and intramolecular ^{13}C-^{19}F dipolar interactions is difficult to answer

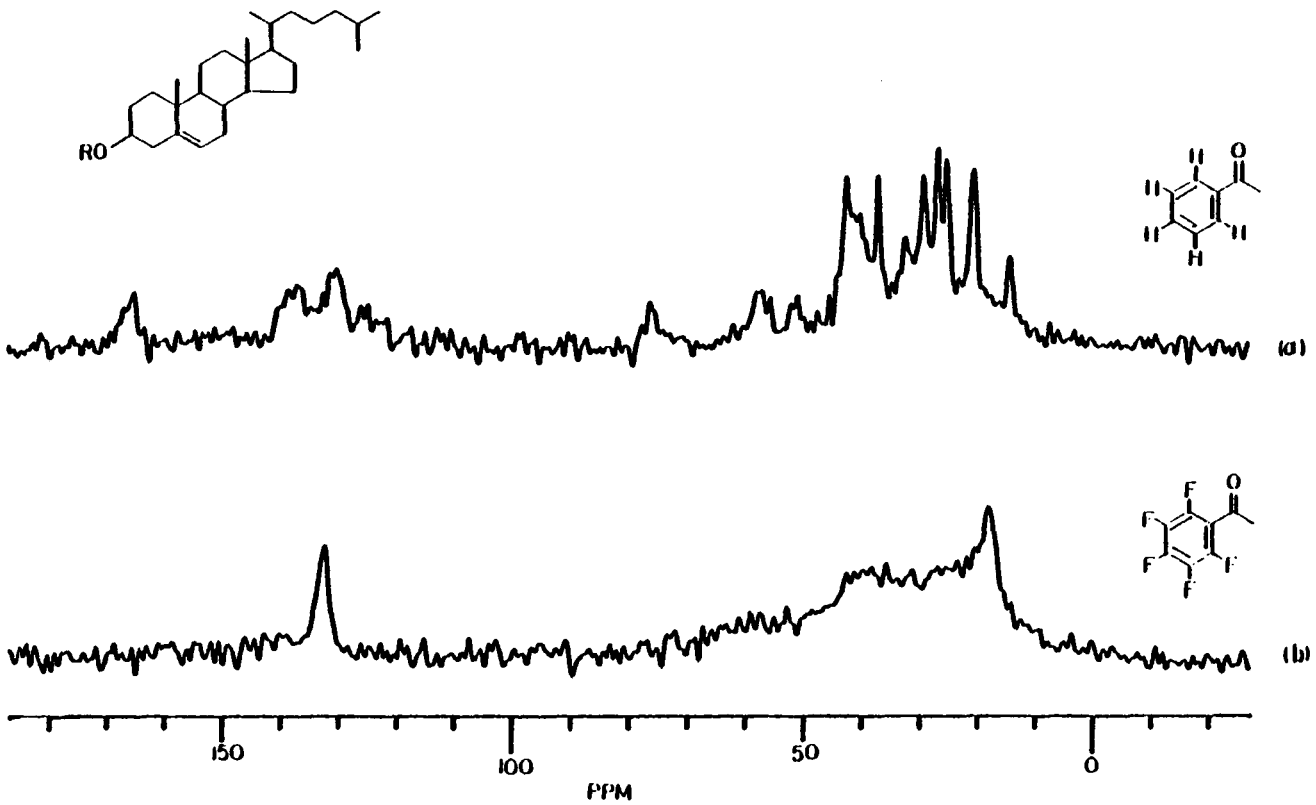

FIGURE 5.22 The 15.0 MHz ^{13}C CP/MAS spectra for cholesteryl benzoate (a) and cholesteryl pentafluorobenzoate (b). Both spectra were obtained from 4000 FID accumulations with a CT = 2.5 ms and pulse repetition time = 2.0 sec.

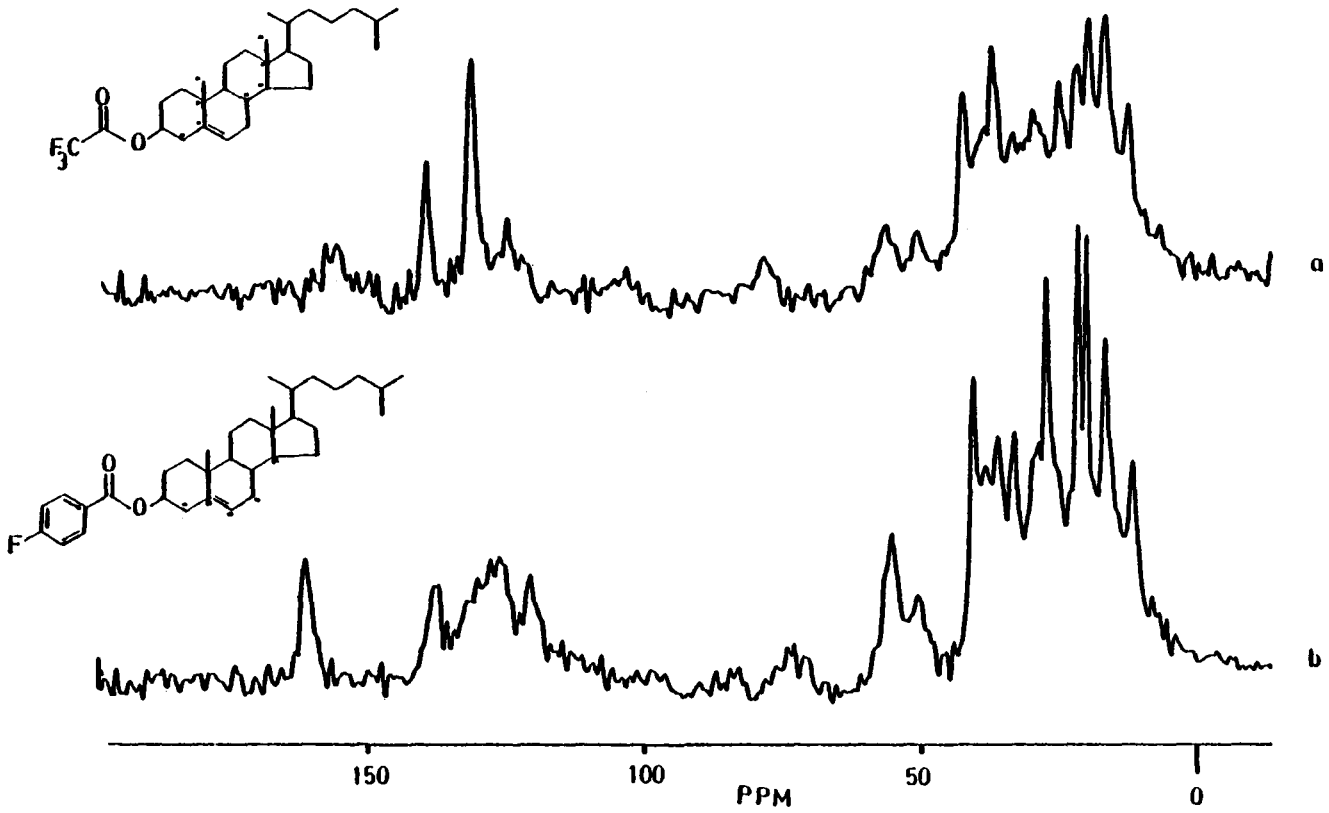

FIGURE 5.23 The 15.0 MHz ^{13}C spectra for cholesteryl trifluoroacetate (a) and cholesteryl p-fluorobenzoate (b). Both spectra were obtained from 4000 FID accumulations with a CT = 2.5 ms and pulse repetition time = 2.0 sec.

from this data. The orientation of the different molecules in the unit cell may be very important. For example, cholesteryl benzoates are a well studied class of liquid crystals and the unit cell has preferred orientation in which a helical structure is introduced into the ordering by the chiral molecular structure (211). The additional "molecular ordering", in combination with the motional processes of the cholesteryl derivatives, are key points to consider when interpreting the data in the present study.

Solid State ^{13}C CP/MAS Study of Derivatized Coal

One Western Virginia bituminous coal sample was derivatized with benzoyl and pentafluorobenzoyl chloride. The purpose of the experiment was to illustrate how the fluorine tagging experiment could be used, in a sample as complex as coal, to assign ^{13}C chemical shift signals for those carbon nuclei in the proximity of the fluorine containing functional group.

Figure 5.24a and 5.24b are the solid state ^{13}C CP/MAS spectra of the benzoylated and pentafluorobenzoylated coal. The two characteristic ^{13}C chemical shift envelopes for aromatic and alkyl carbons are common to both spectra. A distinct shoulder appears at ~160 ppm in the benzoylated coal spectrum (Figure 5.24a) that is not present in the pentafluorobenzoate spectrum (Figure 5.24b). Also, the aromatic region of the pentafluorobenzoate spectrum appears broader than in the benzoate spectrum.

The pentafluorobenzoylated coal spectrum was subtracted from the

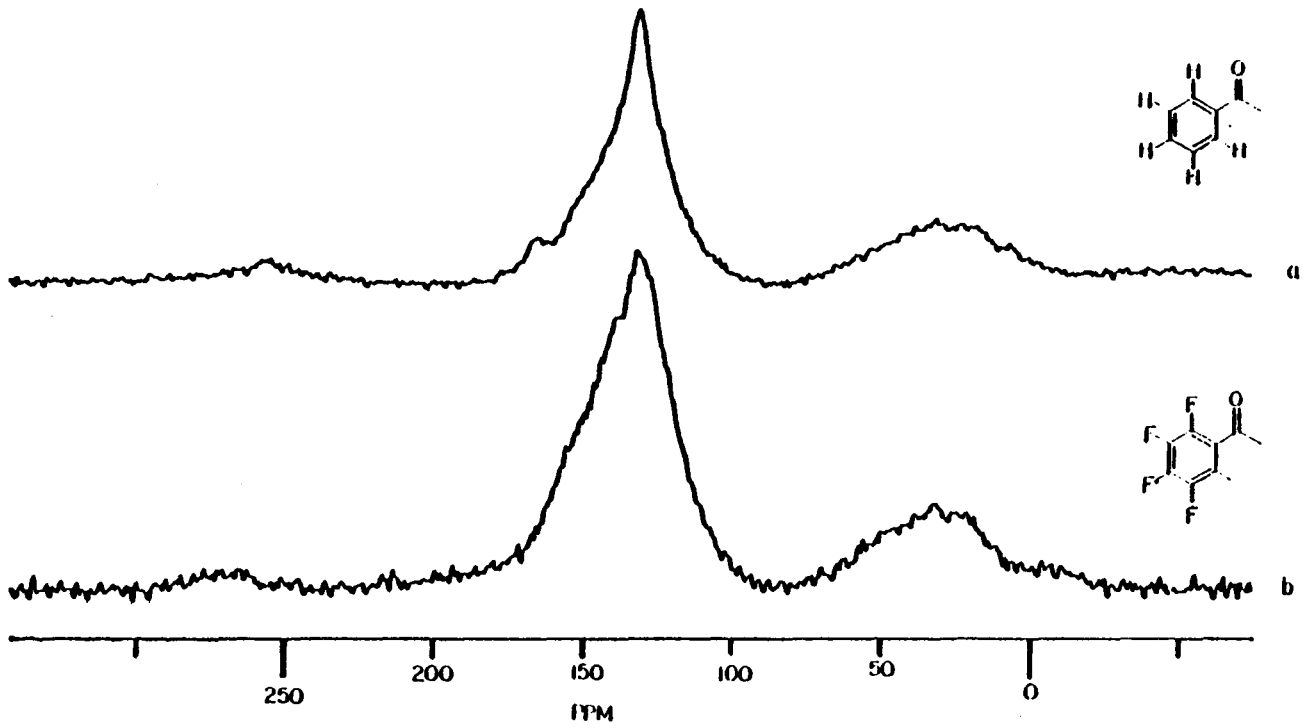

FIGURE 5.24 The 15.0 MHz ^{13}C CP/MAS spectra for a Virginia Bituminous coal derivatized with benzoyl chloride (a) and pentafluorobenzoyl chloride (b). Both spectra were obtained from 12000 FID accumulations with a CT time = 1.5 ms and pulse repetition time = 1.0 sec. No exponential apodization was used in either spectrum.

benzoylated coal spectrum with the resulting spectrum shown in Figure 5.25. The subtracted spectrum contained a large aromatic ^{13}C chemical shift envelope centered at 128 ppm and a low intensity alkyl region. There was a third smaller ^{13}C chemical shift region between ≈ 145-160 ppm. This region could be assigned to aromatic quaternary carbons bonded to hydroxyl, amine, or thiol functional groups. However, the spectral signal-to-noise was very poor, and the complex spectral pattern for the coal system made absolute assignments on the basis of these preliminary results tenuous. Additional studies must be made in this area to determine if the technique is really useful beyond these results. Two potentially useful experiments would involve:

1) Using ^{13}C-^{19}F cross-polarization with proton decoupling. This would permit direct observation of only the carbons dipolar coupled to the ^{19}F nuclei.
2) Derivatization of the sample with p-fluorobenzoyl chloride and corresponding solid state ^{19}F NMR with proton decoupling. The potential advantage of this technique capitalizes on the large ^{19}F chemical shift range for p-fluorobenzoyl derivatives. Separation of the functional groups derivatized on the coal may be great enough to reduce ^{19}F-^{19}F homonuclear dipolar coupling, thus permitting direct speciation of the derivatized coal sites by their ^{19}F chemical shift.

Unfortunately, because of instrumental limitations neither of these experiments was possible.

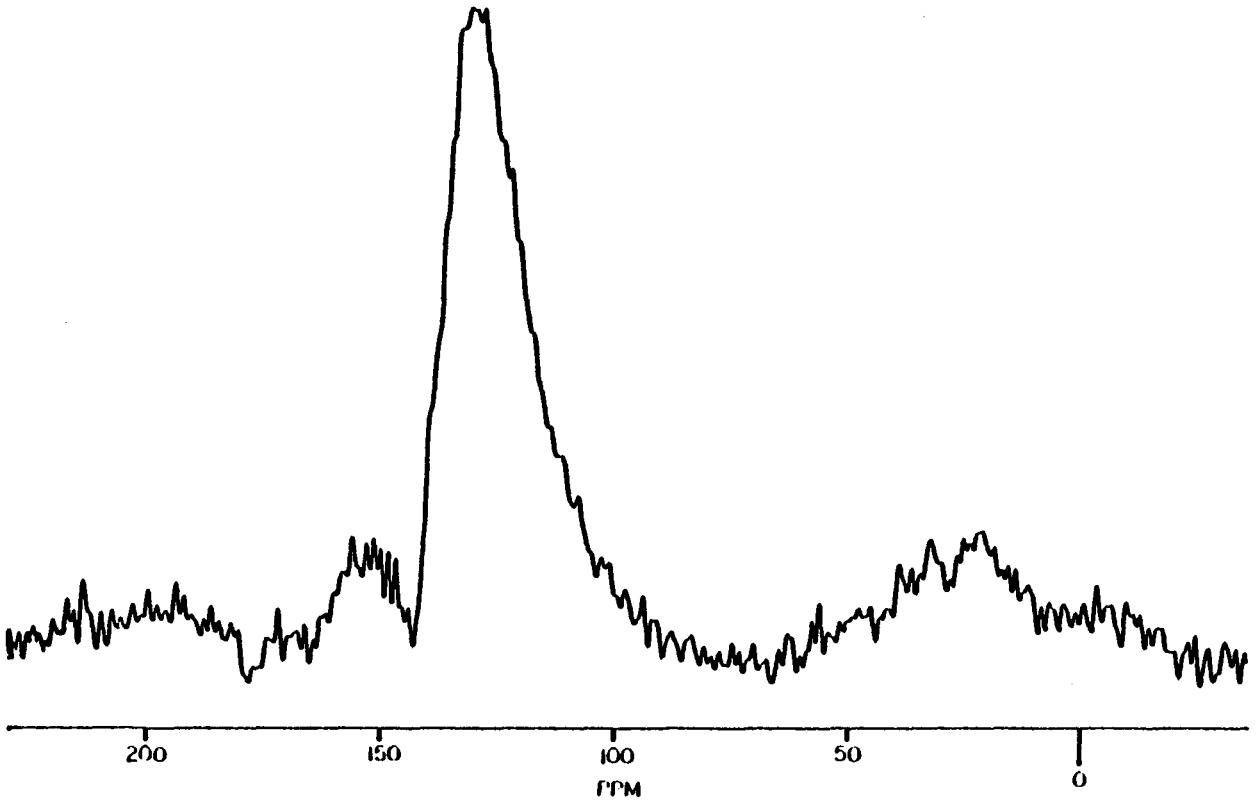

FIGURE 5.25 The solid state ^{13}C spectrum of the Virginia bituminous coal that remains if the ^{13}C CP/MAS spectrum of the coal pentafluorobenzoyl derivatives is subtracted from the ^{13}C CP/MAS spectrum of the coal benzoyl derivatives (i.e. Figure 6.27(a) (-) Figure 6.27(b)). The spectra were subtracted by using a subroutine in the spectrometer's computer.

Solid State ^{29}SI CP/MAS NMR of Derivatized Silica Gel

Using CP/MAS techniques, a number of ^{29}Si NMR spectra were obtained for silica gel whose hydroxyl sites had been derivatized with fluorine tagging reagents. The purpose of the ^{29}Si CP/MAS study of derivatized silica gel surfaces was to critically evaluate the advantages of using ^{19}F dipolar interaction to assign signals in solid state spectra. Silica gel was chosen because it is a well characterized solid with derivatizable surface hydroxyl groups. Studies have shown these hydroxyl groups cover the surface of the silica gel with approximately one group per 20(ϕÅ)^2. Therefore, the ^{29}Si-^{19}F dipole coupling between adjacent derivatized silyl sites should not be substantial. Therefore, the only substantial interaction in the ^{29}Si CP/MAS spectrum that attenuates ^{29}Si signals should be intramolecular ^{29}Si-^{19}F dipolar coupling. The ^{29}Si CP/MAS spectrum (Figure 5.26) of the underivatized silica gel was consistent with results obtained from previous studies (166). Assignments for the three ^{29}Si signals were based on these results.

In the first derivatization study, hydroxyl groups on silica gel were derivatized with benzoyl chloride. The ^{29}Si CP/MAS spectrum for the derivatized silica gel benzoate and underivatized silica gel are shown in Figures 5.27a and 5.27b. In Figure 5.27b, the ^{29}Si signals for the Si*(OSi←)$_4$ (-108.4 ppm) and HOSi*(OSi←)$_3$ (-99.4 ppm) are approximately of equal intensities. The ^{29}Si signal corresponding to (HO)$_2$Si*(OSi←)$_2$ groups was found at -90.0 ppm for derivatized silica gel

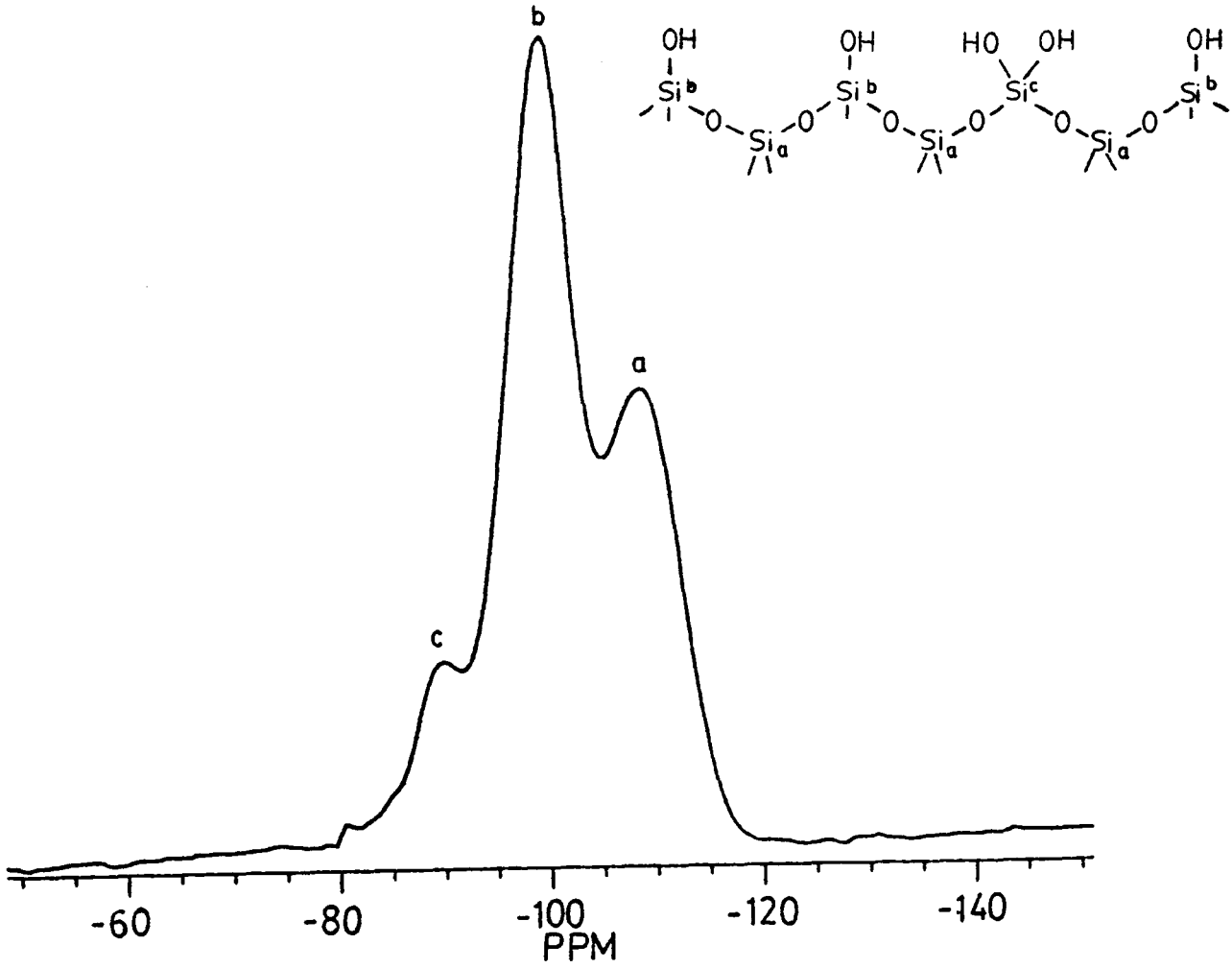

FIGURE 5.26 The 29.70 MHz ^{29}Si CP/MAS NMR spectrum of Baker's Flash Chromatography silica gel. The chemical shift scale is in ppm with respect to liquid Me_4Si (TMS) with larger numbers corresponding to lower shielding. Assignments implied by the structural inserts in this and the following figures are meant to represent typical structural types, not specific structural arrangements in silica gel. The spectrum is the result of 9596 FID accumulations, CT = 10 ms, and pulse repetition time = 1 sec.

FIGURE 5.27

The 29.70 MHz ^{29}Si CP/MAS NMR spectra of Baker's Flash Chromatography silica gel (a) before and (b) after reaction with benzoyl chloride. Spectrum (b) was obtained from 10,000 FID accumulations, CT = 10 ms, and pulse repetition time = 1 sec.

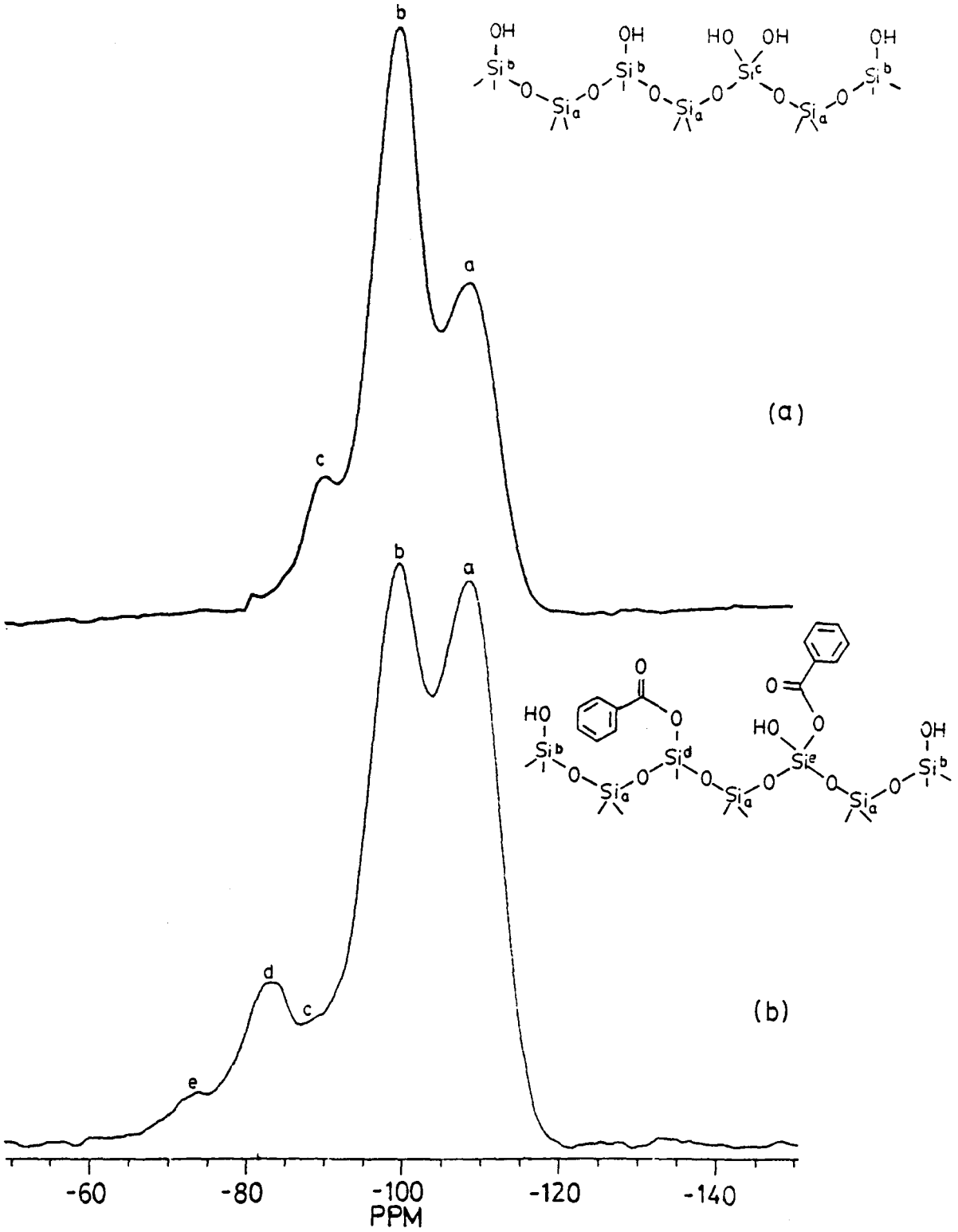
b
a
c
(a)
b
a
d
c
e
(b)
-60
-80
-100
-120
-140
PPM

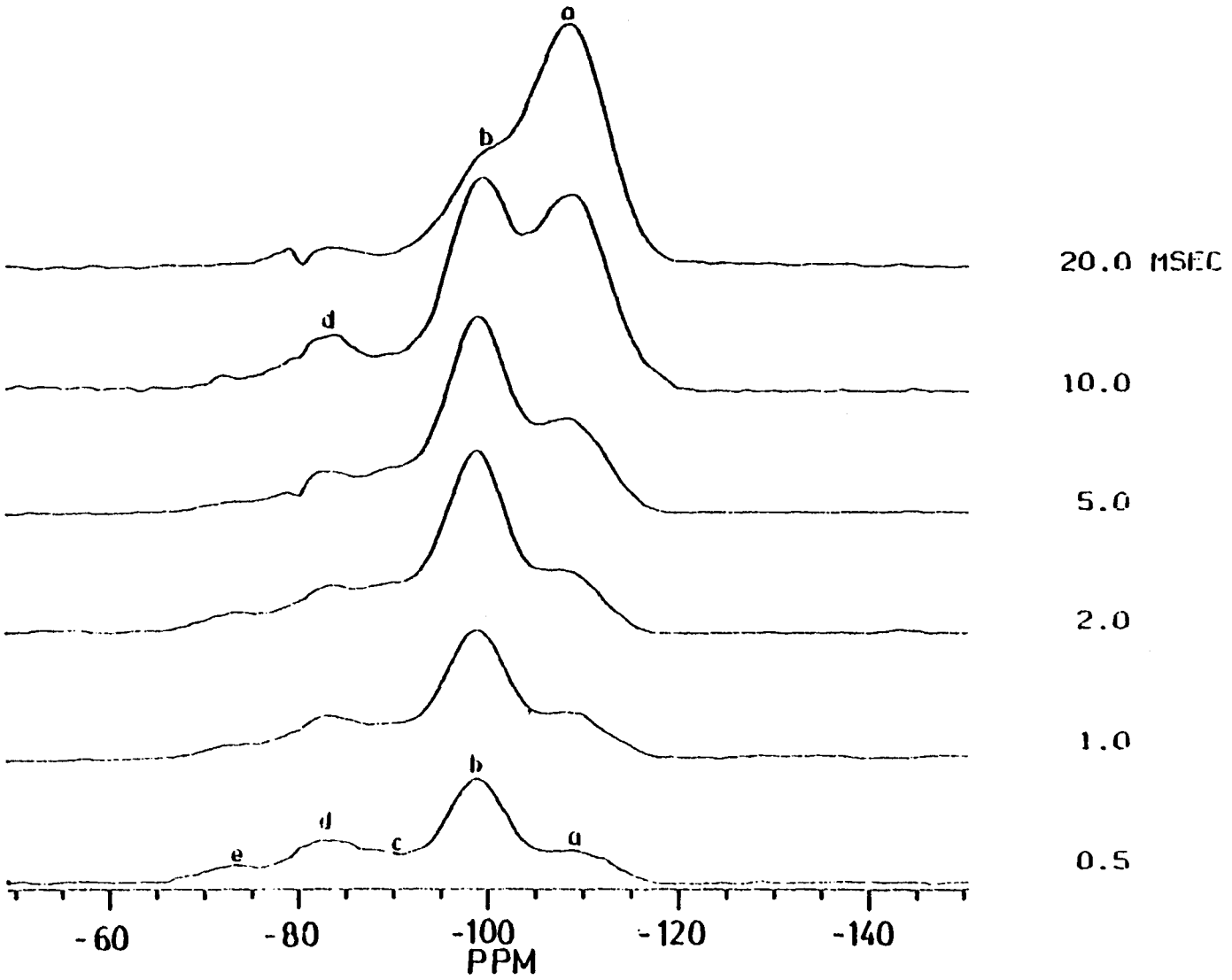

FIGURE 5.28 The 29.70 MHz ^{29}Si CP/MAS NMR spectra of silica gel benzoate obtained at various contact times.

(Figure 5.27a and 5.27b). However, the ^{29}Si chemical shifts for the silica gel benzoate derivative are strongly attenuated. In addition, a very prominent peak appears at -83.1 ppm and a smaller shoulder at -73.8 ppm, which were not observed in the ^{29}Si spectrum for the underivatized silica gel (Figure 5.27a).

The first inclination is to assign these ^{29}Si signals to silicon sites bearing derivatized hydroxyl groups. This assumption would not be unfounded because Sindorf and Maciel (166) reported $(CH_3)_3Si^*$ groups to have a ^{29}Si chemical shift of ≈13 ppm in solid state ^{29}Si CP/MAS NMR spectra. Therefore the benzoate derivative may also have a similar deshielding effect. The ^{29}Si signal at -83.10 ppm is tentatively assigned to the silica site (d) and the signal at -73.8 ppm to silica site (e) (Figure 5.27b).

Cross polarization relaxation (T_{SiH}) data were also obtained for the silica gel benzoate sample, Figure 5.28. This figure shows the dependence of the amplitude of each of the ^{29}Si NMR signals as a function of the cross polarization time using Hartmann-Hahn conditions in a single contact experiment. The data are consistent with earlier reports (182) where the most effective cross polarization time for the resonance at -99.4 ppm was ≈ 10 msec and the resonance at -108.4 (~20 ms).

A second derivatized silica gel benzoate sample was not analyzed by the ^{29}Si CP/MAS NMR technique until ≈2.5 months after the derivative preparation (Figure 5.29). This figure shows a pronounced increase in

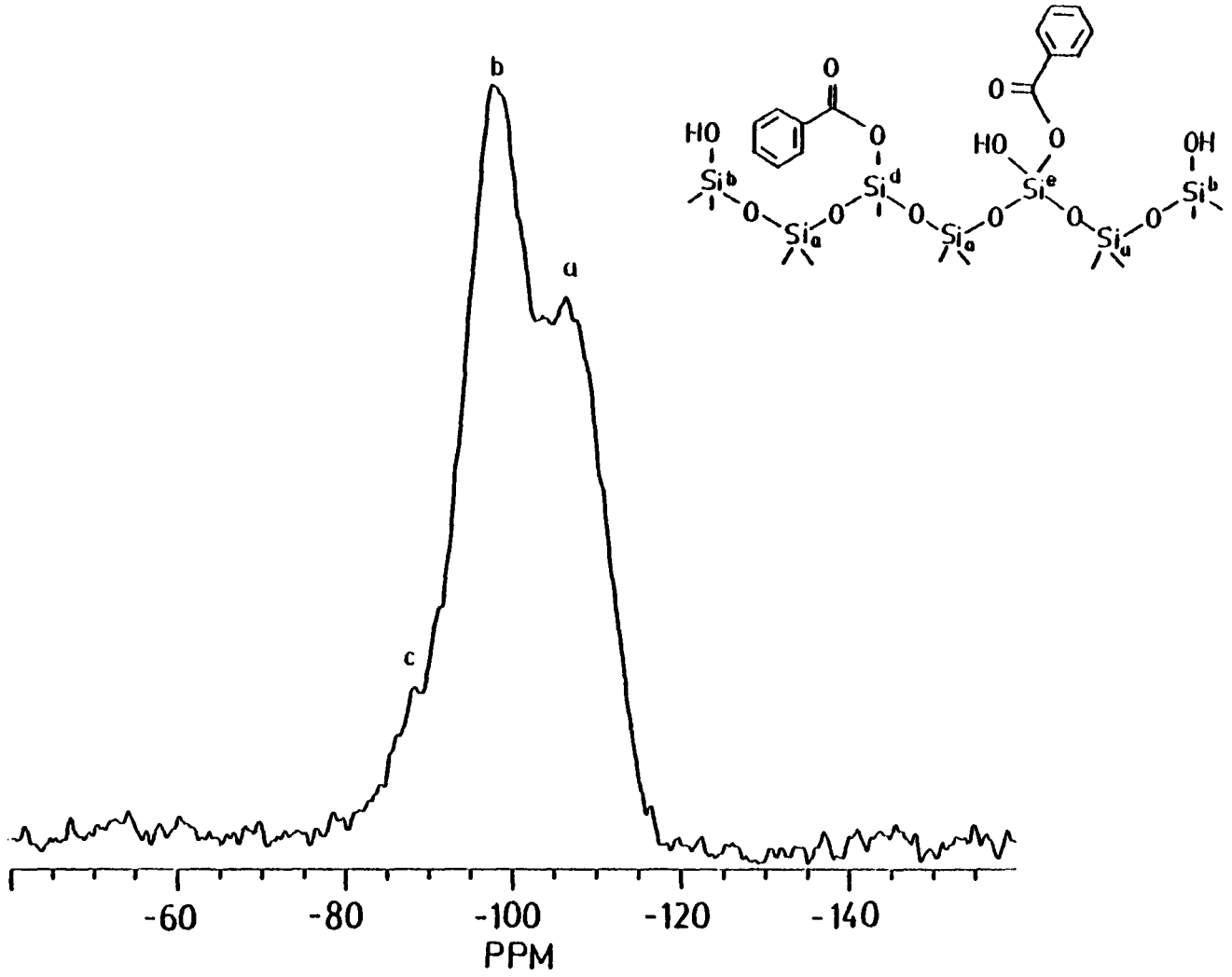

FIGURE 5.29 The 29,70 MHz ^{29}Si CP/MAS NMR spectrum of silica gel benzoate taken 2.5 months after derivatization.

the intensity of the ^{29}Si signal at -99.4 ppm and a distinct shoulder at -89.5 ppm. The peak appearing at -83.1 ppm (Figure 5.28b) is absent in this spectrum. This spectrum appears very similar to the ^{29}Si spectrum of underivatized silica gel (Figure 5.28a). Two explanations may be extended concerning Figure 5.29: a) the silica gel may not have been derivatized in the initial reaction and/or b) the derivatives on the sample may have hydrolyzed before being analyzed by ^{29}Si CP/MAS NMR.

Two pentafluorobenzoate samples of silica gel were also analyzed by ^{29}Si CP/MAS in a manner similar to the silica gel benzoate derivatives. Figure 5.29c is the ^{29}Si CP/MAS NMR spectrum of silica gel pentafluorobenzoate taken 2 weeks after derivatization. The ^{29}Si intensities for the ^{29}Si signal at -99.9 and -108.3 ppm are attenuated like those found in the ^{29}Si silica gel benzoate spectrum (Figure 5.30b). However, the signal at -99.9 ppm is slightly more intense than the signal at -108.3 ppm indicating that the derivatization of the silica gel with pentafluorobenzoyl chloride may have been less effective compared to the benzoyl chloride reaction. The peak at -90.0 ppm corresponding to structural site c on the underivatized silica gel (Figure 5.30) has been significantly reduced, suggesting that at least one of the diol -OH groups has been derivatized (Table 5.10).

The ^{29}Si signals at -83.1 and -73.8 ppm, which were present in the ^{29}Si spectrum of silica gel benzoate, are now absent (Figure 5.30b) in the ^{29}Si spectrum of silica gel pentafluorobenzoate. This indicates that the ^{29}Si signals for those sites have been attenuated due to ^{29}Si-^{19}F dipole coupling. The data are quite consistent with the

FIGURE 5.30

The 29.70 MHz ^{29}Si CP/MAS spectra for underivatized silica gel (a), silica gel benzoate (b), and silica gel pentafluorobenzoate (c). Each spectrum was obtained from $\approx$10000 FID accumulations under similar pulse conditions.

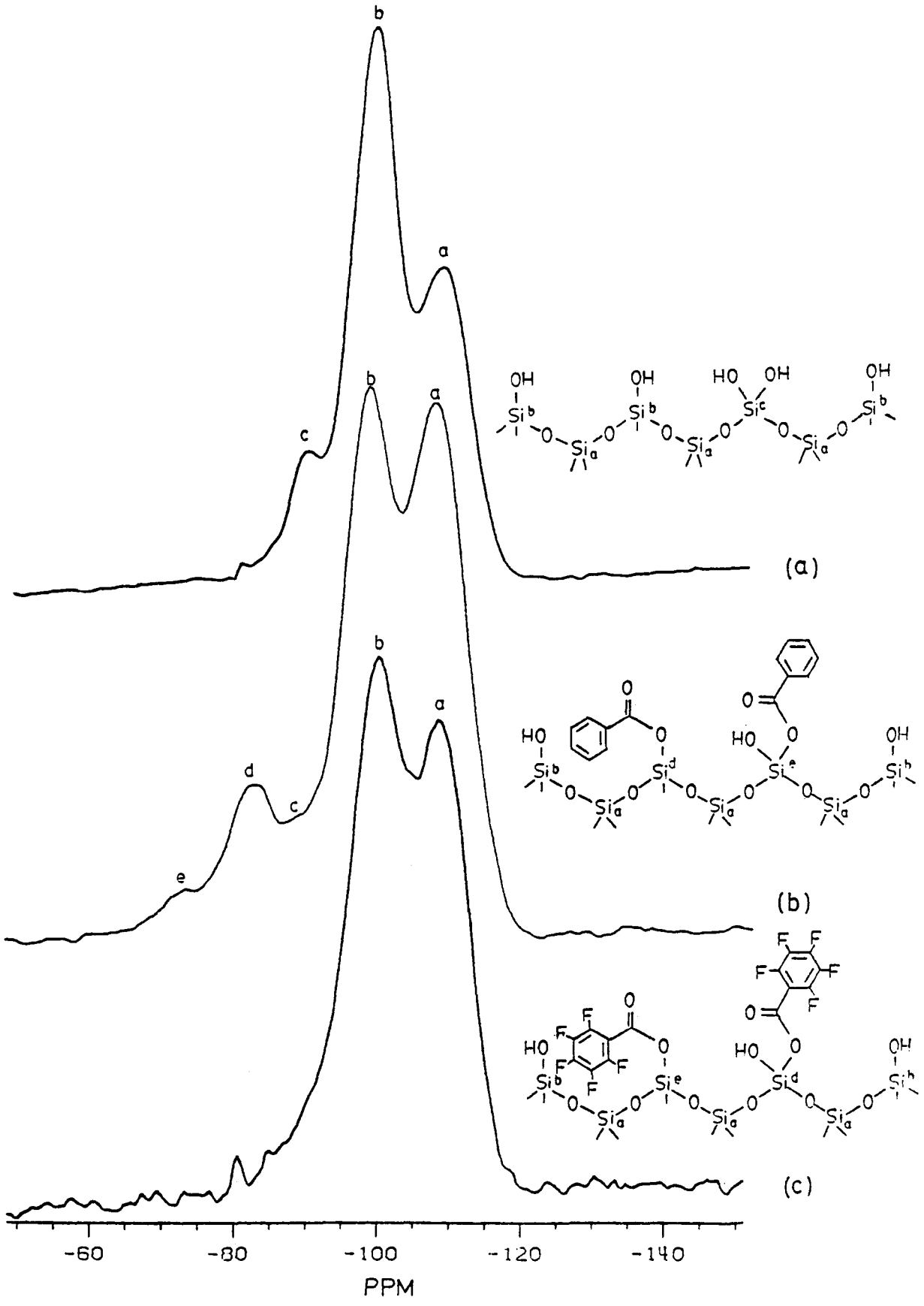
b
a
c
b
a
(a)
b
a
d
c
e
(b)
F
F
F
F
F
O
HO
OH
(c)
-60
-80
-100
-120
-140
PPM

Table 5.10

Measured S/N Ratios for Silica Gel Derivatives

Samples	SiOH	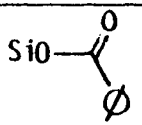	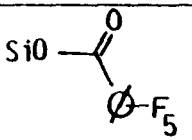	$Si-O-CH_2CF_3$
Approximate sample wgt (mg)	500	500	500	500
Number of accumulations	9596	10,000	8728	20,000
Relative signal (calculated)	1.00	1.04	0.91	2.08
Measured signal/nosie S/N ratio				
$(HO)_2Si^*-(OSi\lessdot)_2$	43.4	21.8	13.9	9.5
$HOSi^*-(OSi\lessdot)_3$	191.8	116.9	78.3	49.0
$Si^*-(OSi\lessdot)_4$	107.9	104.8	68.9	74.5
$ROSi^*-(OSi\lessdot)_3$	-	30.6	-	-
$(RO)_2-Si^*-(OSi\lessdot)_2$	-	7.2	-	-

Table 5.10 (continued)

S/N values normalized to SiOH				
$(HO)_2Si^*-(OSi\lessgtr)_2$	43.4	20.9	15.3	4.6
$HOSi^*-(OSi\lessgtr)_3$	191.8	112.4	86.0	23.6
$Si^*-(OSi\lessgtr)_4$	107.9	100.8	75.7	35.6
$ROSi^*-(OSi\lessgtr)_3$	-	29.4	-	-
$(RO)_2-Si^*-(OSi\lessgtr)_2$	-	6.9	-	-

previously reported data concerning 1-adamantyl fluorobenzoate and sterol fluorobenzoates. There it was found if anisotropic motion was present in both the fluorine tag (i.e., rotation of the 1-adamantyl ring about its C_{3v} axis) the intramolecular ^{13}C-^{19}F coupling was modulated to a certain extent. However, in cases of decreasing anisotropic motion the ^{13}C-^{19}F intramolecular coupling was more intense (e.g., as found for the testosterone pentafluorobenzoate).

If we assume the ^{29}Si sites on the surface of the silica gel are relatively rigid (i.e., having little anisotropic motion), then the ^{29}Si-^{19}F dipole coupling is only modulated by the rotation of the aromatic ring. Therefore, assuming there is not substantial ^{29}Si-^{19}F dipolar coupling between adjacent tagged sites the intramolecular ^{29}Si-^{19}F coupling only reduces the signal intensities of those ^{29}Si signals in the proximity of the tag. This is reflected by the overall decrease in the (normalized) S/N values for each ^{29}Si signal (Table 5.10).

The ^{29}Si CP/MAS spectrum taken after 2.5 months shows that some derivatized sites have been hydrolyzed, Figure 5.31. The spectrum is very similar to that of its silica gel benzoate analog, Figure 5.29.

In the final example, ^{29}Si CP/MAS spectrum for silica gel derivatized with 2,2,2-trifluorodiazoethane and analyzed apprximately 2 weeks after preparation is shown in Figure 5.32. Based on the information in this spectrum and in Table 5.10, the 2,2,2-trifluoro-diazoethane reacts with silica gel hydroxyl groups more efficiently than the acid chloride reagents. The trifluoroethylsilyl ether may also be less susceptable to hydrolysis compared to the silica ester.

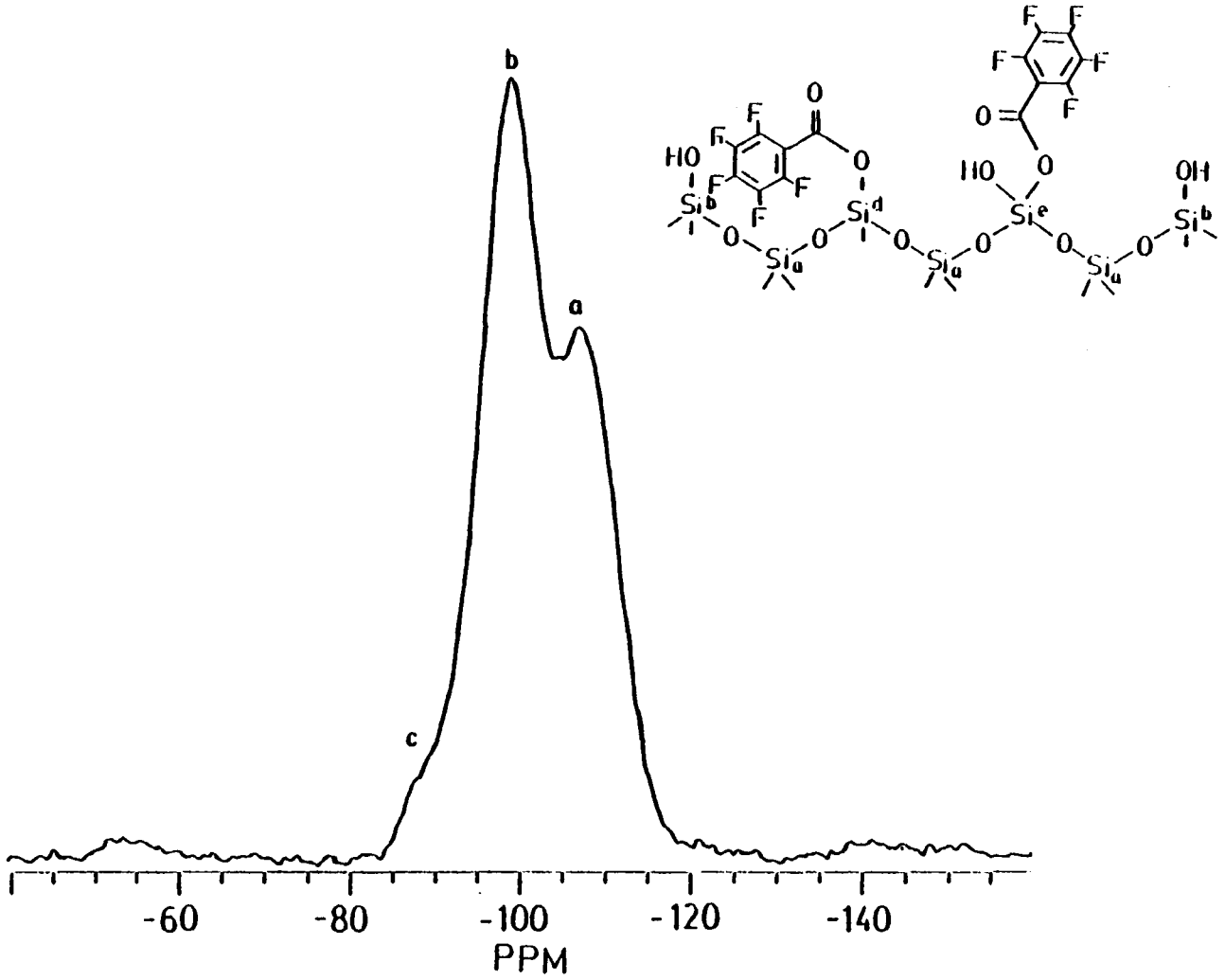

FIGURE 5.31 The 29.70 MHz ^{29}Si CP/MAS spectrum of silica gel pentafluorobenzoate taken 2.5 months after derivatization.

The ^{29}Si CP/MAS spectrum for the silica gel 2,2,2-trifluoroethyl ether derivatives (Figure 5.32c) are also consistent with the previously discussed data concerning silica gel pentafluorobenzoate derivatives. Intramolecular ^{29}Si-^{19}F dipolar coupling drastically attenuates the ^{29}Si signals for all silica sites (a, b, and c, Figure 5.30a). The structural sites at c being reduced because of the following possibilities:

1) the protonated hydroxyl sites have been "capped" with a derivative that increases the distance between the Si atom and any available hydrogen atom. This could lead to dramatic differences in the optimum contact times for the various silicon sites.
2) the ^{29}Si-^{19}F dipole interaction dominates and attenuates the signal intensities.

The second possibility is the more likely one based on the model studies. The reduction in intensities is readily observed in Table 5.10 where S/N values twice the number of spectral accumulations were taken, versus the underivatized silica gel.

Figure 5.33 is the ^{29}Si CP/MAS spectrum of silica gel 2,2,2-tri-fluoroethyl derivatives taken ~ 2.5 months after preparation. Compared to the ^{29}Si spectrum of the silica gel 2,2,2-trifluoroethyl ethers taken two weeks after preparation (Figure 5.32c), little hydrolysis of the derivatives appears to occur. This is in sharp contrast to the silica gel benzoyl derivatives (Figures 5.29 and 5.31) where the ^{29}Si spectra indicated these derivatives had been almost completely hydroylzed.

The 29.70 MHz ^{29}Si CP/MAS spectra for underivatized silica gel (a), silica gel benzoate (b), and silica gel pentafluorobenzoate (c). Each spectrum was obtained from $\approx$10000 FID accumulations under similar pulse conditions.

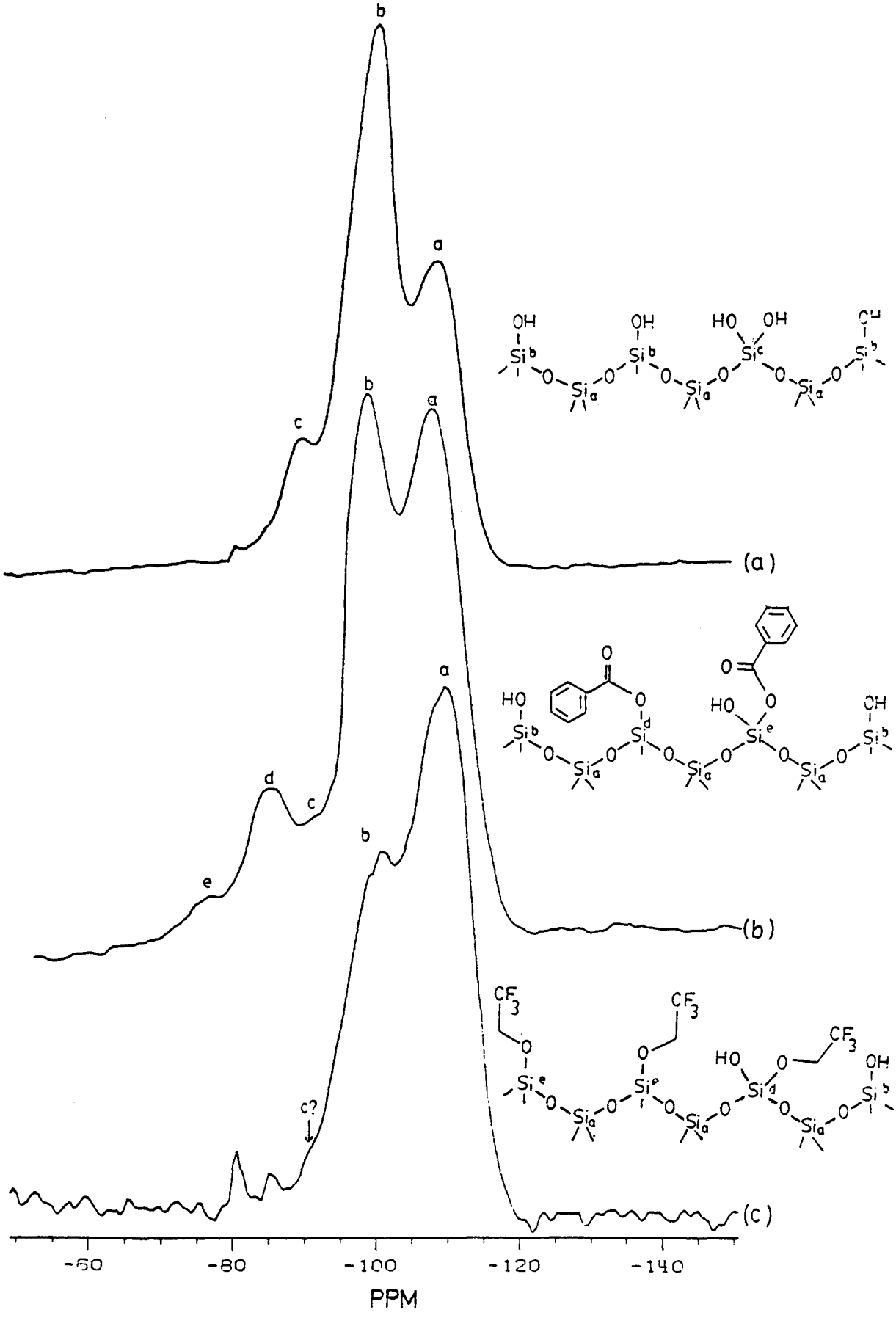
b
a
c
(a)
b
a
d
c
e
(b)
a
b
c?
(c)
-60
-80
-100
-120
-140
PPM

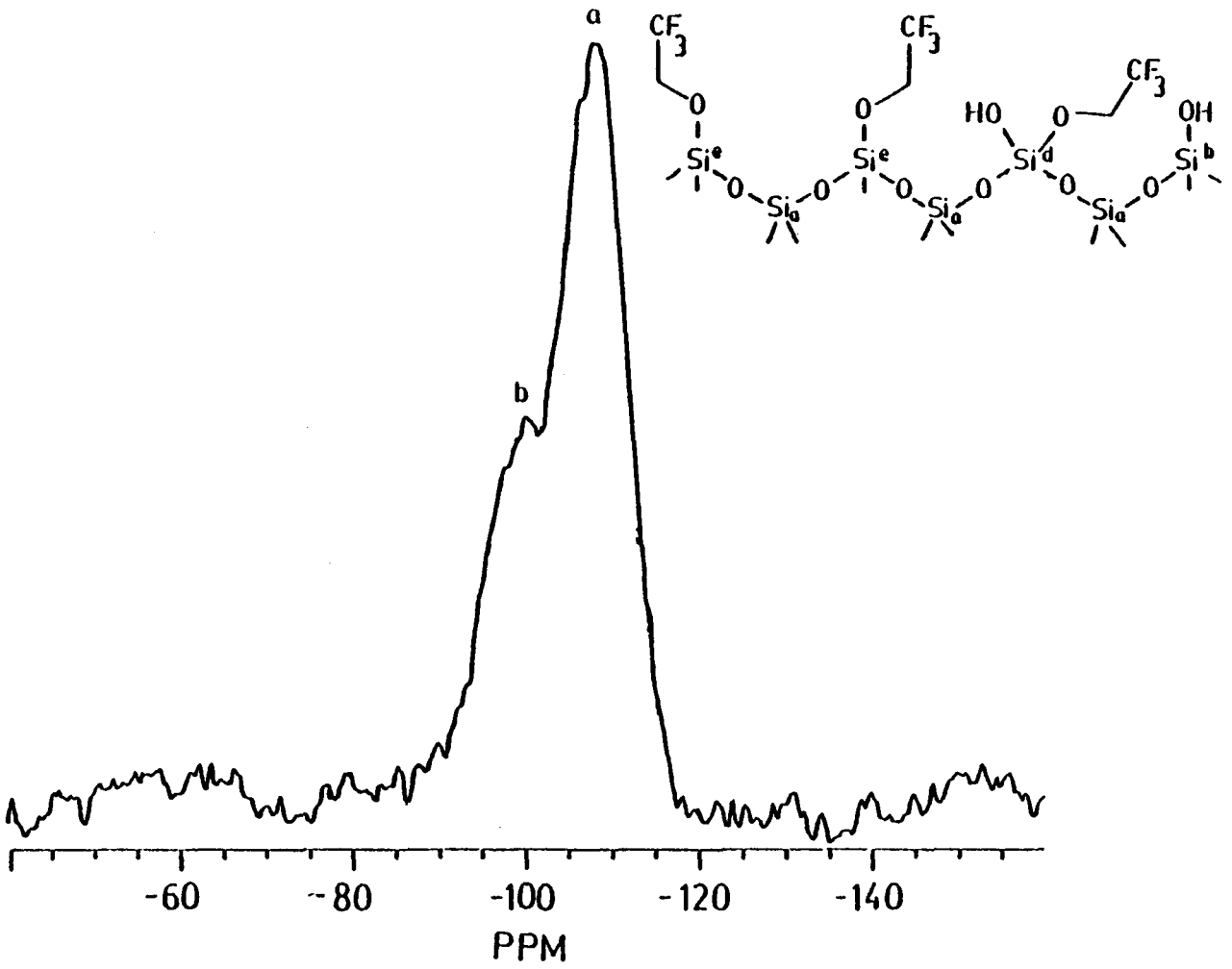

FIGURE 5.33 The 29.70 MHz ^{29}Si CP/MAS NMR spectrum for silica gel 2,2,2-trifluoroethyl ether derivatives taken 2.5 months after derivatization.

CONCLUSION

The results described in this chapter demonstrate that tagging active sites on solid material with fluorine derivatives significantly attenuates the solid state ^{13}C CP/MAS signals of these derivatized solids. Several conclusions are discussed below:

1. The ^{13}C CP/MAS NMR spectra of 1-adamantyl fluorinated benzoate derivatives show that ^{13}C-^{19}F dipolar interactions are significant in these small molecules. The ^{13}C NMR signal attenuations for model systems reflect both intra-and intermolecular coupling contributions.

2. Experimental results show that intramolecular ^{13}C-^{19}F dipole coupling could be reduced by either MAS or anisotropic molecular motion. Signals for ^{13}C nuclei directly bonded to or within ≈1.5 Å of a ^{19}F nucleus were attenuated or eliminated in the ^{13}C CP/MAS spectrum. However, ^{13}C-^{19}F dipole interactions on the order of ≈2 kHz (i.e., corresponds to ^{13}C-^{19}F internuclear distances of >3 Å) are modulated by MAS and complex anisotropic molecular motion of the molecule (i.e., rotation of adamantane ring about a C_{3v} axis and rotation of the aromatic ring about a C_{2v} axis).

3. Formation of thiourea/1-adamantyl benzoates can separate intra-and intermolecular dipole interactions. As presented for 1-adamantyl, pentafluorobenzoate, and p-fluorobenzote derivatives (Figure 5.17 and 5.18), well resolved chemical signals for the adamantyl ring carbons can be obtained indicating intermolecular dipole contributions have been reduced.

4. By plotting S/N ratios (obtained from ^{13}C CP/MAS NMR spectra of thiourea/1-adamantyl pentafluorobenzoate inclusion complexes) versus $1/r^3$ values, it was shown that dipolar interaction was proportional to the distance between the two interacting nuclei.

5. The ^{13}C CP/MAS spectra of steroids derivatized with fluorine tagging reagents indicate that inter-and intramolecular ^{13}C-^{19}F dipole coupling strongly attenuate spectral signals. The data strengthens the hypothesis that anisotropic molecular motion can modulate the ^{13}C-^{19}F dipole coupling, as illustrated by the ^{13}C CP/MAS spectrum of testosterone benzoate and pentafluorobenzoate. The absence of a major symmetry axis in the molecule may reduces anisotropic motion, thereby, ^{13}C-^{19}F dipole coupling is not efficiently modulated and ^{13}C signal attenuation is more severe.

6. Studies concerning derivatization of silica gel hydroxyl groups with ^{19}F tagging reagents and subsequent analysis by ^{29}Si CP/MAS NMR clearly demonstrate advantages in using ^{29}Si-^{19}F dipolar coupling to analyze active sites present on these solids. Results were very consistent with data discussed in this chapter. We did observe appreciable ^{29}Si line attenuation due to ^{29}Si-^{19}F dipolar interactions, as hoped.

Future Work

One technique used to obtain ^{13}C CP/MAS spectrum of fluorinated hydrocarbons is a triple resonance experiment in which simultaneous

decoupling of ^{1}H and ^{19}F eliminates dipolar broadening from both nuclei. This can be achieved by using a probe equipped with a single rf coil tuned to $^{13}C/^{1}H$ resonance surrounded by a "saddle" coil tuned to the ^{19}F resonance (119). Carbon magnetization is created by the routine ^{13}C-^{1}H Hartmann-Hahn cross-polarization contact experiment then the ^{13}C FID is subjected to strong ^{1}H and ^{19}F irradiation.

A second technique, used by Schilling (224) calls for no major modifications to the probehead such as the addition of the saddle coil. The probe assembly is a standard ^{13}C single-coil probehead where the decoupler circuit has been double tuned to both the fluorine and proton resonance frequencies. This approach yields a bandwidth of 1.5 kHz at 7W for protons and a bandwidth of 3.0 kHz at 30W of rf power for fluorine. Dorn and coworkers (225) are currently studying the potential of using these techniques (or modifications of the methods) in relation to this and other ^{13}C NMR problems requiring simultaneous ^{1}H and ^{19}F decoupling.

The advantage of using ^{19}F decoupling would be that contributions from both intermolecular and intramolecular ^{13}C-^{19}F dipolar interactions could be easily studied. For example, in this work, the fluorinated molecules were diluted by inclathration into a host lattice. This action reduced the ^{13}C-^{19}F <u>inter</u>molecular dipole interaction while leaving the <u>intra</u>molecular interaction as the dominant contribution to the ^{13}C signal reduction in the 1-adamantyl fluorobenzoate systems. Using ^{19}F decoupling one should be able to vary the power of the ^{19}F decoupling r.f. field. Therefore, the magnitude of the ^{13}C-^{19}F

intermolecular coupling could be studied by changing the strength of the ^{19}F decoupling field. For example, ^{13}C-^{19}F intermolecular dipole interactions arising from ^{13}C and ^{19}F nuclei separated by 4Å would exhibit weaker dipole coupling and would require lower r.f. coupling power to be eliminated. However, coupling between nuclei separated by 2Å or less would undoubtedly require more power (3) for complete decoupling.

References

1. Spratt, M. P.; Dorn, H. C.; Meng, Y. Anal Chem. 1985, 57, 76-81.

2. Spratt, M. P.; Dorn, H. C.; Armistead, D.; Motell, E. Anal. Chem. 1985, 57, 359-361.

3. Ward, T. C.; Lin, T. S. in "ACS Advances in Chemistry Series-Polymer Blends and Composites in Multiphase Systems," Hans, C. D., ed., No. 206, 1984, pp. 59-75.

4. Pfeffer, P. E.; Hicks, K. B.; Frey, M. H.; Opella, S. J.; Earl, W. J. J. Magn. Reson. 1983, 55, 344-346.

5. Cairns, T.; Siegmund, E. G.; and Rader, B. Anal. Chem. 1981, 53, 1217-1222.

6. Ehrsson, H.; Walle, T.; Brotell, H. Acta Pharm. Suec. 1971, 8, 319-328.

7. Walle, T.; Ehrsson, H. Acta. Pharm. Suec. 1971, 8, 27-38.

8. Walle, T.; Ehrsson, H. Acta Pharm. Suec. 1970, 7, 389-406.

9. Ervik, M.; Walle, T.; Ehrsson, H. Acta. Pharm. Suec. 1970, 7, 625-634.

10. Brown, W. E.; Seamon, K. B. Anal. Biochemistry 1978, 87, 211-222.

11. Bode, J.; Blumenstein, M.; Raftery. M. A. Biochemistry, 1975, 14, 1146-1152.

12. Bode, J.; Blumenstein, M.; Raftery, M. A. Biochemistry, 1975, 14, 1153-1160.

13. Huestis, W. H.; Raftery, M. A. Biochemsitry, 1972, 11, 1648-1654.

14. Seamon, K. B.; Hartshorne, D. J.; Bothner-By, A. A. Biochemistry, 1977, 16, 4039-4046.

15. Bendall, M. R.; Lowe, G. Eur. J. Biochem. 1976, 65, 481-491.

16. Bendall, M. R.; Lowe, G. Eur. J. Biochem. 1976, 65, 493-502.

17. Bendall, M. R.; Lowe, G. FEBS Letters, 1976, 72, 231-234.

18. Huestis, W. H.; Raftery, M. A. Biochemistry, 1971, 10, 1181-1186.

19. Paselk, R. A.; Levy, D. Biochemistry, 1974, 13, 3340-3346.

20. Gaffield, W.; Lundin, R. E. IARC Sci. Publ. 1978, 19, 87-95.

21. Zuber, G. E.; Staiger, D. B.; Warren, R. J. Anal. Chem. 1983, 55, 64-67.

22. Voelter, W.; Brietmaier, E.; Jung, G.; Bayer, E. Org. Mag. Reson. 1970, 2, 251-257.

23. Holton, R. A, Dept. of Chemistry, Virginia Polytechnic Institute and State University, personal communication.

24. Spratt, M. P.; Dorn, H. C. Anal. Chem., 1984, 56, 2038-2043.

25. LeFevre, J. W.; Kingston, D. G. I., J Org. Chem., in press.

26. Sternberg, H. W. J. Am. Chem. Soc.; Prepr., 1976, 21, 1.

27. Neavel, R. C. "Coal Structure", Advances in Chemistry Series, ACS, 1981, 192, p. 1.

28. Sternberg, H. W.; Delle Donne, C. L., Pantages, P., Moroni, E. C.; Markby, R. E. Fuel 1971, 50, 432-435.

29. Sternberg, H. W.; Delle Donne, C. L., Fuel 1974, 53, 172-177.

30. Ignasiak, B. S.; Gawlak, M. Fuel, 1977, 56, 216-219.

31. Alemany, L. B.; King, S. R.; Stock, L. M. Fuel, 1978, 57, 738-748.

32. Alemany, L. B.; Grant, D. M.; Pugmire, R. J.; Stock, L. M. Fuel 1984, 63, 513-521.

33. Hodek, W.; Kolling, G. Fuel 1975, 52, 220-224.

34. Larsen, J. W.; Green, T. K.; Choudhury, P.; Kuemmerle, E. W. "Coal Structure", Advances in Chemistry Series, ACS, 1981, 192, p. 277.

35. Hombach, H. P. Erdrol und Kohle, Erdgus, Petrochemie, Compendium, 1975, 74, (274), 750-753.

36. Larsen, J. W.; Kuemmerle, E. W. Fuel, 1976, 55, 162-164.

37. Franz, J. A.; Skiens, W. E. Fuel, 1978, 57, 502-504.

38. Sharma, D. K.; Mirza, Z. B.; Sarkar, M. K. Fuel, 1983, 62, 292-294.

39. Ouchi, K.; Makabe, M.; Itoh, H. Proc. Int. Kohenwiss. Tag. 1981, 133-138.

40. Makabe, M.; Ouchi, K. Fuel, 1979, 58, 43-47.

41. Deno, N. C.; Greigger, B. A.; Stround, S. G. Fuel, 1978, 57, 455-459.

42. Verheyen, T. V.; Johns, R. B. Anal. Chem. 1983, 55, 1564-1568.

43. Seyferth, D.; Duncan, D. P.; Sternberg, H. W. Fuel, 1979, 58, 74-75.

44. Bockrath, B. C.; Naceti, R. P. Fuel Process Technology 1979 (2), p. 143.

45. Schweighardt, F. K.; Retcofoky, H. L.; Friedman, S.; Hough, M. Anal. Chem. 1978, 50, 368-370.

46. Schwager, I.; Yen, T. F. Anal. Chem. 1979, 57, 569.

47. Snape, C. E.; Smith, C. A. Anal. Chem. 1982, 54, 20-25.

48. Tomkins, B. A.; Ho, C. -h. Anal. Chem. 1982, 54, 91-96.

49. Later, D. W.; Andors, T. G.; Lee, M. L. Anal. Chem. 1983, 55, 2126-2132.

50. Later, D. W.; Lee, M. L.; Wislon, B. W. Anal. Chem. 1983, 55, 117-123.

51. Tomkins, B. A.; Feldman, C. Anal. Chem. Acta. 1980, 119, 283-290.

52. Bartle, K. D.; Matthews, R. S.; Stadelhofer, J. W. App. Spec. 1980, 34, 615.

53. Spratt, M. P.; Roy, J. T.; Dorn, H. C. Anal. Chem., submitted for publication, Fuel.

54. Morris, G. A.; Freeman, R. J. Am. Chem. Soc. 1979, 101, 760-762.

55. Farcasiu, M. Fuel, 56, 1977, 9-13.

56. Hellgeth, J. W., Taylor, L. T. Fuel, 1984, 63, 961-968.

57. Sleevi, P.; Glass, T. E.; Dorn, Anal. Chem. 1979, 57, 1931-1934.

58. Manatt, S. L. J. Am. Chem. Soc. 1966, 88, 1323-1324.

59. Leader, G. R. Anal. Chem. 1982, 45, 1700-1706.

60. Koller, K. L.; Dorn, H. C. Anal. Chem. 1982, 54, 529-533.

61. Shue, F. F.; Yen, T. F. Anal. Chem. 1982, 54, 1641-1642.

62. Taft, R. W.; Prosser, F.; Goodman, L.; Davis, G. T. J. Chem. Phys. 1963, 38, 380-387.

63. Watanabe, N.; Niki, E. Proc. Ipn. Acad. 1978, 54, 194-199.

64. Bayer, E.; Albert, K.; Nieder, M.; Grom, E.; Keller, T. Adv. Chromatogr. 1979, 14, 525-529.

65. Bayer, E.; Albert, K.; Nieder, M.; Grom, E.; Keller, T. J. Chromatogr. 1979, 186, 497-501

66. Bayer, E.; Albert, K.; Nieder, M.; Grom, E.; Zhu, A. Fresenius' Z. Anal. Chem. 1980, 52, (304) 111.

67. Buddrus, J.; Herzog, H. Org. Mag. Reson. 1980, 13, 153-156.

68. Haw, J. F.; Glass, T. E.; Hausler, D. W.; Motell, E.; Dorn, H. C. Anal. Chem. 1980 52, 1135-1140.

69. Bayer, E.; Albert, K.; Nieder, M.; Grom, E.; Wolff, G.; and Rindlisbacher, M. Anal. Chem. 1982, 54, 1747-1750.

70. Haw, J. F.; Glass, T. E.; Dorn, H. C. Anal. Chem. 1981, 53, 2327-2332.

71. Haw, J. F.; Glass, T. E.; Dorn, H. C. Anal. Chem. 1981, 53, 2332-2336.

72. Haw, J. F.; Glass, T. E.; Dorn, H. C. Anal. Chem. 1983, 55, 22-29.

73. Glass, T. E.; Dorn, H. C. J. Magn. Reson. 1983, 51, 527-529.

74. Glass, T. E.; Dorn, H. C. J. Magn. Reson. 1983, 52, 578-581.

75. Dorn, H. C. Anal. Chem. 1984, 56, 747A-758A.

76. Buddrus, J.; Herzog, H.; Cooper, J. W. J. Magn. Reson. 1981, 44, 453-459

77. Buddrus, J.; Herzog, H. Anal. Chem. 1983, 55, 1611-1614.

78. Roy, J. T.; Dorn, H. C. submitted for publication in J. Org. Chem.

79. Haw, J. F.; Glass, T. E.; Dorn, H. C. J. Magn. Reson. 1982, 49, 22-30.

80. Snyder, L. R.; Kirkland, J. J. "Introduction to Modern Liquid Chromatography," John Wiley and Sons, New York, 1979, pp. 246-264.

81. Harris, R. K., "Nuclear Magnetic Resonance Spectroscopy," Pitman Book Ltd., London, 1983.

82. Maciel, G. E., "High Resolution Nuclear Magnetic Resonance of Solids," Science, 1984, 226, 282-294.

83. Yannoni, C. S., "High-Resolution NMR in Solids: The CP-MAS Experiment," Acc. Chem. Res. 1982, 15, 201-208.

84. Jelinksi, L. W., "Modern NMR Spectroscopy," Chem. and Engin. News 1984, 62 (45), 26-47.

85. Jelinksi, L. W., "High Resolution NMR of Solids," AT&T Bell lab. Report, 1984.

86. Slichter, C. P., "Principles of Magnetic Resonance," 2nd. ed., Springer-Verlag, New York, 1978.

87. Mehring, M., "Principles of High Resolution NMR in Solids," 2nd. ed., Springer-Verlag, New York, 1983.

88. Abragam, A., "Principles of Nuclear Magnetism," Oxford University Press, London, 1983.

89. Fyfe, C. A., "Solid State NMR for Chemists," C. F. C. Press, Guelph, Ontario, Canada, 1983.

90. Haeberlen, U., "High Resolution NMR in Solids: Selective Averaging (Suppl. 1, Adv. Magn. Reson. J. S. Waugh, ed.), Academic Press, New York, 1976.

91. Griffin, R. G., Anal. Chem. 1977, 49, 951-960.

92. reference 88, pp. 150-151.

93. Wehrli, F. W.; Wirthlin, T.; "Interpretation of Carbon-13 NMR Spectra," Heyden, London, 1978, pp. 48-57.

94. Early, T. A.; Haw, J. F.; Bax, A.; Maciel, G. E.; Paur, M. S. J. Phys. Chem. 1984, 88, 324-327.

95. reference 85, p. 6.

96. Martin, M. L.; Martin, G. J.; Delpuech, J. J. "Practical NMR Spectrtoscopy," Heydon, London, 1980, p. 17.

97. Andrew, E. R. "Progress in Nuclear Magnetic Resonance Spectroscopy," Vol. 8, Emsley, J. W.; Fenney, J.; Sutcliffe, L. H., eds., Pergamon Press, New York, 1972, pp. 1-39.

98. Andrew, E. R. "Nuclear Magnetic Resonance Spectrsocopy in Solids," Phi. Trans. Roy. Soc. London, 1981, A299, 505-520.

99. Schaefer, J.; Stejskal, E. D.; Buchdahl, R. Macromolecules, 1977, 10, 384-387.

100. Waugh, J. S.; Huber, L. M.; Haeberlen, V. Phys. Rev. Lett. 1968, 20, 180.

101. Lowe, I. J. Phys. Rev. Lett. 1959, 2, 285-287.

102. Andrew, E. R.; Bradbury, A.; Eades, R. G. Nature (London), 1958, 182, 1659-1663.

103. Andrew, E. R.; Bradbury, A.; Eades, R. G. Nature (London), 1959, 183, 1802-1807.

104. reference 87, p. 43.

105. Stejskal, E. O.; Schaefer, J.; McKay, R. A. J. Magn. Reson. 1977, 25, 569-573.

106. Doskocilova, D.; Schneider, B. Adv. Collid Interface Sci. 1978, 9, 63-69.

107. Schneider, B.; Doskocilova, D.l Babka, J.; Ruzicka, Z. J. Magn. Reson. 1980, 37, 41-49.

108. Lippmaa, E. T.; Alla, M.; Pehk, T. J.; Engelhardt, G. J. Am. Chem. Soc. 1978, 100, 1929-1931.

109. Eckman, R.; Alla, M.; Pines, A. J. Magn. Reson. 1980, 41, 440-446

110. Andrew, E. R.; Firth, M.; Jasinski, A.; Randall, P. J. Phys. Lett. 1970, 31A, 446-448.

111. Andrew, E. R.; Farnell, L. F.; Gledhill, T. D. Phys. Rev. Lett. 1967, 19, 6-7.

112. Andrew, E. R.; Wynn, V. T. Proc. Roy. Soc. London, 1966, 291A, 257-261.

113. Kessemeier, H.; Nordberg, R. E. Phys. Rev. 1967, 155, 321-331.

114. Andrew, E. R.; Bradbury, A.; Eades, R. G.; Jeaks, G. J. Nature, (London), 1960, 188, 1096-1099.

115. Griffin, R. G.; Ellett, J. D.; Mehring, M.; Bullitt, J. G.; Waugh, J. S. J. Chem. Phys. 1972, 57, 2147-2155.

116. Dixon, W. T.; Schaefer, J.; Sefcik, M. D.; Stejskal, E. O.; McKay, R. A. J. Magn. Reson. 1981, 45, 173-181.

117. Dixon, W. T.; Schaefer, J.; Sefcik, M. D.; Stejskal, E. O.; McKay, R. A. J. Magn. Reson. 1982, 49, 341-347.

118. reference 85, p. 8.

119. Flemming, W. W.; Fyfe, C. A.; Kendrick, R. D.; Lyerla, J. R.; Vanni, A.; Yannoni, C. S. in "Polymer Characterization by ESR and NMR," Woodward, A. E.; Bovey, F. A., eds. ACS Symposium Series Vol. 142, 1980, pp. 193-217.

120. Lyerla, J. R.; Yannoni, C. S. IBM J. Res. Develp. 1983, 27, 302-312.

121. Farrar, T. C.; Becker, E. D. "Pulse and Fourier Transform NMR, Introdcution to Theory and Methods," Academic Press, New York, 1971.

122. reference 88, p. 111

123. Abragam, A.; Kambe, K. Phys. Rev. 1953, 91, 894-895.

124. Pines, A.; Gibby, M. G.; Waugh, J. S. J. Chem. Phys. 1973, 59, 569-590.

125. reference 86, pp. 188-214

126. reference 88, pp. 133-158

127. reference 86, pp. 238-240.

128. Hartman, S. R.; Hahn, E. L. Phys. Rev. 1962, 128, 2042-2053.

129. Maier, G.; Haeberlen, U.; Wolf, H. C.; Hausser, K. H. Phys. Lett., 1967, 7, 384-387.

130. Lau, P.; Stehlik, D.; Hausser, K. H. J. Magn. Reson. 1970, 15, 270-282.

131. Goldman, M.; Chapellier, M.; Vu. Huang, C.; Abragam, A. Phys. Rev. 1974, B10, 226-238.

132. Jacquinot, J. F.; Wenchenach, W. T.; Goldman, M.; Abragam, A. Phys. Rev. Lett. 1974, 32, 1096-1099.

133. Demco, D.; Kaplan, S.; Pausak, S.; Waugh, J. S. Chem. Phys. Lett. 1975, 1, 77-78.

134. Schwab, M.; Hahn, E. L. J. Chem. Phys. 1970, 52, 3152-3167.

135. Stejskal, E. O.; Schaefer, J. J. Magn. Reson. 1975, 18, 560-563.

136. Flemming, W. W.; Fyfe, C. A.; Lyerla, J. R.; Vanni, H.; Yannoni, C. S. Macromolecules 1980, 13, 460-465.

137. VanderHart, D. L.; Earl, W. L.; Garroway, A. N. J. Magn. Reson. 1981, 44, 361-401.

138. Schaefer, J.; Stejskal, E. O. "Top. in Carbon-13 NMR Spectroscopy" 1980, 3, 283.

139. Schaefer, J.; Stejskal, E. O.; Steger, T. R.; Sefcik, M. D.; McKay, R. A. Macromolecules 1980, 13, 1121-1126.

140. Fyfe, C. "Solid State NMR for Chemists," CFC Press, Guelph Ontario, Canada (1983) p. 380.

141. Kroker, R.; Schneider, M.; Harmann, K. "Progress in Organic Coatings," 1, (1973), p. 23.

142. Gilpin, R. K.; Burke, M. F. Anal. Chem. 1975, 45, 1383-1389.

143. Leyden, D. E.; Luttrell, G. H. Anal Chem. 1975, 47, 1612-1617.

144. Leal, L.; Anderson, D. L.; Bowman, R. G.; Burwell, R. L., Jr. Basolo, F. J. Am. Chem. Soc. 1975, 97, 5125-5129.

145. Horvath, C.; Melander, W. J. Chromatogr. Sci. 1977, 15, 393-404.

146. Clark, H. C.; Davies, J. A.; Fyfe, C. A.; Hayes, P. J.; Wasylishen, R. E. Organometallics 1982, 2, 177-180.

147. Clark, H. C.; Davies, J. A.; Fyfe, C. A.; Hayes, P. J.; Wasylishen, R. E. J. Am. Chem. Soc. 1983, 105, 6577-6584.

148. "Magnetic Resonance in Colloid and Interface Science," Fraissand, J. P.; Resing, H. A., eds.; Reidel: Dordrecht, Holland, 1980, p.

149. Gay, I. D. J. Phys. Chem. 1974, 78, 38-42.

150. Gay, I. D.; Liang, S. J. of Catal. 1976, 44, 306-313.

151. Kriz, J. F.; Gay, I. D. J. Phys. Chem. 1978, 80, 2951-2953.

152. Gay, I. D.; Kriz, J. F. J Phys. Chem. 1978, 80, 319-321.

153. Fyfe, C. A.; Lyerla, J. R.; Thomas, J. M. Agnew. Chem. Intl. Ed. 1981, 20, 96-101.

154. Montrewx, A.; Petit, F.; Blanchard, M. J. Mol. Catal. 1980, 8, 97-111.

155. Sefcik, M. D. J. Am. Chem. Soc. 1979, 101, 2164-2170.

156. Derouawe, E. G.; Gilson, J. P.; Nagy, J. B. J. Mol Catal. 1981, 10, 331-338.

157. Dessan, R. M.; LaPierre, R. B. J. of Catal. 1982, 78, 136-142.

158. Gay, I. D. J. Phys. Chem. 1980, 84, 3230-3232.

159. Duncan, T. M.; Yates, J. T., Jr.; Vaughan, R. W. J. Chem. Phys. 1979, 71, 3129-3130.

160. Duncan, T. M.; Yates, J. T., Jr.; Vaughan, R. W. J. Chem. Phys. 1980, 73, 975-985.

161. Sefcik, M. D.; Schaefer, J.; Stejskal, E. O. in "Magnetic Resonance in Colloid and Interface Science," Resing, H. A.; Wade, C. G., Eds.; ACS Symp. Series 1976, 34, p. 109.

162. Kaplan, S.; Resing, H. A.; Waugh, J. S. J. Chem. Phys. 1973, 59, 5681-5687.

163. Resing, H. A.; Soltfeldt-Ellingsen, D.; Garoway, A. N.; Weber, D. C.; Pinnavaia, T. J.; Unger, K. in "Magnetic Resonance in Colloid and Interface Science," Fraissard, J. P.; Resing, H. A.; Eds.; Reidel: Dordrecht, Holland, 1980, p. 239.

164. Resing, H. A.; Slotfeldt-Ellingsen, D. J. Magn. Reson. 1980, 38, 401-407.

165. Slotfeldt-Ellingsen, D.; Resing, H. A. J. Phys. Chem. 1980, 84, 2204-2209.

166. Sindorf, D. W.; Maciel, G. E. J. Am. Chem. Soc. 1983, 105, 1848-1857.

167. Ripmeester, J. A.; Davidson, D. W. Bull. Mag. Reson. 1980, 2, 139-151.

168. Ripmeester, J. A. J. Am. Chem. Soc. 1982, 104, 289-290.

169. Ito, T.; Fraissard, J. J. Chem. Phys. 1982, 76, 5225-5231.

170. Barrer, R. M. in "Zeolites and Clay Minerals as Sorbents and Molecular Sieves," Academic Press: London, 1978, p 81.

171. Fyfe, C. A.; Thomas, J. M.; Klinowski, J.; Gobbi, G. C. Angew. Chem. Intl. Ed. 1983, 22, 259-275.

172. Lippmaa, E.; Samoson, A.; Magi, M.; Teeaar, R.; Schraml, J.; Gotz, J.; J. Non. Cryst. Solids 1982, 50, 215-222.

173. Lippmaa, E.; Magi, M.; Samoson, A.; Tarmak, M.; Engelhardt, G. J. Am. Chem. Soc. 1981, 103, 4992-4996.

174. Engelhardt, G.; Lippmaa, E.; Magi, M. J. Chem. Soc. Chem. Commun. 1981, 712-713.

175. Klinowski, J.; Thomas, J. M.; Andier, M.; Vasudevan, S.; Fyfe, C. A.; Hartman, J. S., J. C. S. Chem. Comm. 1981, 570-571.

176. Thomas, J. M.; Klinowski, J.; Fyfe, C. A.; Hartmann, J. S.; Bursill, L. A., J. Chem. Soc. Chem. Comm. 1981, 678-679.

177. Ramdas, S.; Thomas, J. M.; Klinowski, J.; Fyfe, C. A.; Hartmann, J. S. Nature (London), 1981, 292, 228-231.

178. Klinowski, J.; Ramdas, S.; Thomas, J. M.; Fyfe, C. A.; Hartmann, J. S. J. Chem. Soc., Faraday Trans 2, 1982, 78, 1025- 1050.

179. Engelhardt, G.; Lohse, U.; Lippmaa, E.; Tarmark, M.; Magi, M. Z. Inorg. Allgem. Chem. 1981, 482, 49-53.

180. Fyfe, C. A.; Gobbi, G. C.; Murphy, W. J.; Ozubko, R. S.; Slack, D. A., J. Am. Chem. Soc., in press.

181. Fyfe, C. A.; Gobbi, G. C.; Kennedy, G. J.; deShutter, C. T.; in Murphy, W. J.; Ozubko, R. S.; Slack, D. A. Chem. Lett. in press.

182. Maciel, G. E.; Sindorf, D. W. J. Am. Chem. Soc. 1980, 102, 7606-7607.

183. Sindorf, D. W.; Maciel, G. E. J. Am. Chem. Soc. 1981, 103, 4263-4265.

184. Sindorf, D. W.; Maciel, G. E. J. Phys. Chem. 1982, 86, 5208-5219.

185. Maciel, G. E.; Haw, J. F.; Chuang, I. S.; Hawkins, B. L.; Early, T. A.; McKay, D. R.; Petrakis, L. J. Am. Chem. Soc. 1983, 105, 5529-5535.

186. Haw, J. F.; Chuang, I. S.; Hawkins, B. L.; Maciel, G. E. J. Am. Chem. Soc. 1983, 105, 7206-7207.

187. Bemi, L.; Clark, H. C.; Davies, J. A.; Fyfe, C. A.; Wasylishen, R. E. J. Orgamomet. Chem. 1982, 224, C5-C10.

188. Bemi, L.; Clark, H. C.; Davies, J. A.; Fyfe, C. A.; Wasylishen, R. E. J. Am. Chem. Soc. 1982, 104, 438-445.

189. Rothwell, W. P.; Shen, W. X.; Lunsford, J. H. J. Am. Chem. Soc. 1984, 106, 2452-2453.

190. Schoonheydt, R. A.; VanWouwe, D.; Leeman, H. Zeolites 1982, 2, 109.

191. reference 89, p. 406.

192. Fyfe, C. A.; Wasylishen, R. E.; Childs, R. F.; Lock, C. L. J. Am. Am. Chem. Soc. 1984, 106, 4016-4020.

193. Ellett, D., Jr.; Haeberlen, U.; Waugh, J. S. Polymer Letters 1969, 7, 71-74.

194. English, A. D.; Vega, A. J. Macromolecules 1979, 12, 353-354.

195. English, A. D.; Vega, A. J. Macromolecules 1980, 13, 1635-1647.

196. Hull, W. E.; Sykes, B. D. J. Mol. Biol. 1975, 98, 121-153.

197. Gent, M. P. N.; Cottam, P. F.; Ho, C. Proc. Natl. Acad. Sci. USA 1978, 75, 630-634.

198. Gent, M. P. N.; Ho, C. Biochemistry 1978, 17, 3023-3038.

199. Rutar, V.; Blinc, R.; Ehrenberg, L. J. Mag. Res. 1980, 40, 225-231.

200. O'Donnell, D. J.; Ackerman, J. J. H.; Maciel, G. E. J. Agric. Food Chem. 1981, 29, 574-582.

201. Haw, J. F.; Maciel, G. E. Anal. Chem. 1983, 55, 1262-1267.

202. Danyluk, S. S.; Schwartz, H. M. Argonne Natl. Lab., Report 1979 "^{13}C CP/MAS Stuides of Biophysical Systems" No. CONF 70048 5-1 Avail. NTIS.

203. Jacob, G. S.; Schaefer, J.; Stejskal, E. O.; McKay R. A. Biochem. Biophy. Res. Commun. 1980, 97, 1176-1177.

204. Schaefer, J.; McKay, R. A.; Stejskal, E. O. J. Mag. Reson. 1979, 34, 443-447.

205. Schaefer, J.; Skokut, T. A.; Stejskal, E. O.; McKay, R. A.; Varner, J. E. J. Biol. Chem. 1981, 256, 11574-11579.

206. Schaefer, J.; Skokut, T. A.; Stejskal, E. O.; McKay, R. A.; Varner, J. E. Proc. Natl. Acad. Sci. USA, 1981, 78, 5978.

207. Stejskal, E. O.; Schaefer, J.; McKay, R. A. J. Magn. Reson. 1984, 57, 471-485.

208. Henrichs, P. M.; Linder, M. J. Magn. Reson. 1984, 58, 458-461.

209. Maricq, M. M.; Waugh, J. S. J. Chem. Phys. 1979, 70, 3300-3316.

210. Kaiser, E. M.; Woodruff, R. A. J. Org. Chem. 1970, 35, 1198-1199.

211. Reich, H. J.; Jautelat, M.; Messe, M. T.; Weigert, F. J.; Roberts, J. D. J. Am. Chem. Soc. 1969, 91, 7445-7454.

212. Locke, D. C.; Schmermund, J. T.; Banner, B. Anal. Chem. 1972, 44, 90-92.

213. Sindorf, D. W.; Maciel, G. E. J. Am. Chem. Soc. 1983, 105, 1487-1493.

214. Gibson, D. F. R.; McDowell, C. A. Mol. Phys. 1961, 4, 125-134.

215. Ault, A.; Kopet, R. J. Chem. Ed. 1969, 46, 612-613.

216. Hexem, J. G.; Frey, M. H.; Opella, S. J. J. Chem. Phys. 1982, 77, 38-47.

217. Cooper, J. W. Comput. Chem. 1976, 1, 55-58

218. McBriety, V. T. Polymers, 1974, 15, 503-511.

219. Schaefer, J.; SEfcik, M. D.; Stejskal, E. O.; McKay, R. A. Macrolmolecules 1981, 14, 188-192.

220. Opella, S. J.; Frey, M. H.; Cross, T. A. J. Am. Chem. Soc. 1979, 101, 5856-5857.

221. Diehl, P.; Khetrapal, C. L. in "NMR-Basic Principles and Progress," Diehl, P; Fluck, E.; Kesfeld, R. eds., Springer Verlag, Berlin, Vol. 1, 1969, p.1

222. Rothwell, W. P.; Waugh, J. S. J. Chem. Phys. 1981, 74, 2721-2784.

223. Suwelack, D.; Rothwell, W. P.; Waugh, J. S. J. Chem. Phys. 1980, 73, 2559-2562.

224. Schilling, F. C. J. Magn. Reson. 1982, 47, 61-67.

225. Dorn, H. C.; Glass, T. E; Allen. L. unpublished results.

The vita has been removed from the scanned document

SOLUTION AND SOLID STATE NMR STUDIES OF FLUORINE TAGGING REAGENTS

BY

Michael Phillip Spratt

(ABSTRACT)

A series of studies are presented in which fluorine tagging reagents are used to analyze complex mixtures for compounds containing active hydrogen functional groups (e.g., hydroxyl, amine, thiol, and carboxylic groups). The existence of these derivatized functional groups is determined by utilizing a number of solution and solid-state nuclear magnetic resonance (NMR) techniques.

In solution NMR studies p-fluorobenzoyl chloride was the fluorine tagging reagent of choice because of a large ^{19}F chemical shift range for the different derivatized substrates (~10 ppm) and generally good reaction yields. Various classes of sterol and amino acid p-fluorobenzoyl derivatives were characterized on the basis of their ^{19}F NMR isotropic chemical shifts. The presence (or absence) of hydroxyl, amine, and carboxylic acid functional groups in coal extract and pyrolysis products was also determined.

The versality of the p-fluorobenzoyl chloride as the fluorine tagging reagent in ^{19}F NMR was enhanced by: a) enriching the carbonyl carbon of the acid chloride with labelled ^{13}C isotope, thus synthesizing a dual ^{19}F and ^{13}C NMR sensitive reagent and b) using the reagent in

conjuction with LC-NMR. The extension to either technique added another dimension to the NMR spectral data obtained from the p-fluorobenzoyl tagging reagent in solution NMR.

Finally, preliminary data is presented illustrating how fluorine tagging reagents may be used to study functional groups (and atoms present in the immediate proximity of the group) existing on solid material utilizing solid state NMR. Functional groups on the solid material are tagged with a fluorinated reagent. The sample is then analyzed using solid state NMR with cross polarization (CP), magic angle spinning (MAS), and high-power proton decoupling. The ^{19}F dipolar coupling interactions, created by the presence of the fluorine tag, attenuate signals for these nuclei in the immediate proximity of the tagged site. A series of 1-adamantanol, steroid, and silica gel fluorinated derivatives show that the effects of the ^{19}F dipolar interactions were modulated by complex anisotropic molecular motions (i.e., solid system with little motion, exhibiting greater signal attenuations due to ^{19}F dipolar coupling).